USGS
science for a changing world

Water Availability and Use Science Program
Prepared in cooperation with the Coachella Valley Water District

Detection and Measurement of Land Subsidence and Uplift Using Global Positioning System Surveys and Interferometric Synthetic Aperture Radar, Coachella Valley, California, 2010–17

Scientific Investigations Report 2020–5093

U.S. Department of the Interior
U.S. Geological Survey

Cover Photos:
Background: Natural color image of the Coachella Valley, California.
Upper right: Photograph showing the moon setting over Global Positioning System (GPS) equipment at geodetic monument TOR2. Photograph by Justin T. Brandt, U.S. Geological Survey, 2015.
Lower right: Photograph showing GPS equipment at geodetic monument 116.8 adjacent the Coachella Branch of the All-American Canal. Photograph by James F. Howle, U.S. Geological Survey, 2015.
Center left: Photograph showing valley vista, water tank, and GPS equipment at geodetic monument DEEP. Photograph by James F. Howle, U.S. Geological Survey, 2015.

Detection and Measurement of Land Subsidence and Uplift Using Global Positioning System Surveys and Interferometric Synthetic Aperture Radar, Coachella Valley, California, 2010–17

By Michelle Sneed and Justin T. Brandt

Water Availability and Use Science Program

Prepared in cooperation with the Coachella Valley Water District

Scientific Investigations Report 2020–5093

U.S. Department of the Interior
U.S. Geological Survey

U.S. Department of the Interior
DAVID BERNHARDT, Secretary

U.S. Geological Survey
James F. Reilly II, Director

U.S. Geological Survey, Reston, Virginia: 2020

Suggested citation:
Sneed, M., and Brandt, J.T., 2020, Detection and measurement of land subsidence and uplift using Global Positioning System surveys and interferometric synthetic aperture radar, Coachella Valley, California, 2010–17: U.S. Geological Survey Scientific Investigations Report 2020–5093, 74 p., https://doi.org/10.3133/sir20205093.

Associated data for this publication:
Sneed, M., 2020, Global Positioning System survey data for 2015 and interferometric synthetic aperture radar data for 1995–2017, Coachella Valley, Riverside County, California: U.S. Geological Survey data release, https://doi.org/10.5066/P9B35CNL.

ISSN 2328-0328 (online)

Acknowledgments

The authors gratefully acknowledge the Coachella Valley Water District for their support and assistance during this study. We thank the Scripps Orbit and Permanent Array Center for allowing free access to continuous Global Positioning System data. We thank the University NAVSTAR (Navigation Satellite Timing and Ranging) Consortium (UNAVCO) for providing Global Positioning System equipment and exceptional technical support for the 2010 and 2015 Global Positioning System surveys. We thank the California Department of Transportation for providing fixed-height tripods for the 2010 and 2015 GPS surveys. Radar data used to produce the interferograms shown in this report were obtained from the European Space Agency through their free and open-data policy and the German Aerospace Center through research proposal GEO1609 for purposes of research and development.

Contents

Figures

Tables

Conversion Factors

U.S. customary units to International System of Units

Multiply	By	To obtain
	Length	
inch (in.)	2.54	centimeter (cm)
inch (in.)	25.4	millimeter (mm)
foot (ft)	0.3048	meter (m)
mile (mi)	1.609	kilometer (km)
	Area	
square mile (mi^2)	259.0	hectare (ha)
square mile (mi^2)	2.590	square kilometer (km^2)
	Subsidence rate	
foot per year (ft/yr)	0.3048	hectare (ha)
foot per year (ft/yr)	304.8	millimeter per year (mm/yr)
inch per year (in/yr)	25.4	millimeter per year (mm/yr)

Temperature in degrees Fahrenheit (°F) may be converted to degrees Celsius (°C) as follows:

$$°C = (°F – 32) / 1.8.$$

Datum

Horizontal coordinate information is referenced to the North American Datum of 1983 (NAD 83).

Vertical coordinate information is referenced to the National Geodetic Vertical Datum of 1929 (NGVD 29).

Ellipsoid heights: In this report, Global Positioning System (GPS) measurements of horizontal coordinates and ellipsoid heights are based on the North American Datum of 1983 (NAD 83).

Elevation, as used in this report, refers to distance above the vertical datum.

Vertical displacements determined by interferometric synthetic aperture radar (InSAR) and coordinates determined by Global Positioning System (GPS) surveying generally are reported in metric units. The industry standard for GPS usage is that field measurements and subsequently computations, including standard error determinations, are done in the metric system. The use of dual units in this report is intended to facilitate application of the data by maintaining the integrity of the original units of measurement for InSAR and GPS surveying.

Abbreviations and Acronyms

CGPS	continuous Global Positioning System
CVWD	Coachella Valley Water District
DLR	German Aerospace Center
GPS	Global Positioning System
InSAR	interferometric synthetic aperture radar
SAR	synthetic aperture radar
SOPAC	Scripps Orbit and Permanent Array Center
USGS	U.S. Geological Survey

Well-Numbering System

Wells are identified and numbered according to their location in the rectangular system for the subdivision of public lands. Identification consists of the township number, north or south; the range number, east or west; and the section number. Each section is divided into sixteen 40-acre tracts lettered consecutively (except I and O), beginning with "A" in the northeast corner of the section and progressing in a sinusoidal manner to "R" in the southeast corner. Within the 40-acre tract, wells are sequentially numbered in the order they are inventoried. The final letter refers to the base line and meridian. In California, there are three base lines and meridians; Humboldt (H), Mount Diablo (M), and San Bernardino (S). All wells in the study area are referenced to the San Bernardino base line and meridian (S). Well numbers consist of 15 characters and follow the format 005S006E23K002S. In this report, well numbers are abbreviated and written 5S/6E-23K2. The following diagram shows how the number for well 5S/6E-23K2 is derived.

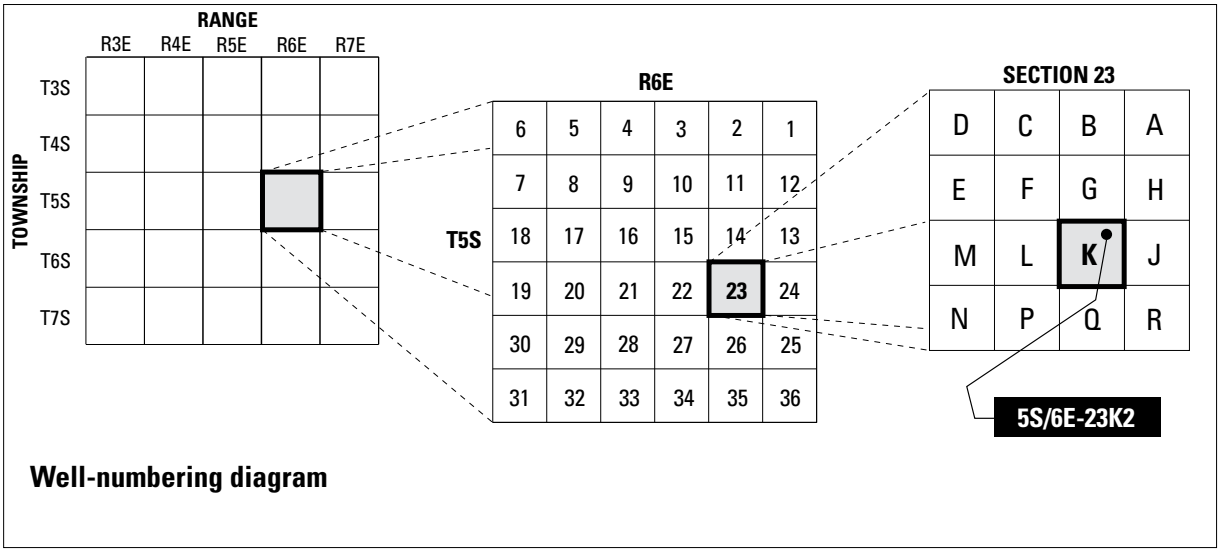

Well-numbering diagram

Detection and Measurement of Land Subsidence and Uplift Using Global Positioning System Surveys and Interferometric Synthetic Aperture Radar, Coachella Valley, California, 2010–17

By Michelle Sneed and Justin T. Brandt

Abstract

Groundwater has been a major source of agricultural, recreational, municipal, and domestic supply in the Coachella Valley of California since the early 1920s. Pumping of groundwater resulted in groundwater-level declines as large as 50 feet (ft) or 15 meters (m) by the late 1940s. Because of concerns that the declines could cause land subsidence, the Coachella Valley Water District (CVWD) and the U.S. Geological Survey (USGS) have cooperatively investigated subsidence in the Coachella Valley since 1996.

Importation of Colorado River water to the southern Coachella Valley began in 1949, resulting in a reduction in groundwater pumping and a recovery of groundwater levels during the 1950s through the 1970s. Since the late 1970s, the demand for water in the valley increased to the point that groundwater levels again declined in response to increased pumping and, consequently, increased the potential for land subsidence caused by aquifer-system compaction. Several management actions to increase recharge or to reduce reliance on groundwater have been implemented since as early as 1973 to address overdraft in the Coachella Valley. The implementation of three particular projects has markedly improved groundwater conditions in some of the historically most overdrafted areas of the valley: (1) groundwater substitution with surface-water imports since 2006 using Colorado River water through the Mid-Valley Pipeline project, which was expanded through 2017; (2) budget-based, tiered rates since 2009; and (3) managed aquifer recharge at the Thomas E. Levy Groundwater Replenishment Facility since 2009.

Global Positioning System (GPS) surveying and interferometric synthetic aperture radar (InSAR) methods were used to determine the location, extent, and magnitude of the vertical land-surface changes in the Coachella Valley during 2010–17, updating 1993–2010 information presented in previous USGS reports. The GPS measurements taken at 24 geodetic monuments in August 2010 and September 2015 indicated that the land-surface elevation was stable at 17 monuments but changed at seven monuments during the 5-year period. Subsidence ranged from 0.17 to 0.43 ±0.09 ft (52 to 132 ±28 millimeters, or mm) at three monuments, and uplift ranged from 0.11 to 0.18 ±0.09 ft (33 to 54 ±28 mm) at four monuments between 2010 and 2015. At two of the monuments that subsided, the subsidence rates decreased between 2010 and 2015 from those computed between 2005 and 2010. Data prior to 2010 were not available for the third monument that subsided; thus, the 2010–15 subsidence rate could not be compared to an earlier period. At three of the monuments that uplifted between 2010 and 2015, data collected in 2005 and 2010 indicated stability. Data prior to 2010 were not available for the fourth monument that uplifted; thus, the 2010–15 uplift rate could not be compared to an earlier period.

InSAR analyses for December 28, 2014–June 27, 2017, indicated that the land surface uplifted as much as about 0.20 ft (60 mm) near the Whitewater River Groundwater Replenishment Facility in the northern Coachella Valley and subsided as much as about 0.26 ft (80 mm) in the La Quinta area and less in Palm Desert, Indian Wells, and other localized areas in the southern Coachella Valley. These areas were identified as subsidence areas in previous reports covering periods during 1993–2010. The comparison of 2014–17 subsidence rates with those derived for 1995–2010 generally indicated a substantial slowing of subsidence, however. Analyses of deformation in the northern Coachella Valley were not included in the previous reports, so a comparison to deformation during the earlier period could not be made.

Water levels in wells near the subsiding geodetic monuments, in and near the three subsiding areas shown by InSAR, and throughout the valley generally indicated seasonal fluctuations and longer-term stability or rising groundwater levels since about 2010. These results mark a reversal in trends of groundwater-level declines during the preceding decades.

This trend reversal provides new insights into aquifer-system mechanics. Although many areas have stopped subsiding, and a few have even uplifted, the few areas that did subside during 2010–17—albeit at a slower rate—indicate a mixed aquifer-system response. Subsidence when groundwater levels are stable or recovering indicates that residual compaction may have occurred. At the same time, coarse-grained materials and thin aquitards may have expanded as groundwater levels recovered. The continued valley-wide stabilization and recovery of groundwater levels since 2010 likely is a result of various projects designed to increase recharge or to reduce reliance on groundwater.

Introduction

The Coachella Valley Water District (CVWD) works cooperatively with local stakeholders to manage the water supply for a large part of the Coachella Valley (fig. 1). Groundwater has been a major source of agricultural, recreational, municipal, and domestic water supply in the Coachella Valley of California, United States, since the early 1920s. Although there has been no documented subsidence between the early 1920s and late 1940s, pumping of groundwater resulted in groundwater-level declines as much as 50 feet (ft), or 15 meters (m), during that timeframe. In 1949, the importation of Colorado River water began to the southern Coachella Valley via the Coachella Canal, which is a branch of the All-American Canal (fig. 1). As a result of the importation of surface water, pumping of groundwater decreased in the southern Coachella Valley during the 1950s through the 1970s, and groundwater levels in some wells recovered as much as 50 ft (15 m). Starting in the 1970s, however, the demand for water in the Coachella Valley had increased to the point that groundwater levels again declined in response to increased pumping, except in some northern areas of the valley near the Whitewater River Groundwater Replenishment Facility. By about 2010, groundwater levels in many wells in the southern Coachella Valley had declined 50–100 ft (15–30 m), and groundwater levels in some wells were at their lowest recorded levels. Since about 2010, however, the combination of several management agreements, water management agency projects, and actions by the CVWD, have markedly improved groundwater conditions in some of the historically most overdrafted areas of the valley. The agreements, projects, and actions include the Quantification Settlement Agreement, conservation programs including budget-based, tiered rates; managed aquifer-recharge (MAR) projects; and groundwater substitution for golf-course irrigation and for other non-potable water uses through the Mid-Valley Pipeline Project (Coachella Valley Water District, 2012; undated) Monitoring has tracked the effect that these agreements and the related projects have had on groundwater levels.

Declining groundwater levels can contribute to or induce land subsidence in aquifer systems that consist of a substantial fraction of unconsolidated fine-grained sediment (silts and clays; Galloway and others, 1999). Because of the potential for groundwater pumping to cause land subsidence, the CVWD entered into a cooperative agreement with the U.S. Geological Survey (USGS) in the mid-1990s to monitor vertical changes in land surface to determine if land was subsiding in the Coachella Valley.

As much as 0.5 ±0.3 ft (150 ±90 millimeters, or mm) of subsidence in the southern Coachella Valley between 1930 and 1996 was reported by Ikehara and others (1997). As much as about 2 ft (600 mm) of subsidence along the largely urbanized southwestern margins of the Coachella Valley between 1995 and 2010 was reported by Sneed and others (2014). Land subsidence can disrupt surface drainage and water-supply or flood-control conveyances; cause earth fissures; and damage wells, buildings, roads, and utility infrastructure. A large earth fissure was discovered in 1948 about 2 miles (mi), or 3 kilometers (km), north of Lake Cahuilla in La Quinta (Coachella Valley Water District, unpublished field notes, 1948). Because subsidence had not been documented in the southern Coachella Valley prior to the report by Ikehara and others (1997), it is not known if this fissure formed in response to differential land subsidence (different magnitudes of subsidence across the landscape) during the earlier period (early 1920s–late 1940s) of groundwater-level declines. However, fissuring has recurred in this area (Clay Stevens, TerraPacific Consultants, Inc., written commun., 2006). Subsidence-related earth fissures and reactivated surface faults have been identified in many other groundwater basins in the western United States (Holzer, 1984). More recently, subsidence-induced damage to the Coachella Canal prompted the CVWD to reroute a section in the La Quinta area during 2014–15.

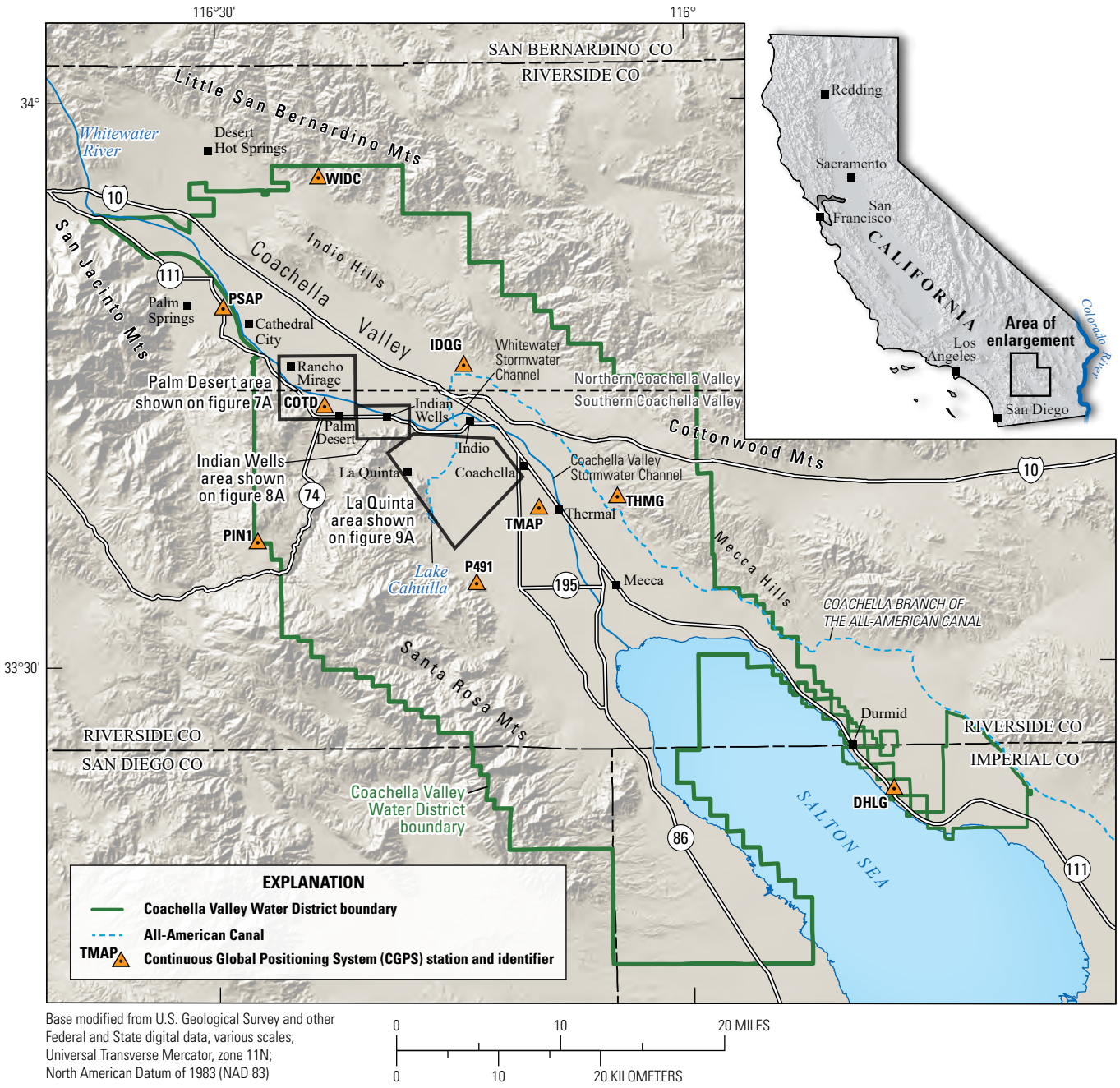

Figure 1. Location of study area and nine continuous Global Positioning System (CGPS) stations in or near Coachella Valley, California.

Objectives, Purpose, and Scope

The objectives of this study were to detect and quantify land subsidence in the Coachella Valley from 2010 through 2017 by completing Global Positioning System (GPS) surveys at the established geodetic network of monuments and by analyzing interferometric synthetic aperture radar (InSAR) data. The purpose of this report is to present the results and interpretations of GPS data collected at the monuments in the monitoring network in the southern Coachella Valley during surveys in 2010 and 2015 and to show detailed maps of vertical land-surface changes generated by analyzing InSAR data collected throughout the Coachella Valley between 2010 and 2017. The GPS and InSAR data supporting the conclusions of this report are available in Sneed (2020). Groundwater levels for 2010–17 also are examined and compared with the GPS measurements and the InSAR-generated maps to determine if the vertical changes in land surface could be related to the changes in groundwater levels. For the southern Coachella Valley, these new results are compared to previous results. This comparison facilitates analyses in a longer-term context and updates previous analogous results for 1993–2010. Analyses of deformation in the northern Coachella Valley were not done for 1993–2010; therefore, a comparison to deformation that may have occurred during the earlier period could not be made.

Description of Study Area

The Coachella Valley is a 65-mi (100-km) long, northwest-southeast trending valley in southeastern California (fig. 1). The valley covers about 400 square miles (mi^2), or 1,000 square kilometers (km^2; California Department of Water Resources, 1964) and includes the cities of Desert Hot Springs, Palm Springs, Cathedral City, Rancho Mirage, Palm Desert, Indian Wells, La Quinta, Indio, Coachella, Thermal, and Mecca, which are interspersed with about 125 golf courses. In this report, the southern Coachella Valley represents the southern half of the Coachella Valley, which extends from about the communities of Palm Desert, Indian Wells, and Indio, on the north, to the Salton Sea on the south (fig. 1). The northern Coachella Valley represents the northern half of the Coachella Valley, which includes the communities of Desert Hot Springs, Palm Springs, and Rancho Mirage and extends to the northwest near the intersection of Interstate 10 and Highway 111. Agriculture and smaller urban centers, such as Coachella, Thermal, and Mecca, are common in the southern Coachella Valley. The valley is bordered by the San Jacinto and Santa Rosa Mountains on the west, the Little San Bernardino Mountains on the north, the Cottonwood Mountains and the Mecca Hills on the east, and the Salton Sea on the south (fig. 1). The Coachella Valley is drained primarily by the Whitewater River, which flows into the Whitewater Stormwater Channel, then into the Coachella Valley Stormwater Channel, and eventually discharges into the Salton Sea (fig. 1). Land-surface elevations vary from more than 230 ft (70 m) below sea level at the Salton Sea to more than 10,000 ft (3,000 m) above sea level at the peaks of the surrounding mountains.

The climate of the Coachella Valley floor is arid. Average annual rainfall ranges from less than 4 inches (in.), or 100 mm, on the valley floor, to more than 40 in. (1,000 mm) on the crests of the mountains to the west and north of the valley (PRISM Climate Group, 2015). Temperatures range from more than 104 degrees Fahrenheit (°F) on the valley floor in the summer to below 32 °F in the surrounding mountains in the winter (PRISM Climate Group, 2015).

Previous Land-Subsidence Studies in the Coachella Valley

This study is the sixth in a series of Coachella Valley land-subsidence studies that have been completed by the USGS in cooperation with the CVWD. In 1996, the USGS established a geodetic network of monuments to monitor vertical changes in land surface in the southern Coachella Valley by using GPS surveys and to establish baseline values for comparisons with results of future surveys. This geodetic network has been surveyed periodically to determine the distribution and magnitude of land subsidence. The development of the geodetic monitoring network and its use to detect areas of possible land subsidence in Coachella Valley by comparing historical leveling measurements with GPS surveying measurements taken in 1996 were documented by Ikehara and others (1997). The vertical changes in land surface between 1996 and the earliest historical leveling measurements at monuments in the monitoring network did not exceed 0.5 ft (150 mm; Ikehara and others, 1997). The uncertainty (±0.3 ft or ±90 mm) of these calculated vertical changes in land surface is large because the historical leveling surveys were done at different times and, sometimes, by different agencies using different methods. Furthermore, the methods used for the leveling surveys had different accuracy standards, and the networks covered different geographic extents (Ikehara and others, 1997). The GPS measurements indicated small magnitudes of subsidence between 1996 and 1998 at some monuments in the monitoring network (Sneed and others, 2001). The GPS measurements indicated most monuments were fairly stable between 1998 and 2000 (Sneed and others, 2002), although subsequent GPS data processing indicated small magnitudes of subsidence at some monuments (Sneed and Brandt, 2007). The GPS measurements indicated that some monuments were fairly stable, whereas others subsided between 2000 and 2005 (Sneed and Brandt, 2007) and between 2005 and 2010 (Sneed and others, 2014).

Interferometric synthetic aperture radar (InSAR) data have been analyzed periodically to complement the GPS surveys and to assess subsidence removed from the geodetic network. InSAR methods were used to detect and quantify land subsidence throughout much of the Coachella Valley. InSAR measurements taken between 1995 and 2010 indicated as much as 1.97 ft (600 mm) of land subsidence in areas near Palm Desert, Indian Wells, and La Quinta (Sneed and others, 2001, 2002, 2014; Sneed and Brandt, 2007).

Tectonic and Hydrogeologic Setting

The Coachella Valley is the northernmost extent of the Salton Trough, which is the landward extension of the spreading-ridge and transform-fault complex of the Gulf of California (not shown) segment of the East Pacific Rise (Sylvester and Smith, 1976; Fuis and Mooney, 1990; McKibben, 1993). Near the end of the Miocene, a spreading center separating the western Farallon plate from the eastern Pacific plate was obliquely subducted under the North American continent (Atwater, 1970; McKibben, 1993). The modern Gulf of California and the Salton Trough formed about 12 million years ago, after subduction ceased, and when the formation of an inland belt of northwest-to-southeast crustal extension, alkali basalt volcanism, tectonic subsidence, and basin sedimentation began (Atwater, 1970; McKibben, 1993). Prior to about 6 million years ago, the shear zone constituting the principal tectonic boundary between the Pacific and North American plates appears to have shifted about 155 mi (250 km) inland to this belt, initiating the formation of the modern Gulf of California and the Salton Trough (Atwater, 1970; McKibben, 1993). As the Salton Trough opened, it was filled with sediment from the delta of the Colorado River. The river has been building its delta from the east, into the trough, since about 5 million years ago, and sedimentation apparently has kept pace with the tectonic subsidence (McKibben, 1993). The relation between tectonic subsidence, which is on a geologic time scale, and land subsidence, caused by much shorter-term groundwater-level declines measured during this study, is unknown in the study area, although tectonically induced subsidence rates south of the study area have been reported to be about 0.007 ft/yr (2 mm/yr) since the 1700s (Meltzner and others, 2006; Crowell and others, 2013).

The Coachella Valley is filled with as much as 13,000 ft (4,000 m) of sediment (Ajala and others, 2019); the upper 2,000 ft (600 m) constitute the aquifer system that is the primary source of groundwater supply (California Department of Water Resources, 1979). The aquifer system consists of a complex unconsolidated to partly consolidated assemblage of gravel, sand, silt, and clay of alluvial and lacustrine origins (fig. 2). Sediment tends to be finer grained with more silt and clay in the southern Coachella Valley compared to the northern Coachella Valley because of the greater distance from sediment source areas in the north and because of lacustrine deposition in the ancient Lake Cahuilla (California Department of Water Resources, 1964, 1979). In the southern Coachella Valley, the aquifer system consists of a semiperched zone that is fairly persistent southeast of Indio, an upper aquifer, a confining layer composed of lacustrine deposits, and a lower aquifer. In the northern Coachella Valley, the confining layer is absent such that the aquifer system is not subdivided and is considered the upper aquifer throughout its thickness. The general direction of groundwater flow is southeast toward the Salton Sea (California Department of Water Resources, 1964, 1979).

The near-surface semiperched zone consists of silt, clay, and fine sand. The semiperched zone is as much as 100 ft (30 m) thick and is generally an effective barrier to deep percolation (California Department of Water Resources, 1964, 1979). The upper aquifer consists of unconsolidated and partly consolidated silty sand and gravel with interbeds of silt and clay. In general, the upper aquifer is 150–300 ft (45–90 m) thick. The aquifer is unconfined, except where it is overlain by the semiperched zone southeast of Indio. In the southern Coachella Valley, the upper aquifer is separated from the lower aquifer by a confining layer of silt and clay that is 100 to 200 ft (30 to 60 m) thick. The lower aquifer is the most productive source of groundwater in the southern Coachella Valley; it consists of unconsolidated and partly consolidated silty sand and gravel with interbeds of silt and clay. The top of the lower aquifer is about 300 to 600 ft (90 to 180 m) below land surface. Available data indicate that the lower aquifer is at least 500 ft (150 m) thick and could be as much as 2,000 ft (600 m) thick (California Department of Water Resources, 1964, 1979).

Geologic structures in the Coachella Valley have a marked influence on the location and movement of groundwater (California Department of Water Resources, 1964). The principal structural features of Coachella Valley are faults and fault-related drag and compressional folds. The most notable fault system is the northwest–southeast trending San Andreas fault zone that flanks the eastern side of the valley (fig. 2). Although movement within the San Andreas fault zone is predominantly right lateral, vertical displacement has downdropped the southwest block (California Department of Water Resources, 1964). The faults may have either juxtaposed consolidated rocks against partly consolidated or unconsolidated water-bearing deposits or displaced preferential flow paths in the partly consolidated or unconsolidated water-bearing deposits. This juxtaposition and displacement, in conjunction with cementation, compaction, and extreme deformation of water-bearing deposits adjacent to faults, may have created low-permeability zones that can act as barriers to groundwater flow.

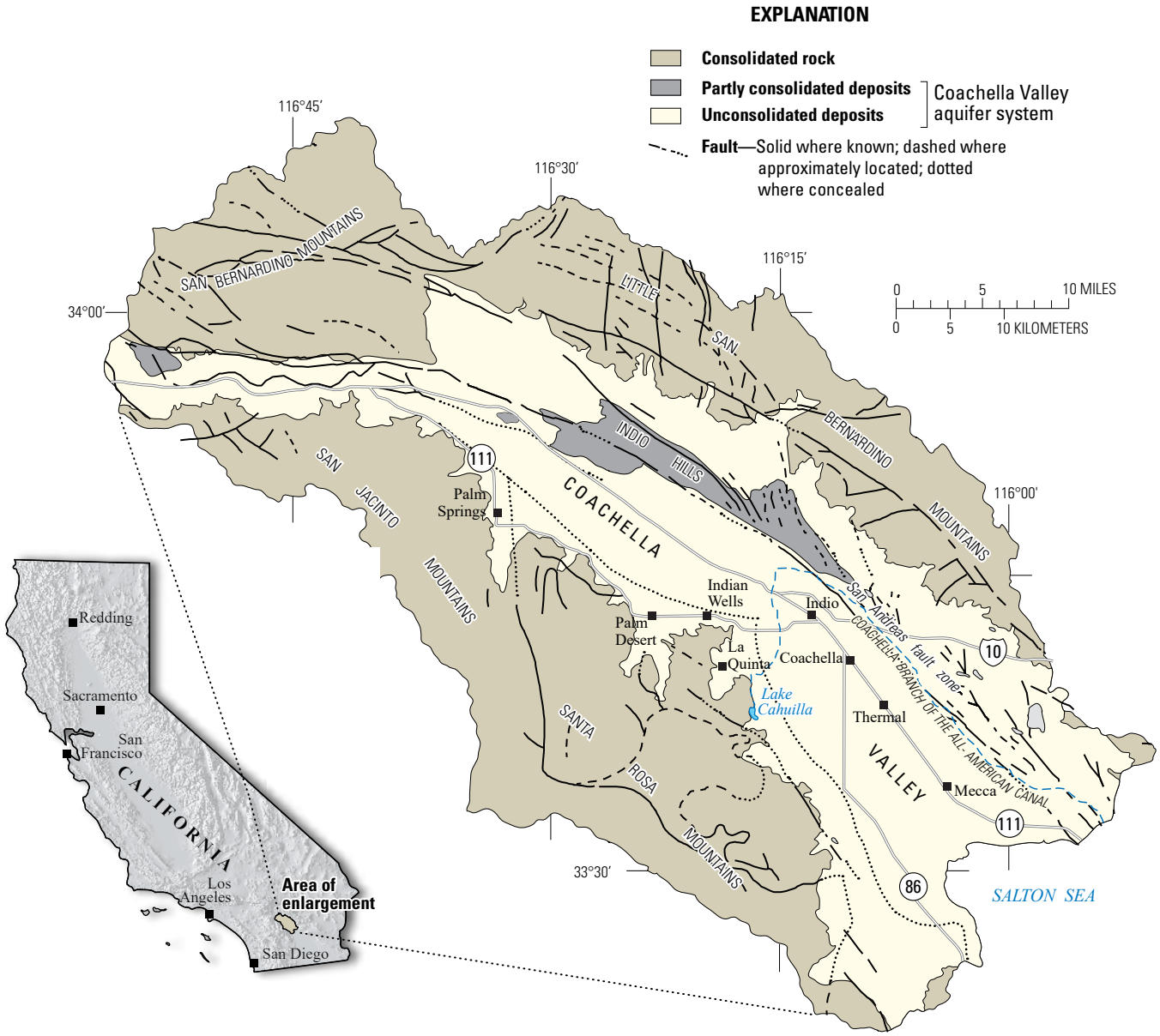

Figure 2. Generalized geology of the Coachella Valley, California. Figure modified from Tyley (1971).

Mechanics of Pumping-Induced Land Subsidence

Land can subside as a result of groundwater pumping in valleys containing aquifer systems that are, at least in part, made up of fine-grained sediment and that have undergone extensive groundwater development (Poland, 1984). The pore structure of a sedimentary aquifer system is supported by the granular skeleton of the aquifer system and the pore-fluid pressure of the groundwater that fills the intergranular pore space (Meinzer, 1928). When groundwater is withdrawn in quantities that result in reduced pore-fluid pressure and in groundwater-level decline, the reduction of the pore-fluid pressure support increases the intergranular stress, or effective stress, on the skeleton. An increase in effective stress compresses the skeleton. This deformation is sometimes inelastic (non-recoverable), resulting in vertical compaction of the aquifer system, a permanent reduction in aquifer-system storage capacity, and land subsidence. An aquifer-system skeleton that primarily consists of fine-grained sediments, such as silt and clay, is much more compressible than one that primarily consists of coarse-grained sediments, such as sand and gravel. Inelastic compaction of coarse-grained sediment generally is negligible (Ireland and others, 1984; Hanson, 1989; Sneed and Galloway, 2000).

Aquifer-system deformation can be elastic (recoverable) if the effective stress imposed on the skeleton is less than any previous maximum effective stress (Terzaghi, 1925). The greatest historical effective stress imposed on the aquifer system—sometimes the result of the lowest groundwater level—is the "preconsolidation stress," and the corresponding (lowest) groundwater level is the "preconsolidation head" (Leake and Prudic, 1991). If the effective stress does not exceed the preconsolidation stress, then the aquifer system undergoes elastic compression, which is recovered if water levels (pore-fluid pressures) subsequently increase. If the effective stress exceeds the preconsolidation stress, the pore structure of the granular matrix of the fine-grained sediment is rearranged; this new configuration results in a reduction of pore volume and, thus, inelastic compaction of the aquifer system. Furthermore, the compressibility of the fine-grained sediment constituting an aquitard, and any resulting compaction under stress exceeding the preconsolidation stress, is 20 to more than 100 times greater than under stress less than the preconsolidation stress (Riley, 1998).

This simple compaction model does not account for delayed drainage from low-permeability fine-grained sediment. For a developed aquifer system with an appreciable thickness of fine-grained sediment, a substantial part of the total compaction can be residual compaction (Sneed and Galloway, 2000). Residual compaction occurs in thick aquitards as heads in the thick aquitards equilibrate with heads in the surrounding aquifers (Terzaghi, 1925). Depending on the thickness and the vertical hydraulic diffusivity of a thick aquitard, fluid-pressure equilibration—and thus compaction—lags behind pressure (or hydraulic head) declines in the adjacent aquifers; associated compaction can require decades or centuries to approach completion. Thus, if the aquifer head declines below the previous lowest level for a relatively short period, the preconsolidation head in the aquitard is not necessarily reset to the new low value (Phillips and others, 2003). For a more complete description of aquifer-system compaction, see Poland (1984); for the history of the aquitard-drainage model, see Holzer's review (1998); and, for a review and selected case studies of land subsidence caused by aquifer-system compaction in the United States, see Galloway and others (1999).

Global Positioning System Surveys

A GPS survey uses a U.S. Department of Defense satellite-based navigation system designed to provide continuous worldwide positioning and navigation capability. For this study, GPS surveys were used to determine the three-dimensional position of monuments in the geodetic monitoring network. This network was established in 1996 by the USGS to measure changes in land-surface elevations at the monuments relative to the results of future surveys (Ikehara and others, 1997).

Land-Subsidence Monitoring Network

The geodetic monitoring network, henceforth referred to as the land-subsidence monitoring network, consists of geodetic monuments used as GPS stations (fig. 3). Most geodetic monuments consist of flat metal disks that are anchored in the ground or to a structure and can be surveyed repeatedly. During the 1996 study by Ikehara and others (1997), historical data for monuments in the southern Coachella Valley were compiled and reviewed to determine the location and the quality of the vertical-control data. Sources of the data included National Oceanic and Atmospheric Administration's National Geodetic Survey, the California Department of Transportation (Caltrans), the Bureau of Reclamation, and the CVWD (Ikehara and others, 1997).

The original subsidence monitoring network in the southern Coachella Valley was established in 1996 and consisted of 17 geodetic monuments. By 2010, the network consisted of 24 monuments as a result of monument replacements or additions during the 14-year period. The history of network modifications through 2010 is given in Sneed and others (2014). The network in 2015 was unchanged from the 2010 configuration (fig. 3). The spacing between the monuments met the generalized network-design criterion established by Zilkoski and others (1997), which requires that the distance between local network points not exceed 6 mi (10 km). The geodetic monuments were examined before each of the GPS surveys to determine if any had been damaged or destroyed and to evaluate their suitability for GPS observations.

Determination of Ellipsoid Heights

GPS measurements were taken at the geodetic monuments to determine their horizontal positions and ellipsoid heights. Ellipsoid height is the vertical distance above a geodetically defined reference ellipsoid; the ellipsoid that closely approximates the Earth's shape in the study area is the North American Datum of 1983 (NAD83). Differences in ellipsoid-height between successive GPS surveys were computed and represented land-surface elevation changes at the monuments. The GPS surveys generally followed established guidelines (Zilkoski and others, 1997), except that the data were processed with single-baseline, rather than multi-baseline, software. Software used for the baseline and least-squares adjustment computations for the 2010 survey was Trimble Geomatics Office, version 1.63. Software used for the baseline and least-squares adjustment computations for the 2015 survey was Trimble Business Center 2.81. The effects of, and compensations for, the use of single-baseline, rather than multi-baseline, software are given in Sneed and others (2014) and apply to this study as well. Other variations to the guidelines were specific to particular surveys and are described in following sections for the 2010 and 2015 surveys and in Sneed and others (2014) for older surveys.

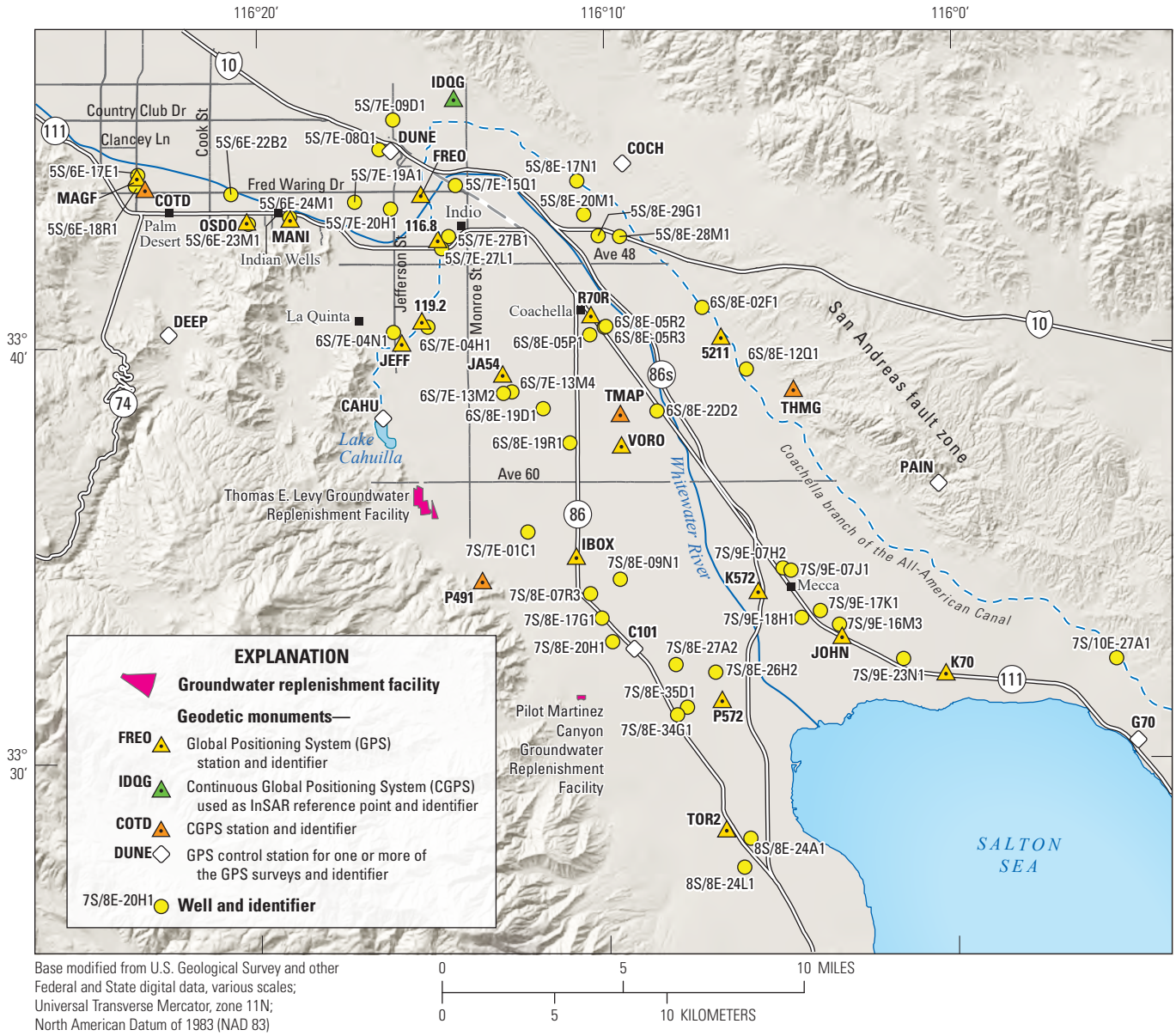

Figure 3. Network of Global Positioning System (GPS) stations and wells used to monitor changes in land-surface elevation and groundwater levels, respectively, in the Coachella Valley, California.

Global Positioning System Survey Methods, 2010 and 2015

The GPS measurements for the 2010 and 2015 surveys were acquired using 7 dual-frequency, full-wavelength, P-code GPS receivers (Topcon GB1000) and compact antennas with ground plane (Topcon PG-A1 Geodetic) at the 24 geodetic monuments between August 23 and 27, 2010, and between September 28 and October 2, 2015, to determine horizontal positions and ellipsoid heights. The GPS measurements were recorded at the monuments on at least 2 days during 1-hour observation periods. Of the 24 geodetic monuments, 7 were used as control stations: DUNE, COCH, DEEP, CAHU, PAIN, C101, and G70 (fig. 3). At these seven stations, GPS measurements were recorded an additional 3 days each during 6.5-hour (or longer) observation periods.

Determining the ellipsoid heights of the 24 geodetic monuments in the network involved 2 phases of least-squares adjustments. During the first phase of least-squares adjustments, horizontal coordinates and ellipsoid heights of the seven Coachella Valley control stations were determined by processing the GPS measurements taken at these monuments with simultaneous measurements at the same three continuous Global Positioning System (CGPS) stations (DHLG, PIN1, and WIDC; fig. 1) used in the 1998, 2000, and 2005 GPS surveys and by using precise satellite orbital data and accurate coordinates of the CGPS stations provided by the International GPS Service (IGS) and Scripps Orbit and Permanent Array Center (SOPAC), respectively. The measurements at the CGPS stations were recorded at 30-second intervals and archived by SOPAC. During the second phase of least-squares adjustments, the 7 control stations were fixed at the positions determined during the first phase, and the horizontal coordinates and ellipsoid heights for the other 17 monuments were calculated. The expected uncertainty of the ellipsoid heights for each survey was ±0.07 ft (±20 mm) at the 95-percent confidence level, which was determined using the maximum ellipsoid-height difference computed from 95 percent of the repeatedly observed baselines used in the adjustment. The expected uncertainty when comparing the results from the two surveys was computed by using the uncertainty for each of the surveys and applying the root sum of squares method. The resulting uncertainty was ±0.09 ft (±28 mm) for comparing the 2010 and 2015 survey results.

Global Positioning System Survey Results

For each of the GPS surveys, the horizontal coordinates and the ellipsoid heights of the monuments were compared to determine the magnitude of horizontal and vertical land-surface changes, respectively. The horizontal changes at the monuments were consistent with the northwest movement of the Pacific Plate with respect to the North American Plate (Shen and others, 2011). The monument ellipsoid heights and their changes with respect to the first GPS measurement at each monument are tabulated in table 1 and graphed as a function of time in figure 4; additionally, the monument ellipsoid-height changes for 1996–2015 and 2010–15 are tabulated in table 1 to provide both long- and short-term context.

Differences in calculated ellipsoid heights at the 11 geodetic monuments surveyed in 1996 and 2015 in the southern Coachella Valley indicate that the calculated ellipsoid heights at these monuments changed –0.36 to +0.03 ft (–111 to +10 mm; table 1; fig. 4). The maximum uncertainty expected for these calculated changes in ellipsoid heights was ±0.18 ft (±54 mm) at the 95-percent confidence level. Changes at 5 of the 11 monuments (DUNE, R70R, 5211, CAHU, and C101) exceeded this value, indicating confidence that the land surface subsided at these monuments between June 1996 and September 2015 (figs. 4*A*, 4*H*, 4*K*, 4*N*, 4*T*; table 1). Ellipsoid-height changes at 6 of the 11 monuments (COCH, PAIN, K572, JOHN, K70, and P572) did not exceed the maximum expected uncertainty, which indicates that the vertical positions of these monuments were similar in June 1996 and September 2015 (figs. 4*B*, 4*P*, 4*R*, 4*S*, 4*U*, 4*V*; table 1).

Differences in calculated ellipsoid heights at the 24 monuments surveyed in 2010 and 2015 indicate changes from –0.43 to +0.18 ft (–132 to +54 mm) during this 5-year period (table 1; fig. 4). The maximum uncertainty expected for these calculated changes in ellipsoid heights was ±0.09 ft (±28 mm) at the 95-percent confidence level. Changes between August 2010 and September 2015 at 7 of the 24 monuments (MAGF, OSDO, JEFF, K572, JOHN, P572, and TOR2) exceeded the maximum expected uncertainty, indicating that land surfaces subsided at 3 monuments (MAGF, OSDO, and JEFF; figs. 4*C*, 4*F*, 4*L*) and uplifted at 4 monuments (K572, JOHN, P572, and TOR2; figs. 4*R*, 4*S*, 4*V*, 4*X*). Between 2005 and 2010, MAGF and OSDO also subsided significantly; no data were available for JEFF for that period (Sneed and others, 2014). For 2010–15, OSDO subsided at the fastest rate at 0.09 foot per year (ft/yr), or 26 millimeters per year (mm/yr), followed by MAGF at 0.05 ft/yr, or 15 mm/yr, and JEFF at 0.03 ft/yr, or 10 mm/yr. The rates for OSDO and MAGF were about half of those calculated for the same monuments for 2005–10 (Sneed and others, 2014). For 2010–15, TOR2 uplifted the fastest at 0.04 ft/yr (11 mm/yr), followed by P572 at 0.03 ft/yr (10 mm/yr), K572 at 0.03 ft/yr (8 mm/yr), and JOHN at 0.02 ft/yr (6 mm/yr). Between 2005 and 2010, P572, K572, and JOHN were fairly stable; no data were available for TOR2 for that period. Ellipsoid-height changes at 17 of the 24 monuments (DUNE, COCH, FREO, MANI, 116.8, R70R, 119.2, DEEP, 5211, JA54, CAHU, VORO, PAIN, IBOX, C101, K70, and G70) did not exceed the maximum expected uncertainty, indicating land-surface elevations at these monuments were similar in August 2010 and September 2015 (figs. 4*A*, 4*B*, 4*D*, 4*E*, 4*G*–4*K*, 4*M*–4*Q*, 4*T*, 4*U*, 4*W*).

Table 1. Horizontal positions and ellipsoid heights of selected geodetic monuments in the Coachella Valley, California, for 1996, 1998, 2000, 2005, 2010, and 2015, and ellipsoid height changes relative to the first measurement for 1996–2015 and 2010–15.

[Latitude, longitude, and ellipsoid height are referenced to the North American Datum of 1983. Negative values for ellipsoid-height change indicate subsidence. **Abbreviations**: m, meter; mm, millimeter; GPS, global positioning system; ±, plus or minus; ft, foot; —, no data]

GPS station	Monument name	Latitude	Longitude	Ellipsoid height (m)						Ellipsoid-height change from 1st measurement (mm)					
				1996 (±0.05 m)	1998 (±0.02 m)	2000 (±0.03 m)	2005 (±0.02 m)	2010 (±0.02 m)	2015 (±0.02 m)	1996	1998	2000	2005	2010	2015
DUNE	DUNEPORT Azimuth	33°44'46”	116°16'10”	–17.354	–17.371	–17.407	–17.436	–17.461	–17.449	0	–17	–53	–82	–107	–95
COCH	COACH 1931	33°44'25”	116°09'30”	33.427	33.436	33.367	33.418	33.402	33.410	0	9	–60	–9	–25	–17
MAGF	Magnesium Falls Drive	33°44'11”	116°23'27”	—	—	27.742	27.604	27.446	27.373	—	—	0	–138	–296	–369
FREO	Fred Waring and Canal	33°43'44”	116°15'17”	—	—	—	—	–22.609	–22.582	—	—	—	—	0	27
MANI	Manitou Drive	33°43'11”	116°19'03”	—	—	2.962	2.916	2.871	2.847	—	—	0	–46	–91	–116
OSDO	Osage Trail and El Dorado Drive	33°43'06”	116°20'19”	—	—	13.484	13.292	13.036	12.904	—	—	0	–192	–448	–580
116.8	116.8 Canal Check Structure	33°42'40”	116°14'50”	—	—	—	—	–24.296	–24.280	—	—	—	—	0	16
R70R	R70 Reset 1958	33°40'49”	116°10'26”	–54.402	–54.433	–54.471	–54.509	–54.538	–54.512	0	–31	–69	–107	–136	–110
119.2	119.2 Canal Check Structure	33°40'42”	116°15'18”	—	—	—	—	–25.400	–25.406	—	—	—	—	0	–6
DEEP	Deep Canyon	33°40'21”	116°22'34”	—	—	190.409	190.402	190.398	190.399	—	—	0	–7	–11	–10
5211	USBR 52.11	33°40'17”	116°06'43”	–32.682	–32.698	–32.740	–32.737	–32.735	–32.754	0	–16	–58	–55	–53	–72
JEFF	Jefferson and Canal	33°40'10”	116°15'52”	—	—	—	—	–25.693	–25.745	—	—	—	—	0	–52
JA54	Jackson and Ave 54	33°39'24”	116°13'00”	—	—	–46.907	–46.991	–47.066	–47.046	—	—	0	–84	–159	–139
CAHU	Lake Cahuilla	33°38'19”	116°16'25”	–30.738	–30.778	–30.815	–30.822	–30.806	–30.826	0	–40	–77	–84	–68	–88
VORO	VORO	33°37'41”	116°09'35”	—	—	—	—	–71.333	–71.337	—	—	—	—	0	–4
PAIN	Painted Canyon	33°36'43”	116°00'30”	93.365	93.352	93.318	93.343	93.332	93.327	0	–13	–47	–22	–33	–38
IBOX	Irrigation Box 2010	33°35'01”	116°10'55”	—	—	—	—	–73.946	–73.948	—	—	—	—	0	–2
K572	K572 1939	33°34'09”	116°05'42”	–91.484	–91.515	–91.523	–91.540	–91.541	–91.500	0	–31	–39	–56	–57	–16
JOHN	Johnson	33°33'03”	116°03'18”	–94.146	–94.158	–94.170	–94.184	–94.169	–94.136	0	–12	–24	–38	–23	10
C101	Caltrans 10.1 1986	33°32'44”	116°09'16”	–50.336	–50.396	–50.419	–50.443	–50.453	–50.447	0	–60	–83	–107	–117	–111
K70	K70 1928	33°32'09”	116°00'21”	–91.483	–91.507	–91.536	–91.525	–91.515	–91.490	0	–24	–53	–42	–32	–7
P572	P572 1939	33°31'32”	116°06'46”	–91.233	–91.259	–91.283	–91.311	–91.295	–91.246	0	–26	–50	–78	–62	–13
G70	G70 1928	33°30'27”	115°54'51”	—	–93.078	–93.111	–93.098	–93.103	–93.088	—	0	–33	–20	–25	–10
TOR2	TORRO2 RM NO 4 1979	33°28'25”	116°06'39”	—	—	—	—	–67.205	–67.151	—	—	—	—	0	54

Table 1. Horizontal positions and ellipsoid heights of selected geodetic monuments in the Coachella Valley, California, for 1996, 1998, 2000, 2005, 2010, and 2015, and ellipsoid height changes relative to the first measurement for 1996–2015 and 2010–15.—Continued

[Latitude, longitude, and ellipsoid height are referenced to the North American Datum of 1983. Negative values for ellipsoid-height change indicate subsidence. **Abbreviations**: m, meter; mm, millimeter; GPS, global positioning system; ±, plus or minus; ft, foot; —, no data]

GPS station	Monument name	Latitude	Longitude	Ellipsoid-height change from 1st measurement (ft)						Ellipsoid-height change for selected periods			
										1996–2015		2010–15	
				1996	1998	2000	2005	2010	2015	mm, ±54 mm	ft, ±0.18 ft	mm, ±28 mm	ft, ±0.09 ft
DUNE	DUNEPORT Azimuth	33°44'46”	116°16'10”	0.000	–0.056	–0.174	–0.269	–0.351	–0.310	–95	–0.31	12	0.04
COCH	COACH 1931	33°44'25”	116°09'30”	0.000	0.030	–0.197	–0.030	–0.082	–0.054	–17	–0.05	8	0.03
MAGF	Magnesium Falls Drive	33°44'11”	116°23'27”	—	—	0.000	–0.453	–0.971	–1.212	—	—	–73	–0.24
FREO	Fred Waring and Canal	33°43'44”	116°15'17”	—	—	—	—	0.000	0.089	—	—	27	0.09
MANI	Manitou Drive	33°43'11”	116°19'03”	—	—	0.000	–0.151	–0.299	–0.379	—	—	–25	–0.08
OSDO	Osage Trail and El Dorado Drive	33°43'06”	116°20'19”	—	—	0.000	–0.630	–1.470	–1.902	—	—	–132	–0.43
116.8	116.8 Canal Check Structure	33°42'40”	116°14'50”	—	—	—	—	0.000	0.052	—	—	16	0.05
R70R	R70 Reset 1958	33°40'49”	116°10'26”	0.000	–0.102	–0.226	–0.351	–0.446	–0.361	–110	–0.36	26	0.09
119.2	119.2 Canal Check Structure	33°40'42”	116°15'18”	—	—	—	—	0.000	–0.018	—	—	–6	–0.02
DEEP	Deep Canyon	33°40'21”	116°22'34”	—	—	0.000	–0.023	–0.036	–0.033	—	—	1	0.00
5211	USBR 52.11	33°40'17”	116°06'43”	0.000	–0.052	–0.190	–0.180	–0.174	–0.238	–72	–0.24	–19	–0.06
JEFF	Jefferson and Canal	33°40'10”	116°15'52”	—	—	—	—	0.000	–0.172	—	—	–52	–0.17
JA54	Jackson and Ave 54	33°39'24”	116°13'00”	—	—	0.000	–0.276	–0.522	–0.456	—	—	20	0.07
CAHU	Lake Cahuilla	33°38'19”	116°16'25”	0.000	–0.131	–0.253	–0.276	–0.223	–0.290	–88	–0.29	–20	–0.07
VORO	VORO	33°37'41”	116°09'35”	—	—	—	—	0.000	–0.014	—	—	–4	–0.01
PAIN	Painted Canyon	33°36'43”	116°00'30”	0.000	–0.043	–0.154	–0.072	–0.108	–0.124	–38	–0.12	–5	–0.02
IBOX	Irrigation Box 2010	33°35'01”	116°10'55”	—	—	—	—	0.000	–0.007	—	—	–2	–0.01
K572	K572 1939	33°34'09”	116°05'42”	0.000	–0.102	–0.128	–0.184	–0.187	–0.052	–16	–0.05	41	0.14
JOHN	Johnson	33°33'03”	116°03'18”	0.000	–0.039	–0.079	–0.125	–0.075	0.032	10	0.03	33	0.11
C101	Caltrans 10.1 1986	33°32'44”	116°09'16”	0.000	–0.197	–0.272	–0.352	–0.384	–0.363	–111	–0.36	6	0.02
K70	K70 1928	33°32'09”	116°00'21”	0.000	–0.079	–0.174	–0.138	–0.105	–0.023	–7	–0.02	25	0.08
P572	P572 1939	33°31'32”	116°06'46”	0.000	–0.085	–0.164	–0.256	–0.203	–0.042	–13	–0.04	49	0.16
G70	G70 1928	33°30'27”	115°54'51”	—	0.000	–0.108	–0.066	–0.082	–0.032	—	—	15	0.05
TOR2	TORRO2 RM NO 4 1979	33°28'25”	116°06'39”	—	—	—	—	0.000	0.177	—	—	54	0.18

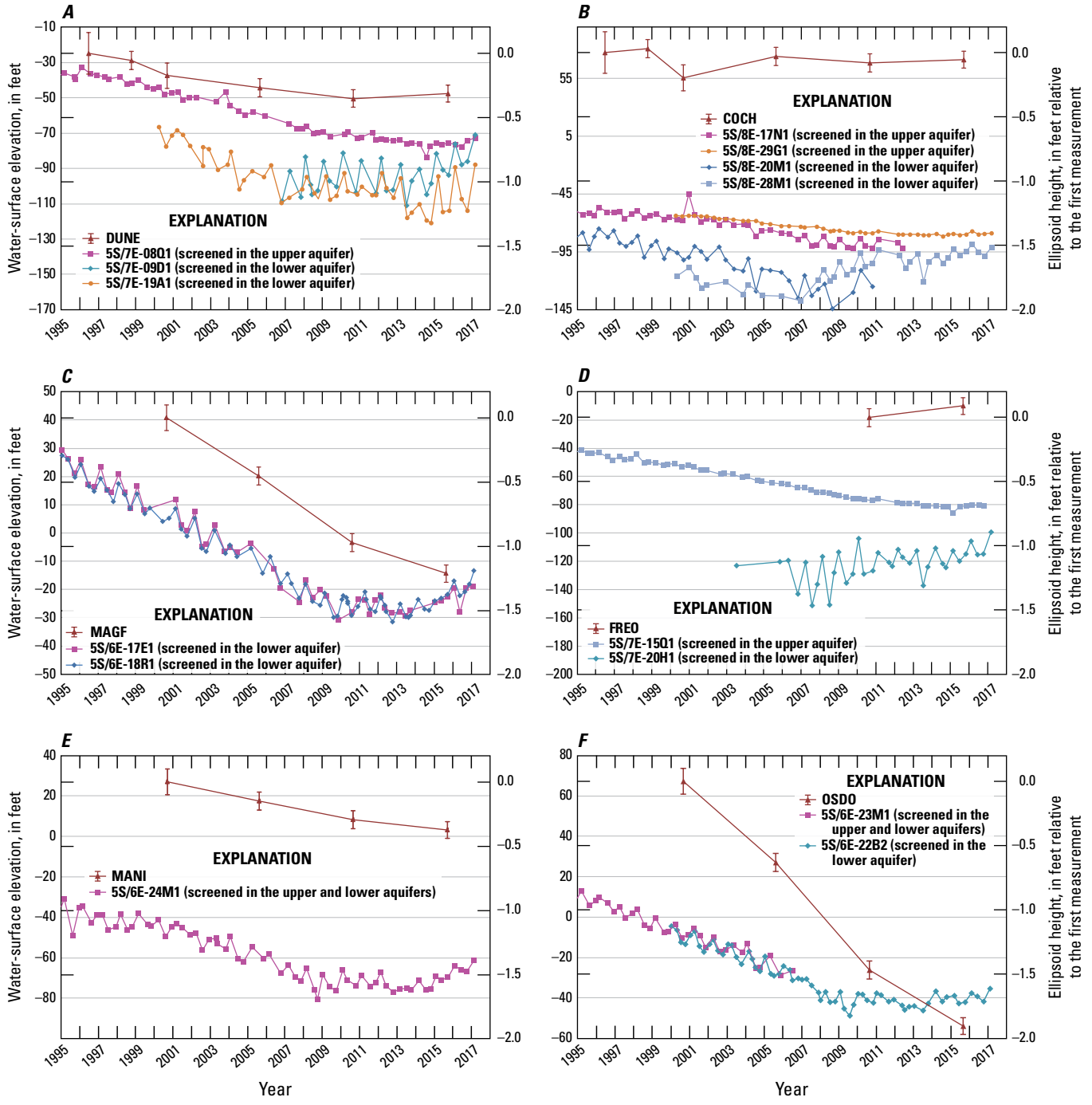

Figure 4. Ellipsoid-height changes relative to the first measurement for selected geodetic monuments in the Coachella Valley, California, and water-surface elevations for selected nearby wells, 1995–2017: *A*, DUNE; *B*, COCH; *C*, MAGF; *D*, FREO; *E*, MANI; *F*, OSDO; *G*, 116.8; *H*, R70R; *I*, 119.2; *J*, DEEP; *K*, 5211; *L*, JEFF; *M*, JA54; *N*, CAHU; *O*, VORO; *P*, PAIN; *Q*, IBOX; *R*, K572; *S*, JOHN; *T*, C101; *U*, K70; *V*, P572; *W*, G70; and, *X*, TOR2. (See figure 3 for locations of wells and geodetic monuments. Note, the scale for water-surface elevations varies among the graphs. Water-surface elevation data are referenced to the National Geodetic Vertical Datum of 1929 and were provided by the Coachella Valley Water District.)

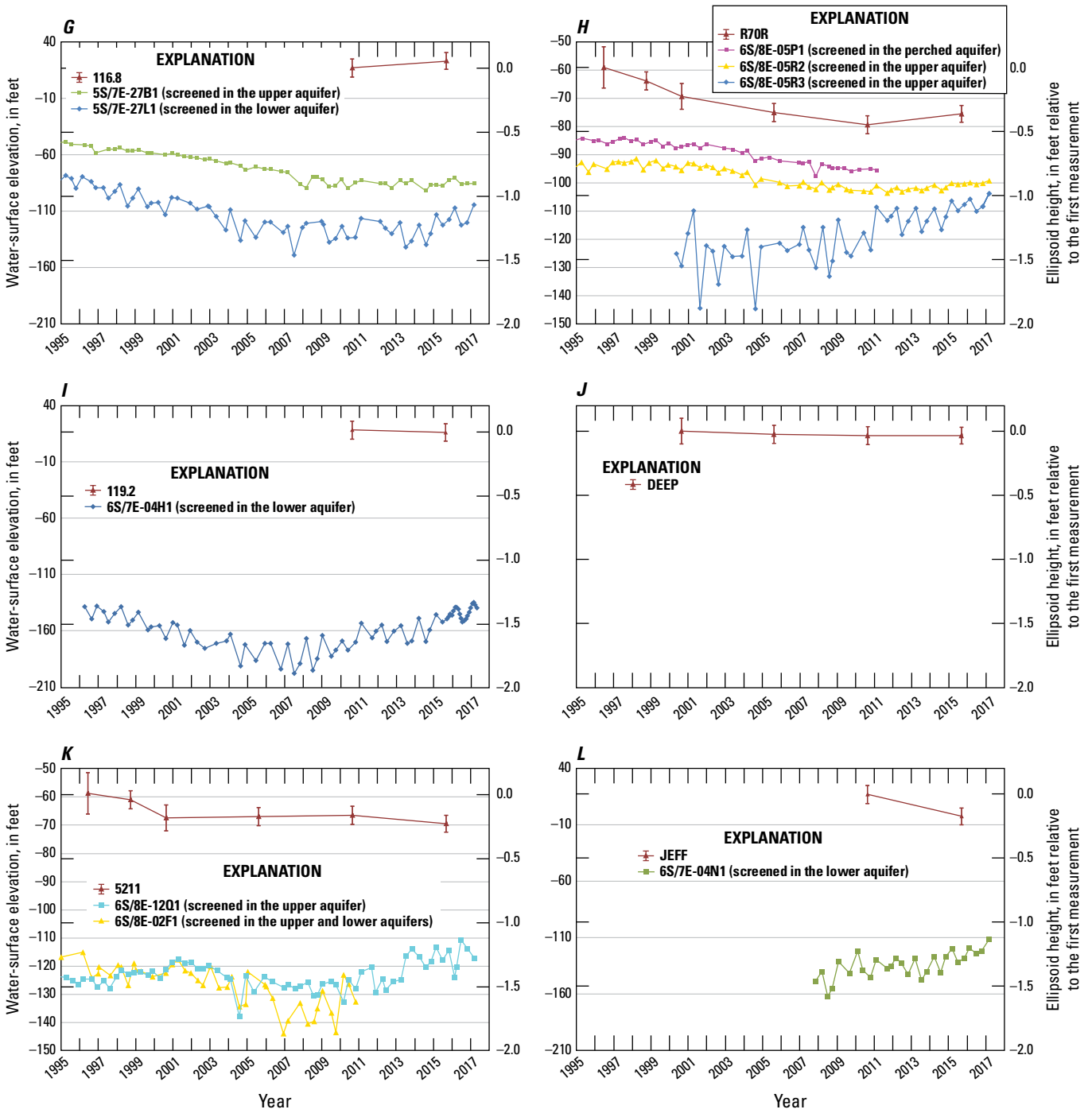

Figure 4. —Continued

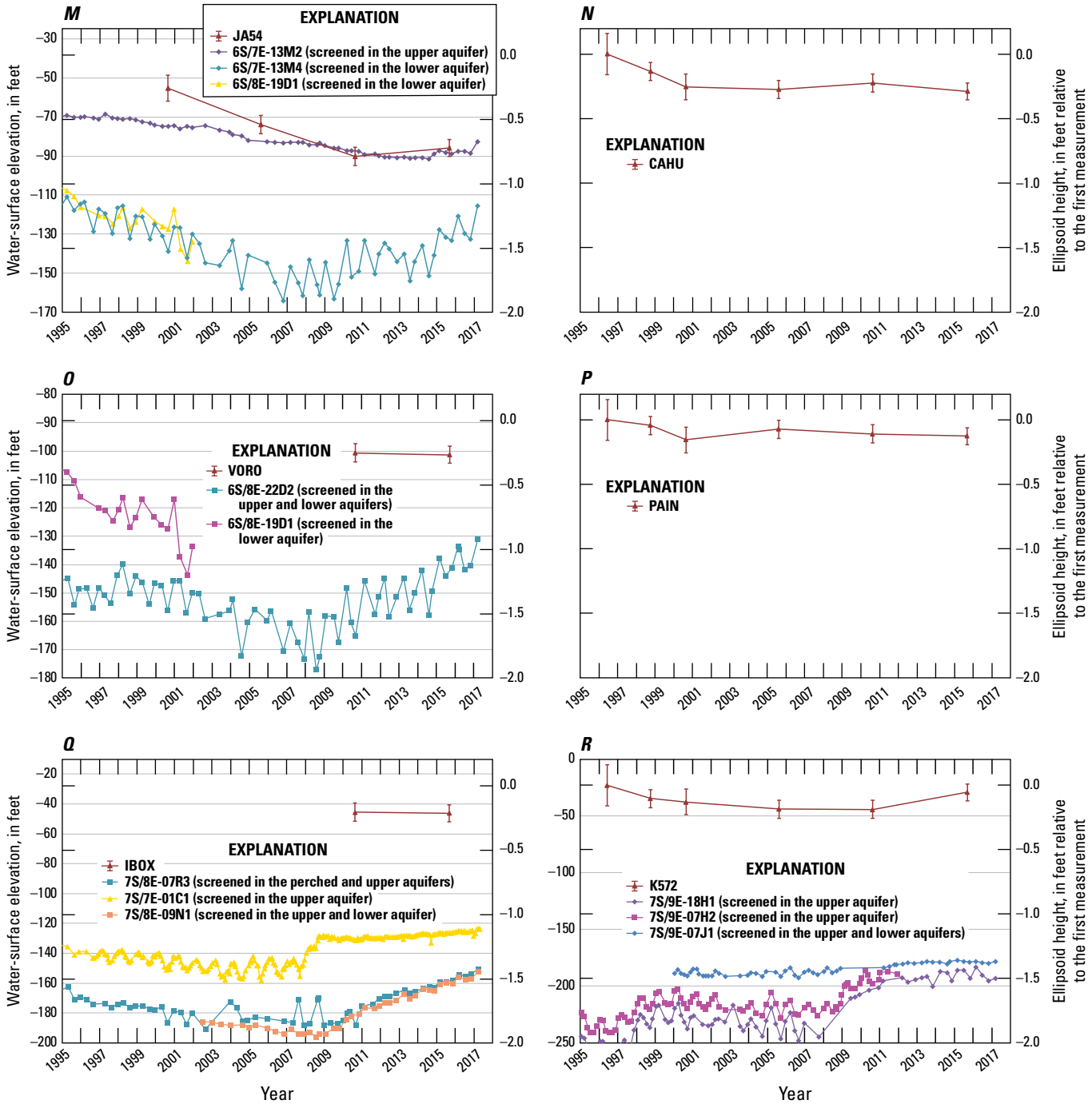

Figure 4. —Continued

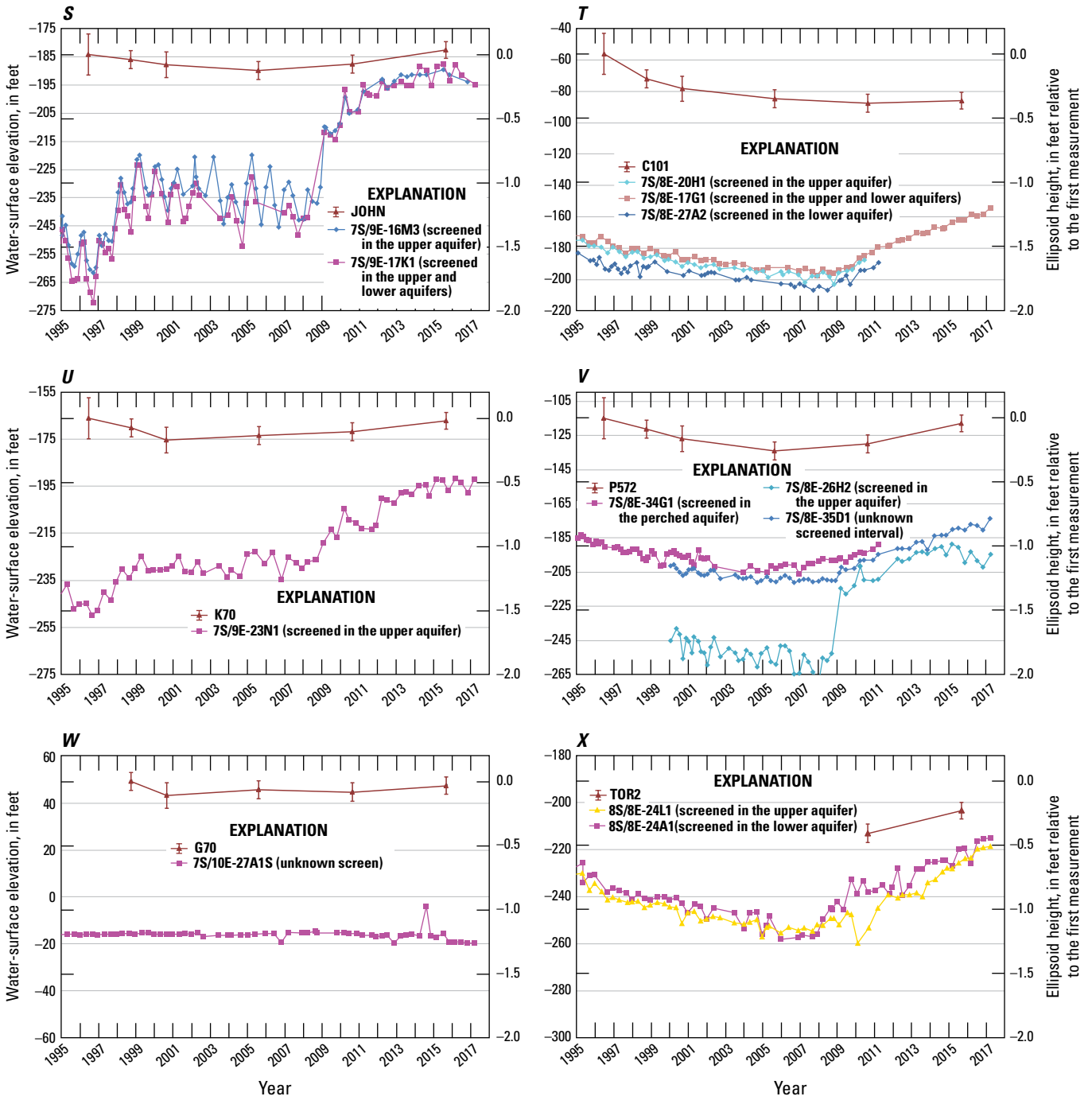

Figure 4. —Continued

Interferometric Synthetic Aperture Radar (InSAR)

The next two sections of this report describe InSAR methodology and results. A third section describes the comparison of subsidence magnitudes derived from GPS and InSAR measurements at selected GPS stations.

Interferometric Synthetic Aperture Radar Methodology

InSAR is a satellite-based, remote-sensing technique that can detect sub-inch land-surface deformation over hundreds of square miles at a spatial resolution (pixel size) of 295 ft (90 m) or better (Bawden and others, 2003). Synthetic aperture radar (SAR) imagery is produced by reflecting radar signals off a target area and measuring the two-way travel time back to the satellite. InSAR uses two SAR scenes of the same area taken at different times and "interferes" (differences) them, resulting in maps called interferograms that show relative ground-elevation change (range change) between the two times. The SAR imagery has two components: amplitude and phase. The amplitude is the radar signal intensity returned to the satellite and depends on the varying reflective properties that delineate features of the landscape such as roads, mountains, structures, and others. The phase component is proportional to the line-of-sight distance from the ground to the satellite (range) and is the component used to measure land-surface displacement (subsidence or uplift). If the ground has moved away from the satellite (subsidence), a more distal phase portion of the waveform is reflected back to the satellite. Conversely, if the ground has moved closer to the satellite (uplift), a more proximal phase portion of the waveform is reflected back to the satellite. The phase difference, or shift, between the two SAR images is then calculated for each pixel. The map of phase shifts, or interferogram, can be depicted with a color scale that shows relative range change between the first and the second SAR acquisitions. Data from two SAR satellites were utilized for this study; the European Space Agency's (ESA) Sentinel-1A (C-band radar signal) and the German Aerospace Center's (DLR) TerraSAR-X (X-band radar signal).

Interferogram quality depends partly on satellite position, atmospheric conditions, ground cover, land-use practices, and timespan of the interferogram. Strict orbital control is required to precisely control the look angle and position of the satellite. Successful application of the InSAR technique is contingent on looking at the same point on the ground from nearly the same position in space so that the horizontal distance between each satellite pass, or perpendicular baseline, is minimized. Perpendicular baselines greater than about 656 ft (200 m) can produce excessive topographic effects (parallax) that can mask range changes. The relatively flat topography of the study area allowed inclusion of SAR image pairs with perpendicular baselines as long as about 920 ft (280 m) without adversely affecting the interferograms.

The principal sources of error in the InSAR method applied to the Coachella Valley result from atmospheric artifacts and agricultural land-use practices (related to ground cover), both of which have deleterious effects on interferograms. Atmospheric artifacts are caused by non-uniform atmospheric water vapor associated with either variable land-surface elevation (higher elevations have less atmosphere) or clouds and fog; water vapor slows the radar signal, causing a phase shift that can lead to erroneous deformation interpretations (Zebker and others, 1997). A digital elevation model (DEM) is used in the interferogram generation process to reduce the topographic effects caused by elevation differences and to georeference the image. Agricultural land-use practices, including the tilling or flooding of farm fields, cause large and non-uniform changes in the amplitude and phase components of radar signals reflected back to the satellite. The non-uniform phase changes can result in spatially decorrelated signals (shown as randomly colored pixels on an interferogram) that cannot be interpreted. Interferograms spanning long periods (generally two or more years) often have poor signal quality because more non-uniform change is likely to have occurred in both urban and non-urban areas (Sneed and others, 2013).

Atmospheric artifacts can be identified by analyzing independent interferograms and can be removed by stacking interferograms. Time-span dependent errors also can be reduced by stacking interferograms. The term "independent interferograms" refers to two or more interferograms that do not share a common SAR image. When apparent ground movement is detected in a single interferogram, or in a set of interferograms that share a common SAR image, then the apparent movement is likely an artifact of atmospheric phase delay or another error source within the common SAR image. When the pixel-by-pixel range displacements of two or more interferograms are summed to create a "stacked interferogram," a cloud in one particular SAR image may not affect the total displacement measured by the stacked interferogram. For example, when two interferograms are generated from three SAR images, the area with a cloud in the common SAR image appears to have increased range (apparent subsidence) in the first interferogram and decreased range (apparent uplift) in the second interferogram. When these two interferograms are added (stacked) together, the equal and opposite apparent deformation is cancelled out, effectively removing the phase change caused by the cloud. Stacking also is beneficial for reducing time-span dependent errors. Stacking two or more interferograms that span shorter periods, which have less timespan-dependent errors, can result in more spatially correlated, longer term interferograms.

The type and density of ground cover also can substantially affect interferogram quality. Densely forested areas are poor reflectors because the typically short wavelengths used in SAR transmitters (C-band has a wavelength of 0.18 ft or 56 mm; X-band has a wavelength of 0.10 ft or 31 mm) are either absorbed or reflected from various canopy depths, resulting in decorrelated signals. In contrast, sparsely vegetated areas and urban centers generally reflect correlated signals because bare ground, roads, and buildings have consistently uniform surfaces. Certain land-use practices, such as the farming, which is prevalent in the southern Coachella Valley, cause decorrelation both in the phase and amplitude components of interferograms because the tilling of farm fields causes relatively large and nonuniform land-surface changes. The Coachella Valley generally is suitable for InSAR analysis because it is fairly flat and arid, and it contains several urban centers; therefore, most of the aforementioned sources of error are not substantial or can be mitigated using the techniques described previously, such as stacking. The short interval between repeat orbital tracks of the Sentinel-1A satellite, as little as 12 days, allowed for the production of interferograms with moderately high spatial correlation in the agriculturally active areas of the southern Coachella Valley; however, data gaps owing to poor spatial correlation were still common in nearly all interferograms.

Post-processing techniques, including image smoothing, image unwrapping, and ordinary kriging, were used to maximize data quality and interpretability of the interferograms. Image smoothing was used in cases where interferograms containing spatially decorrelated areas prevented reliable interpretation at these locations. Computer algorithms were used to adjust the image according to the average phase value of surrounding pixels, thereby reducing noise and increasing spatial correlation (Goldstein and Werner, 1998). Conservative application of smoothing algorithms can be used to avoid over-smoothing an interferogram. Over-smoothing an interferogram can result in the removal of small scale deformation features or local maxima and minima or in the creation of false signals in areas of very low spatial correlation, because successively averaging a set of random pixels inevitably leads to a well correlated set of pixel values that likely are not reliable data points. For this study, smoothing was applied conservatively to facilitate successful unwrapping of each image.

In order to successfully stack and extract range (and ultimately elevation) change information from InSAR data, raw interferograms are unwrapped. Because raw interferograms only contain data values that repeat modulo 2π (when a series of pixels indicate an increasing phase change, the value "wraps" from 2π back to zero), the phase change values are "unwrapped" starting at, and relative to, a selected reference pixel and converted to millimeters of range change. An ideal reference pixel is where the land-surface elevation was stable during the period of the SAR data used and where spatial correlation in the pixel vicinity was quite good. More generally, better spatial correlation of an interferogram results in a higher percentage of the image being unwrapped. If a set of well-correlated pixels are surrounded by poorly correlated pixels, the magnitude of range change across that poorly correlated area cannot be reliably determined.

Following unwrapping, the interferograms were kriged using default parameters for ordinary kriging in ArcMap software to enable range-change interpretations at any location in the image. Each interferogram had different areas of spatial decorrelation, resulting in null values at different locations in the interferograms. The kriging replaced null values with the statistically derived values, resulting in homogenized interferograms with range-change values at every location. Finally, the values of range change were converted to vertical change using the radar look-angle properties, which could then be stacked and interpreted for land-surface elevation change at any location.

The TerraSAR-X satellite began collecting SAR data over the Coachella Valley in April 2009. The Sentinel-1A satellite began collecting SAR data over the Coachella Valley during November 2014. A total of 53 SAR images (16 TerraSAR-X and 37 Sentinel-1A) acquired between April 9, 2009, and July 21, 2017, were processed using the previously described InSAR techniques into 154 interferograms (47 TerraSAR-X and 107 Sentinel-1A; table 2). Of these, 2 TerraSAR-X and 22 Sentinel-1A interferograms from between July 28, 2009, and June 27, 2017, were used for analysis and for the construction of time series at selected locations. These 24 interferograms were selected because of their quality, the time span represented, and time span length, which ranged from 12 days to 528 days (table 2). TerraSAR-X data cover most of the southern Coachella Valley, but none of the northern Coachella Valley (for example, appendix fig. 1.1); whereas Sentinel-1A data cover nearly all of the Coachella Valley (for example, appendix fig. 1.3). The time series for locations within the TerraSAR-X coverage contain two data gaps: from May 16, 2012, to December 28, 2014 (956 days, or about 2.6 years), and from February 27, 2017, to May 22, 2017 (84 days, or nearly 3 months). Locations outside the TerraSAR-X coverage contain only the latter data gap. These data gaps represent periods when SAR data were not collected, were not available through the DLR research proposal (GEO1609), or were not suitable for analysis for the study area. The magnitudes of any surface deformation that may have occurred during these gaps were not estimated.

Table 2. Interferograms interpreted for the Coachella Valley, California, 2009–17.

[mm/dd/yyyy, month/day/year; SAR, synthetic aperture radar; —, not applicable]

New index number	Satellite, track, and for TerraSAR-X only, strip	1st SAR acquisition (mm/dd/yyyy)	2nd SAR acquisition (mm/dd/yyyy)	Time span of SAR pair, in days	Appendix figure number
1	TerraSAR-X, Track 68, Strip 9	04/09/2009	05/23/2009	44	—
2	TerraSAR-X, Track 68, Strip 9	04/09/2009	06/25/2009	77	—
3	TerraSAR-X, Track 68, Strip 9	04/09/2009	07/06/2009	88	—
4	TerraSAR-X, Track 68, Strip 9	04/09/2009	07/28/2009	110	—
5	TerraSAR-X, Track 68, Strip 9	04/09/2009	01/07/2011	638	—
6	TerraSAR-X, Track 68, Strip 9	04/09/2009	02/18/2012	1,045	—
7	TerraSAR-X, Track 68, Strip 9	04/09/2009	04/02/2012	1,089	—
8	TerraSAR-X, Track 68, Strip 9	04/09/2009	05/16/2012	1,133	—
9	TerraSAR-X, Track 68, Strip 9	05/23/2009	06/25/2009	33	—
10	TerraSAR-X, Track 68, Strip 9	05/23/2009	07/06/2009	44	—
11	TerraSAR-X, Track 68, Strip 9	05/23/2009	07/28/2009	66	—
12	TerraSAR-X, Track 68, Strip 9	05/23/2009	01/07/2011	594	—
13	TerraSAR-X, Track 68, Strip 9	05/23/2009	02/18/2012	1,001	—
14	TerraSAR-X, Track 68, Strip 9	05/23/2009	04/02/2012	1,045	—
15	TerraSAR-X, Track 68, Strip 9	05/23/2009	05/16/2012	1,089	—
16	TerraSAR-X, Track 68, Strip 9	06/25/2009	07/06/2009	11	—
17	TerraSAR-X, Track 68, Strip 9	06/25/2009	07/28/2009	33	—
18	TerraSAR-X, Track 68, Strip 9	06/25/2009	01/07/2011	561	—
19	TerraSAR-X, Track 68, Strip 9	06/25/2009	02/18/2012	968	—
20	TerraSAR-X, Track 68, Strip 9	06/25/2009	04/02/2012	1,012	—
21	TerraSAR-X, Track 68, Strip 9	06/25/2009	05/16/2012	1,056	—
22	TerraSAR-X, Track 68, Strip 9	07/06/2009	07/28/2009	22	—
23	TerraSAR-X, Track 68, Strip 9	07/06/2009	01/07/2011	550	—
24	TerraSAR-X, Track 68, Strip 9	07/06/2009	02/18/2012	957	—
25	TerraSAR-X, Track 68, Strip 9	07/06/2009	04/02/2012	1,001	—
26	TerraSAR-X, Track 68, Strip 9	07/06/2009	05/16/2012	1,045	—
27*	TerraSAR-X, Track 68, Strip 9	07/28/2009	01/07/2011	528	1.1
28	TerraSAR-X, Track 68, Strip 9	07/28/2009	02/18/2012	935	—
29	TerraSAR-X, Track 68, Strip 9	07/28/2009	04/02/2012	979	—
30	TerraSAR-X, Track 68, Strip 9	07/28/2009	05/16/2012	1,023	—
31	TerraSAR-X, Track 68, Strip 9	01/07/2011	02/18/2012	407	—
32	TerraSAR-X, Track 68, Strip 9	01/07/2011	04/02/2012	451	—
33*	TerraSAR-X, Track 68, Strip 9	01/07/2011	05/16/2012	495	1.2
34	TerraSAR-X, Track 68, Strip 9	02/18/2012	04/02/2012	44	—
35	TerraSAR-X, Track 68, Strip 9	02/18/2012	05/16/2012	88	—
36	TerraSAR-X, Track 68, Strip 9	04/02/2012	05/16/2012	44	—
37	TerraSAR-X, Track91, Strip 11	04/29/2011	06/01/2011	33	—
38	TerraSAR-X, Track91, Strip 11	04/29/2011	01/18/2012	264	—
39	TerraSAR-X, Track91, Strip 11	04/29/2011	05/07/2012	374	—
40	TerraSAR-X, Track91, Strip 11	04/29/2011	08/03/2012	462	—
41	TerraSAR-X, Track91, Strip 11	06/01/2011	01/18/2012	231	—

Table 2. Interferograms interpreted for the Coachella Valley, California, 2009–17.—Continued

[mm/dd/yyyy, month/day/year; SAR, synthetic aperture radar; —, not applicable]

New index number	Satellite, track, and for TerraSAR-X only, strip	1st SAR acquisition (mm/dd/yyyy)	2nd SAR acquisition (mm/dd/yyyy)	Time span of SAR pair, in days	Appendix figure number
42	TerraSAR-X, Track91, Strip 11	06/01/2011	05/07/2012	341	—
43	TerraSAR-X, Track91, Strip 11	06/01/2011	08/03/2012	429	—
44	TerraSAR-X, Track91, Strip 11	01/18/2012	05/07/2012	110	—
45	TerraSAR-X, Track91, Strip 11	01/18/2012	08/03/2012	198	—
46	TerraSAR-X, Track91, Strip 11	05/07/2012	08/03/2012	88	—
47	TerraSAR-X, Track91, Strip 12	07/23/2012	06/18/2013	330	—
48	Sentinel-1A, Track 173	11/10/2014	12/04/2014	24	—
49	Sentinel-1A, Track 173	11/10/2014	01/21/2015	72	—
50	Sentinel-1A, Track 173	12/04/2014	12/28/2014	24	—
51	Sentinel-1A, Track 173	12/04/2014	01/21/2015	48	—
52	Sentinel-1A, Track 173	12/04/2014	02/14/2015	72	—
53	Sentinel-1A, Track 173	12/04/2014	03/10/2015	96	—
54*[1]	Sentinel-1A, Track 173	12/28/2014	01/21/2015	24	1.3
55	Sentinel-1A, Track 173	12/28/2014	02/14/2015	48	—
56	Sentinel-1A, Track 173	12/28/2014	03/10/2015	72	—
57	Sentinel-1A, Track 173	12/28/2014	04/03/2015	96	—
58*[1]	Sentinel-1A, Track 173	01/21/2015	02/14/2015	24	1.4
59	Sentinel-1A, Track 173	01/21/2015	03/10/2015	48	—
60	Sentinel-1A, Track 173	01/21/2015	04/03/2015	72	—
61	Sentinel-1A, Track 173	01/21/2015	04/27/2015	96	—
62*	Sentinel-1A, Track 173	02/14/2015	03/10/2015	24	1.5
63	Sentinel-1A, Track 173	02/14/2015	04/27/2015	72	—
64*	Sentinel-1A, Track 173	03/10/2015	04/03/2015	24	1.6
65	Sentinel-1A, Track 173	03/10/2015	04/27/2015	48	—
66	Sentinel-1A, Track 173	03/10/2015	05/21/2015	72	—
67	Sentinel-1A, Track 173	03/10/2015	06/14/2015	96	—
68*[2]	Sentinel-1A, Track 173	04/03/2015	04/27/2015	24	1.7
69	Sentinel-1A, Track 173	04/03/2015	05/21/2015	48	—
70	Sentinel-1A, Track 173	04/03/2015	06/14/2015	72	—
71	Sentinel-1A, Track 173	04/03/2015	07/08/2015	96	—
72*[2]	Sentinel-1A, Track 173	04/27/2015	05/21/2015	24	1.8
73	Sentinel-1A, Track 173	04/27/2015	06/14/2015	48	—
74	Sentinel-1A, Track 173	04/27/2015	07/08/2015	72	—
75	Sentinel-1A, Track 173	04/27/2015	08/01/2015	96	—
76*	Sentinel-1A, Track 173	05/21/2015	06/14/2015	24	1.9
77	Sentinel-1A, Track 173	05/21/2015	07/08/2015	48	—
78	Sentinel-1A, Track 173	05/21/2015	08/01/2015	72	—
79	Sentinel-1A, Track 173	05/21/2015	08/25/2015	96	—
80*	Sentinel-1A, Track 173	06/14/2015	07/08/2015	24	1.10
81	Sentinel-1A, Track 173	06/14/2015	08/01/2015	48	—
82	Sentinel-1A, Track 173	06/14/2015	08/25/2015	72	—

Table 2. Interferograms interpreted for the Coachella Valley, California, 2009–17.—Continued

[mm/dd/yyyy, month/day/year; SAR, synthetic aperture radar; —, not applicable]

New index number	Satellite, track, and for TerraSAR-X only, strip	1st SAR acquisition (mm/dd/yyyy)	2nd SAR acquisition (mm/dd/yyyy)	Time span of SAR pair, in days	Appendix figure number
83	Sentinel-1A, Track 173	06/14/2015	09/18/2015	96	—
84*	Sentinel-1A, Track 173	07/08/2015	08/01/2015	24	1.11
85	Sentinel-1A, Track 173	07/08/2015	08/25/2015	48	—
86	Sentinel-1A, Track 173	07/08/2015	10/12/2015	96	—
87	Sentinel-1A, Track 173	08/01/2015	08/25/2015	24	—
88*	Sentinel-1A, Track 173	08/01/2015	09/18/2015	48	1.12
89	Sentinel-1A, Track 173	08/01/2015	10/12/2015	72	—
90	Sentinel-1A, Track 173	08/25/2015	09/18/2015	24	—
91	Sentinel-1A, Track 173	08/25/2015	11/29/2015	96	—
92	Sentinel-1A, Track 173	09/18/2015	10/12/2015	24	—
93	Sentinel-1A, Track 173	09/18/2015	11/29/2015	72	—
94*[3]	Sentinel-1A, Track 173	09/18/2015	12/23/2015	96	1.13
95	Sentinel-1A, Track 173	10/12/2015	11/29/2015	48	—
96	Sentinel-1A, Track 173	11/29/2015	12/23/2015	24	—
97	Sentinel-1A, Track 173	11/29/2015	02/09/2016	72	—
98	Sentinel-1A, Track 173	12/23/2015	02/09/2016	48	—
99*[3]	Sentinel-1A, Track 173	12/23/2015	03/04/2016	72	1.14
100	Sentinel-1A, Track 173	02/09/2016	03/04/2016	24	—
101	Sentinel-1A, Track 173	02/09/2016	03/28/2016	48	—
102	Sentinel-1A, Track 173	02/09/2016	04/21/2016	72	—
103	Sentinel-1A, Track 173	02/09/2016	05/15/2016	96	—
104*	Sentinel-1A, Track 173	03/04/2016	04/21/2016	48	1.15
105	Sentinel-1A, Track 173	03/04/2016	06/08/2016	96	—
106	Sentinel-1A, Track 173	03/28/2016	04/21/2016	24	—
107	Sentinel-1A, Track 173	03/28/2016	05/15/2016	48	—
108	Sentinel-1A, Track 173	03/28/2016	06/08/2016	72	—
109	Sentinel-1A, Track 173	03/28/2016	07/02/2016	96	—
110*	Sentinel-1A, Track 173	04/21/2016	05/15/2016	24	1.16
111	Sentinel-1A, Track 173	04/21/2016	07/02/2016	72	—
112	Sentinel-1A, Track 173	04/21/2016	07/26/2016	96	—
113	Sentinel-1A, Track 173	05/15/2016	06/08/2016	24	—
114*	Sentinel-1A, Track 173	05/15/2016	07/02/2016	48	1.17
115	Sentinel-1A, Track 173	05/15/2016	07/26/2016	72	—
116	Sentinel-1A, Track 173	05/15/2016	08/19/2016	96	—
117	Sentinel-1A, Track 173	06/08/2016	07/02/2016	24	—
118*[4]	Sentinel-1A, Track 173	07/02/2016	07/26/2016	24	1.18
119	Sentinel-1A, Track 173	07/02/2016	10/06/2016	96	—
120	Sentinel-1A, Track 173	07/26/2016	08/19/2016	24	—
121*[4]	Sentinel-1A, Track 173	07/26/2016	10/06/2016	72	1.19
122	Sentinel-1A, Track 173	07/26/2016	10/30/2016	96	—
123	Sentinel-1A, Track 173	08/19/2016	09/12/2016	24	—

Table 2. Interferograms interpreted for the Coachella Valley, California, 2009–17.—Continued

[mm/dd/yyyy, month/day/year; SAR, synthetic aperture radar; —, not applicable]

New index number	Satellite, track, and for TerraSAR-X only, strip	1st SAR acquisition (mm/dd/yyyy)	2nd SAR acquisition (mm/dd/yyyy)	Time span of SAR pair, in days	Appendix figure number
124	Sentinel-1A, Track 173	08/19/2016	10/06/2016	48	—
125	Sentinel-1A, Track 173	08/19/2016	10/30/2016	72	—
126	Sentinel-1A, Track 173	09/12/2016	10/06/2016	24	—
127	Sentinel-1A, Track 173	09/12/2016	10/30/2016	48	—
128*	Sentinel-1A, Track 173	10/06/2016	10/30/2016	24	1.20
129	Sentinel-1A, Track 173	10/06/2016	02/27/2017	144	—
130*	Sentinel-1A, Track 173	10/30/2016	02/27/2017	120	1.21
131	Sentinel-1A, Track 173	02/27/2017	05/10/2017	72	—
132	Sentinel-1A, Track 173	02/27/2017	05/22/2017	84	—
133	Sentinel-1A, Track 173	02/27/2017	06/03/2017	96	—
134	Sentinel-1A, Track 173	05/10/2017	05/22/2017	12	—
135	Sentinel-1A, Track 173	05/10/2017	06/03/2017	24	—
136	Sentinel-1A, Track 173	05/10/2017	06/15/2017	36	—
137	Sentinel-1A, Track 173	05/10/2017	06/27/2017	48	—
138	Sentinel-1A, Track 173	05/10/2017	07/09/2017	60	—
139	Sentinel-1A, Track 173	05/10/2017	07/21/2017	72	—
140*	Sentinel-1A, Track 173	05/22/2017	06/03/2017	12	1.22
141	Sentinel-1A, Track 173	05/22/2017	06/15/2017	24	—
142	Sentinel-1A, Track 173	05/22/2017	06/27/2017	36	—
143	Sentinel-1A, Track 173	05/22/2017	07/09/2017	48	—
144	Sentinel-1A, Track 173	05/22/2017	07/21/2017	60	—
145*	Sentinel-1A, Track 173	06/03/2017	06/15/2017	12	1.23
146	Sentinel-1A, Track 173	06/03/2017	06/27/2017	24	—
147	Sentinel-1A, Track 173	06/03/2017	07/09/2017	36	—
148	Sentinel-1A, Track 173	06/03/2017	07/21/2017	48	—
149*	Sentinel-1A, Track 173	06/15/2017	06/27/2017	12	1.24
150	Sentinel-1A, Track 173	06/15/2017	07/09/2017	24	—
151	Sentinel-1A, Track 173	06/15/2017	07/21/2017	36	—
152	Sentinel-1A, Track 173	06/27/2017	07/09/2017	12	—
153	Sentinel-1A, Track 173	06/27/2017	07/21/2017	24	—
154	Sentinel-1A, Track 173	07/09/2017	07/21/2017	12	—

*Used in interferogram stack (fig. 5*A*) and timeseries (figs. 6*A*–6*E*, 7*B*, 8*B*, 9*B*); shown in appendix 1.

[1]Stacked to produce a single data point for timeseries (figs. 6*A*–6*E*, 7*B*, 8*B*, 9*B*).

[2]Stacked to produce a single data point for timeseries (figs. 6*A*–6*E*, 7*B*, 8*B*, 9*B*).

[3]Stacked to produce a single data point for timeseries (figs. 6*A*–6*E*, 7*B*, 8*B*, 9*B*).

[4]Stacked to produce a single data point for timeseries (figs. 6*A*–6*E*, 7*B*, 8*B*, 9*B*).

A stacked interferogram also was generated using the 22 Sentinel-1A interferograms from December 28, 2014, to June 27, 2017 (fig. 5*A*). A second stacked interferogram was created by adding the December 28, 2014–June 27, 2017, stacked interferogram (fig. 5*A*) to the stacked interferogram for June 27, 1995–September 19, 2010, which was presented in Sneed and others (2014). This second stacked interferogram represents deformation between 1995 and 2017 (fig. 5*B*). Note, the extent of the 1995–2017 interferogram (fig. 5*B*) is less than that of the 2014–17 interferogram (fig. 5*A*) because pre-2014 InSAR data were not processed for the northern Coachella Valley. The 1995–2017 interferogram has several data gaps. The largest gaps are between November 2000 and October 2003, when satellite data were not collected, and between September 2010 and December 2014, when suitable data were not available. The 1995–2017 interferogram does not include any deformation that may have occurred during the data gaps. Although TerraSAR-X results were available for part of the time during September 19, 2010–December 28, 2014, they could not be included in the stack because spatial decorrelation prevented unwrapping the resulting interferograms. Therefore, interpretations of TerraSAR-X interferograms were made by identifying a stable area and interpreting the value of subsidence using the modulo 2π-scale for the location of interest (for an example, refer to appendix fig. 1.1).

Continuous GPS and InSAR results were compared for 2014–17 to assess the quality of the InSAR results at six CGPS sites distributed throughout the Coachella Valley: station PSAP in the northern Coachella Valley and stations COTD, TMAP, IDQG, THMG, and P491 in the southern Coachella Valley (figs. 5, 6). Magnitudes of subsidence derived from CGPS and InSAR analysis were directly compared because continuously collected GPS data generally permit computation of coordinates for most days. The coordinates for CGPS stations were obtained from, and computed by, SOPAC for most days during 2010–17, except for station PSAP, for which data are not available after November 8, 2016. Daily CGPS position time series were downloaded from the Scripps Orbit and Permanent Array Center (2017). Day-to-day CGPS height solutions varied by as much as about 0.10 ft (30 mm), which is likely the result of variable atmospheric conditions, random walk noise, and other effects not directly related to land-surface-elevation change (Zerbini and others, 2001; Williams and others, 2004; Langbein, 2008). To minimize this high-frequency noise and to enable better comparison between changes in GPS heights and InSAR measurements, a 31-day moving average was applied to the CGPS results. The removal of the day-to-day variations in GPS heights did not remove seasonal or long-term deformation trends (fig. 6) and, therefore, permitted more meaningful comparison with InSAR results.

Data from PSAP, COTD, TMAP, IDQG, THMG, and P491 were compared to data from the stacked interferogram (fig. 5*A*). Both datasets span the same, or similar, periods at these locations, which were about 2.5 years. All comparisons cover exactly the same period, December 28, 2014–June 27, 2017, except those for station PSAP. Gaps in PSAP CGPS results prevented comparison with InSAR subsidence magnitudes for exactly the same period; thus, the period lengths differed by 20 days between the two datasets (table 3). The land-surface deformation values derived from each method compared favorably and indicated that these stations generally were stable during the 2.5-year period (table 3). The largest discrepancy in the deformation values derived from the two methods was for PSAP (0.06 ft or 18 mm); the other sites' discrepancies were not more than 0.03 ft (9 mm).

Data from PSAP, COTD, TMAP, IDQG, THMG, and P491 also were compared to data from the interferograms used to produce the time series for December 28, 2014–June 27, 2017 (fig. 6). Of nearly 100 measurement comparisons between the CGPS and InSAR data, 91 percent agreed within 0.05 ft (15 mm) and were not systematically biased. Using the CGPS data as the ground truth, these results indicate that the expected InSAR error is about ±0.05 ft (±15 mm).

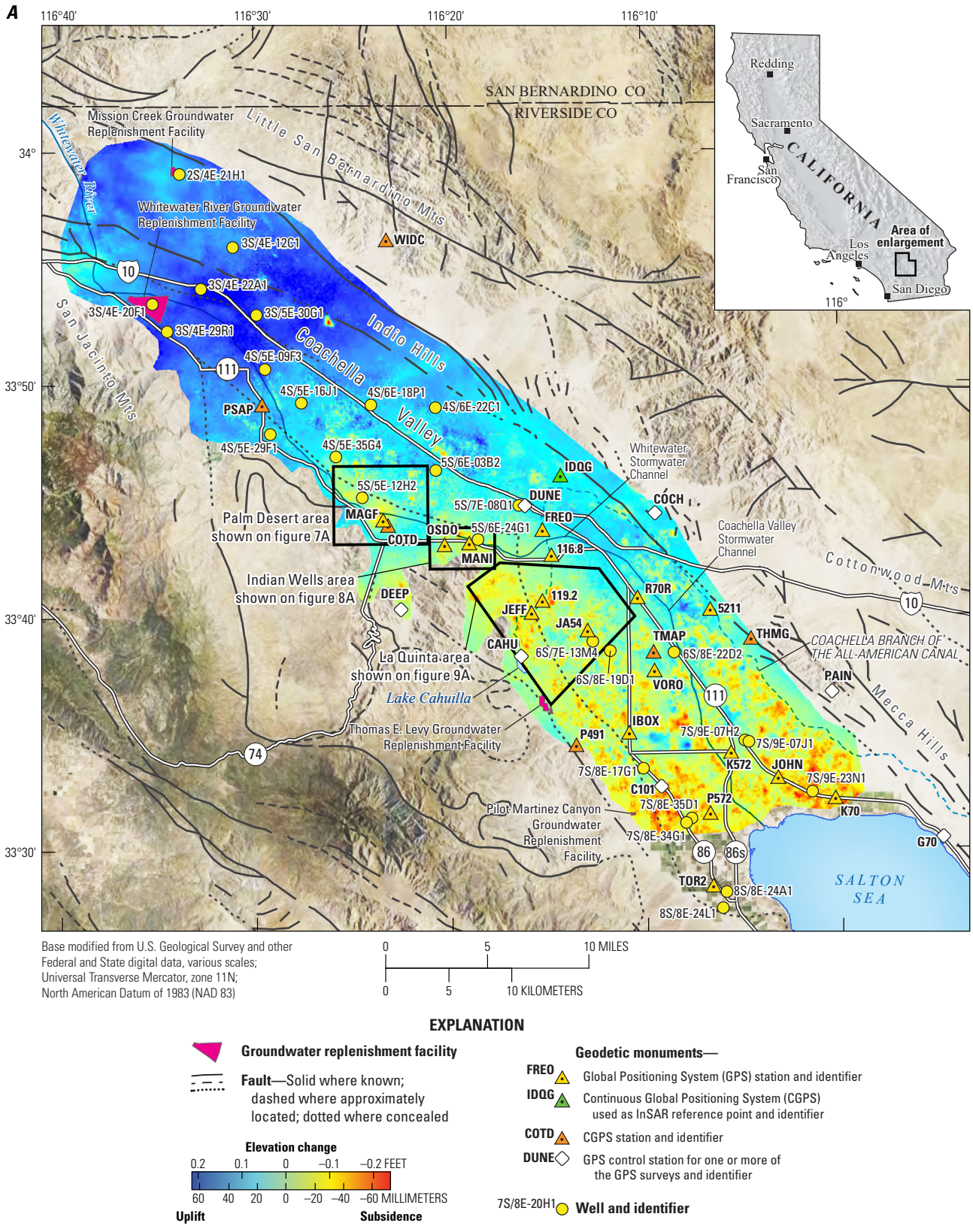

Figure 5. Areas of subsidence and uplift, Global Positioning System (GPS) stations, and continuous GPS (CGPS) stations in the Coachella Valley, California, as shown on a stacked interferogram for *A*, December 28, 2014–June 27, 2017 (excludes February 27, 2017–May 22, 2017), and *B*, June 27, 1995–June 27, 2017 (excludes November 8, 2000–November 30, 2003; September 19, 2010–December 28, 2014; and February 27, 2017–May 22, 2017).

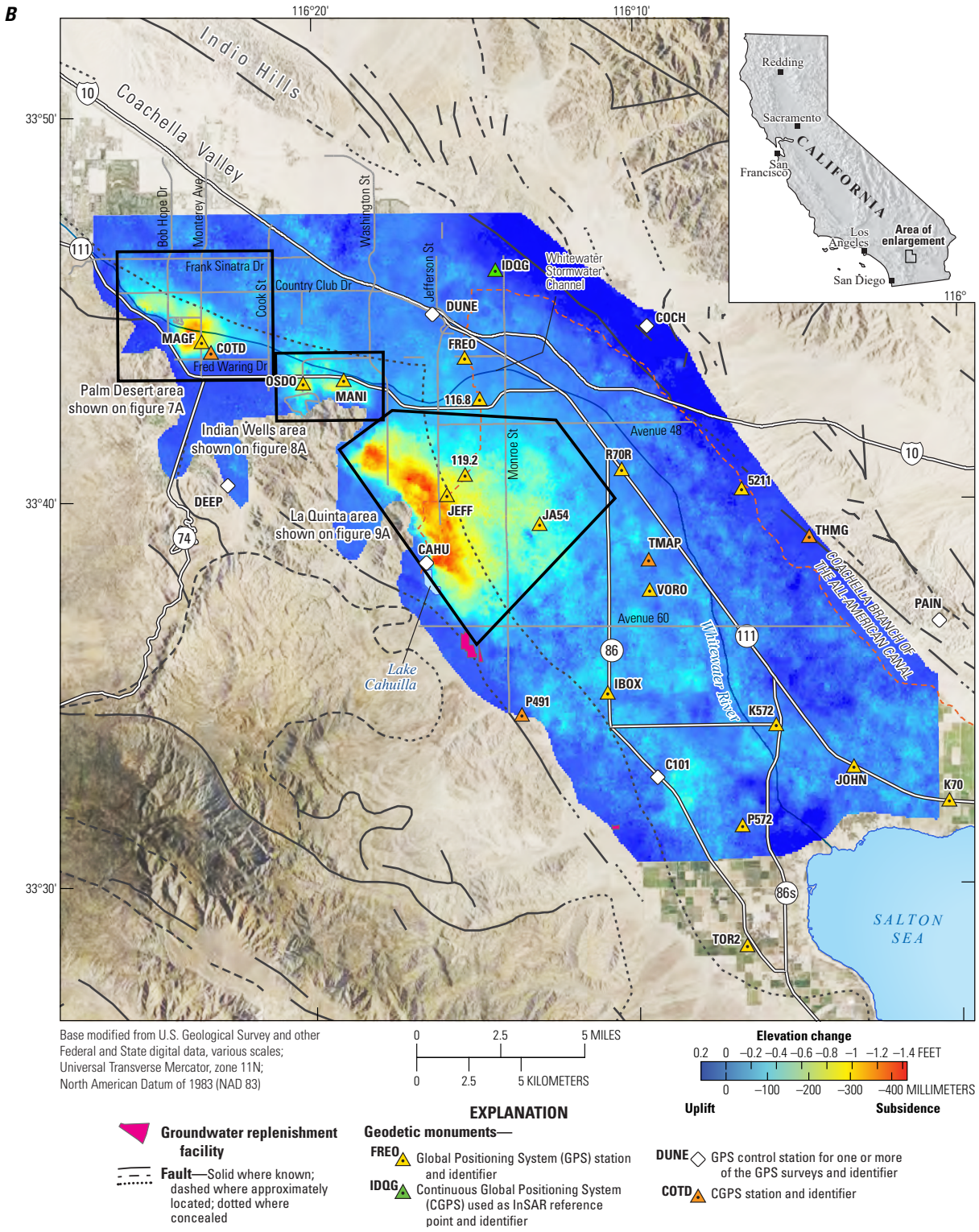

Figure 5. —Continued

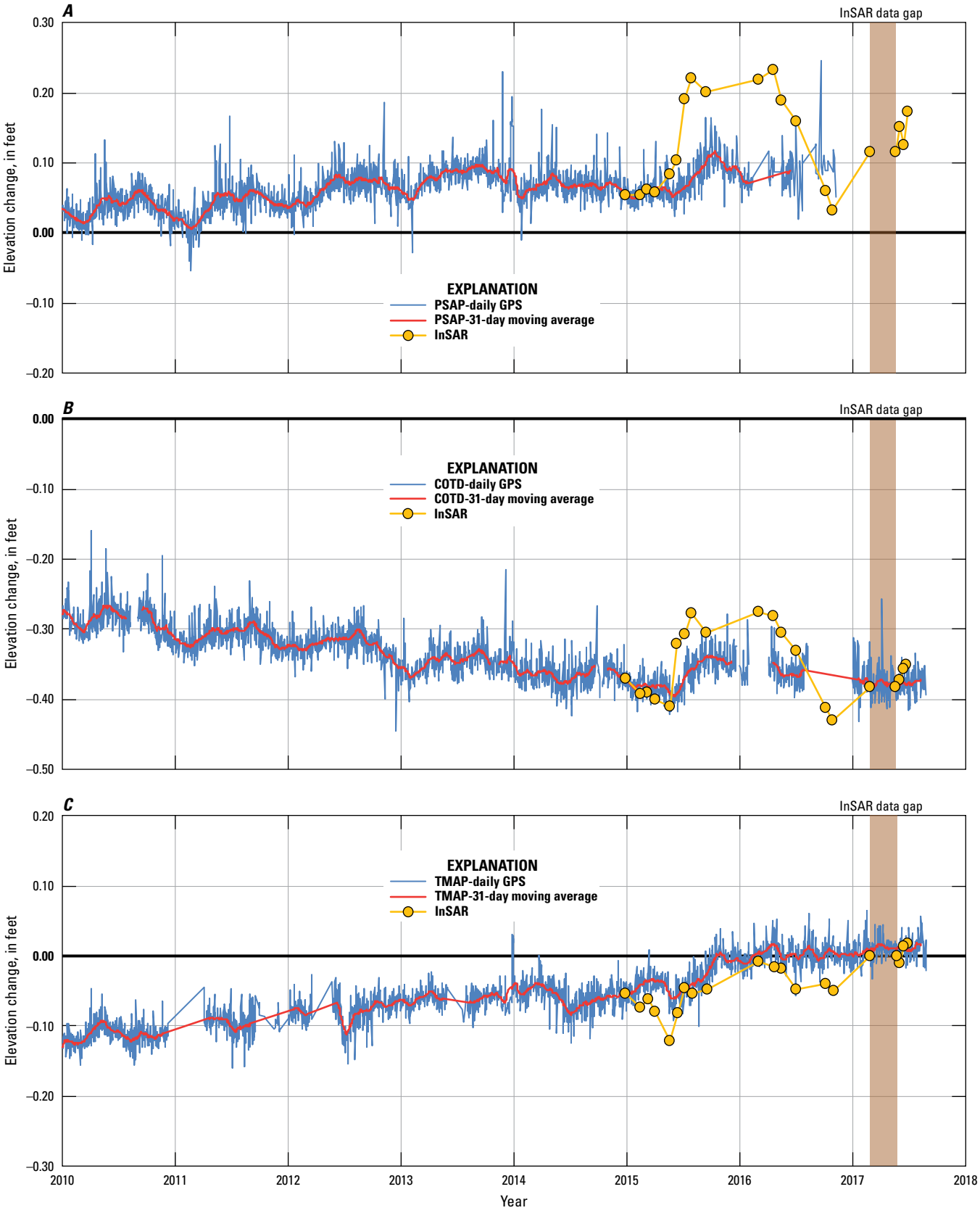

Figure 6. Elevation change measured by continuous Global Positioning System (CGPS) and by interferometric synthetic aperture radar (InSAR) at selected CGPS stations, Coachella Valley, California, 2010–17: *A*, PSAP; *B*, COTD; *C*, TMAP; *D*, IDQG; *E*, THMG; and *F*, P491. (Station locations are shown in figure 5*A*.)

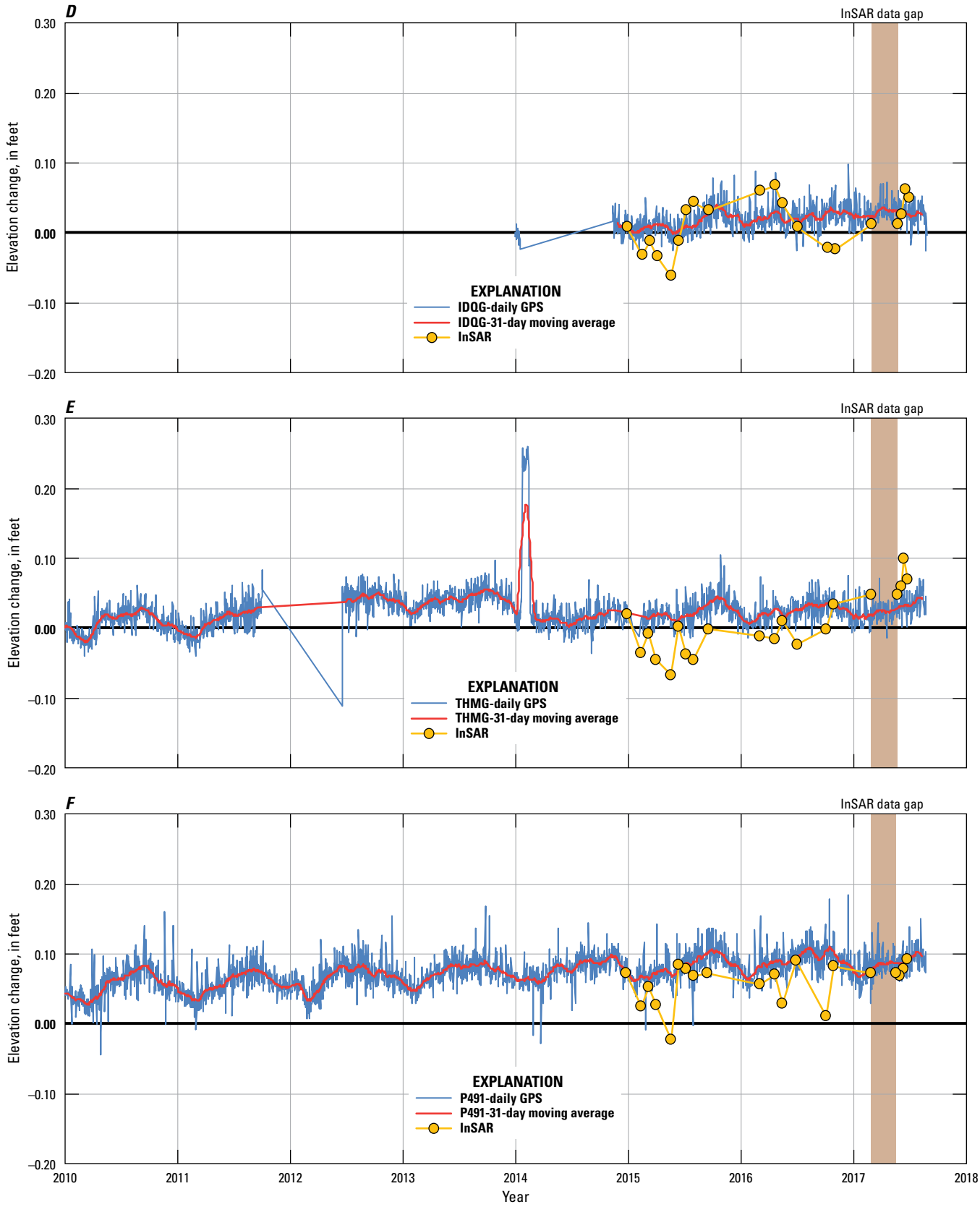

Figure 6. —Continued

Table 3. Deformation values derived from Global Positioning System (GPS) data and from interferometric synthetic aperture radar (InSAR) results, and differences between those values, for selected continuous Global Positioning System (CGPS) stations, Coachella Valley, California.

[mm, millimeter; ft, foot]

CGPS station name	Date range of CGPS and InSAR-derived deformation values	CGPS-derived deformation (31-day moving average), in ft (mm)	InSAR-derived deformation in ft (mm)	Difference between CGPS- and InSAR-derived deformation, in ft (mm)
PSAP	December 28, 2014–June 12, 2016 (CGPS) December 28, 2014–July 2, 2016 (InSAR)	+0.04 ft (+11 mm)	+0.10 ft (+29 mm)	0.06 ft (18 mm)
COTD	December 28, 2014–June 27, 2017	–0.01 ft (–2 mm)	+0.01 ft +(3 mm)	0.02 ft (5 mm)
TMAP	December 28, 2014–June 27, 2017	+0.04 ft (+13 mm)	+0.07 ft (+20 mm)	0.03 ft (7 mm)
IDQG	December 28, 2014–June 27, 2017	+0.02 ft (+6 mm)	+0.05 ft (+15 mm)	0.03 ft (9 mm)
THMG	December 28, 2014–June 27, 2017	+0.01 ft (+4 mm)	+0.04 ft (+12 mm)	0.03 ft (8 mm)
P491	December 28, 2014–June 27, 2017	+0.02 ft (+5 mm)	–0.01 ft (–2 mm)	0.03 ft (7 mm)

Interferometric Synthetic Aperture Radar Results

The interferograms processed for 2014–17 for the entire Coachella Valley show that most of the northern Coachella Valley uplifted, with the largest magnitudes near the Whitewater River Groundwater Replenishment Facility (fig. 5*A*). In addition, most of the southern Coachella Valley subsided, with the largest magnitudes in the La Quinta area and in small, localized areas near the Salton Sea (fig. 5*A*).

In the northern Coachella Valley, small magnitudes of vertical land-surface deformation ranged from about 0.20 ft (60 mm) of uplift near the Whitewater River Groundwater Replenishment Facility to about 0.03 ft (10 mm) of subsidence. The small magnitudes of subsidence fell within the expected error of the InSAR analyses and tended to correlate with golf courses. The small magnitudes of subsidence correlated with golf courses could be actual land subsidence from local pumping or from land-surface disturbances caused by golf-course activities. Small magnitude land-surface deformation in the northern Coachella Valley also was a conclusion of a subsidence study that analyzed InSAR data for 2003–05 (Martin, 2011).

Three areas in the southern Coachella Valley had the most land subsidence: Palm Desert, Indian Wells, and La Quinta. Maximum subsidence during 2014–17 was about 0.26 ft (80 mm) in a few local areas around La Quinta (including parts of the Coachella Branch of the All-American Canal) and just north of the Salton Sea (fig. 5*A*). At least some of the localized areas near the Salton Sea showing apparent subsidence could either be actual land subsidence or land-surface disturbances caused by farming or other localized ground-disturbing activities. Smaller magnitudes of subsidence were measured throughout the southern Coachella Valley, including in the Palm Desert and Indian Wells areas (fig. 5*A*). These three areas also were identified as areas of subsidence in previous reports (Sneed and others, 2002, 2014; Sneed and Brandt, 2007).

Palm Desert Area

A small magnitude subsidence feature was detected in the Palm Desert area between December 28, 2014, and June 27, 2017 (figs. 5*A*, 7*A*). No data from 2010 to 2014 were available. In many of the shorter term interferograms, the magnitude is about as small as the measurement resolution of InSAR methods. The stacked interferogram for 2014–17 indicates that the extent of subsidence had not changed substantially from the 1993 to 2010 results (Sneed and others, 2014), but the rate of measured subsidence was substantially less. The subsidence feature is approximately 1.2 mi (2 km) in diameter, centered about 0.6 mi (1 km) north of Fred Waring Drive and 0.6 mi (1 km) east of the intersection of Bob Hope Drive and Hwy 111 (fig. 7*A*). This feature is approximately bounded by Country Club Drive on the north, Fred Waring Drive on the south, Highway 111 and Bob Hope Drive on the west, and Portola Avenue on the east. The maximum subsidence was about 0.20 ft (60 mm) and is about 0.3 mi (0.5 km) north of PD1 (fig. 7*A*). The deformation time series for the location of previously identified maximum subsidence in the Palm Desert area (Sneed and others, 2014; PD1 in fig. 7*A*) shows periods of uplift and of subsidence during 2014–17 (fig. 7*B*) totaling to about 0.08 ft (25 mm) of subsidence, or about 0.03 ft/yr (10 mm/yr), and adding only a small magnitude of subsidence to the 1.97 ft (600 mm) measured at PD1 between 1995 and 2010. The 2014–17 subsidence rate is about one-fourth of the average rate calculated from the 1995–2010 InSAR results at this location, indicating subsidence rates slowed substantially (Sneed and others, 2014).

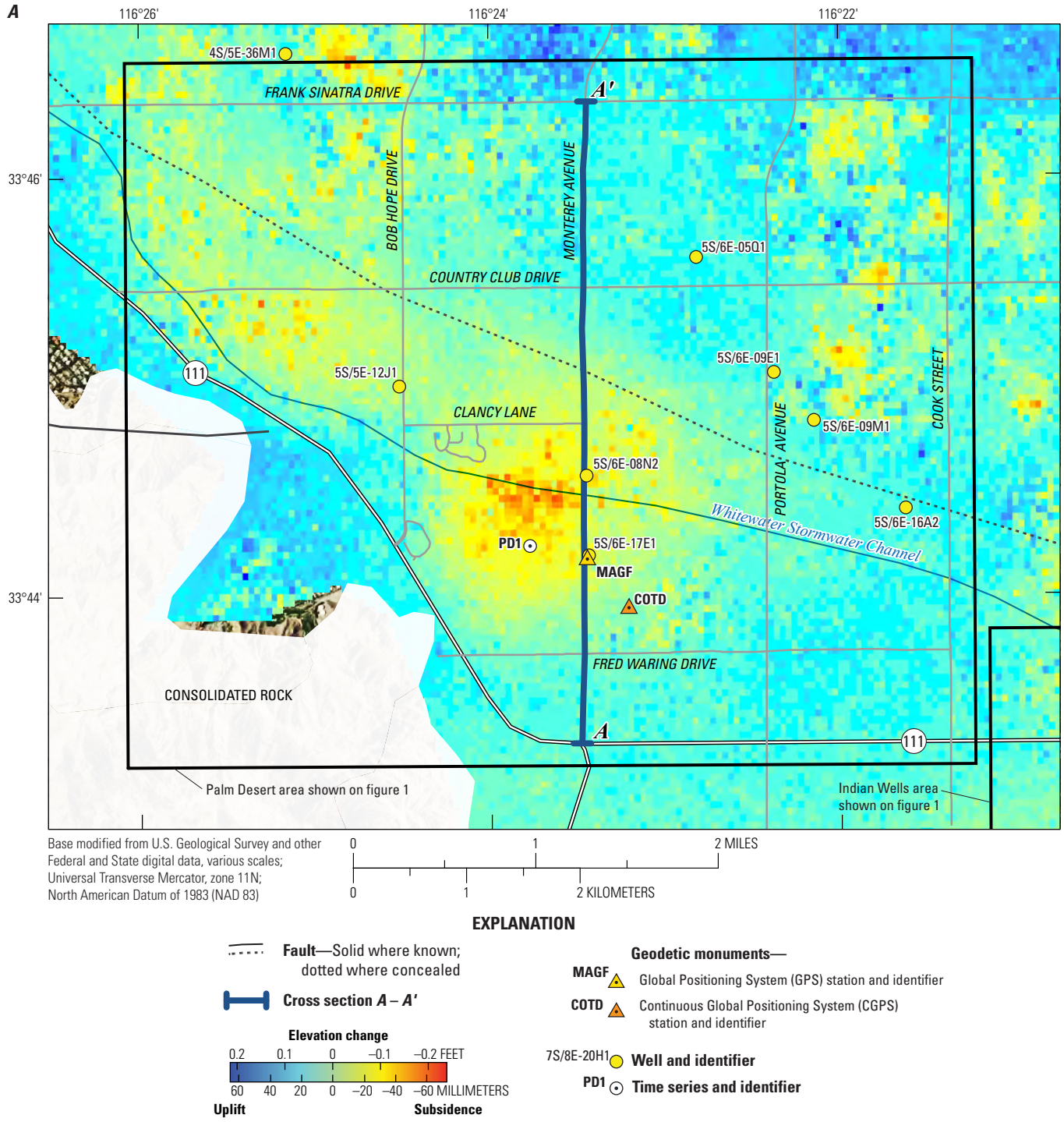

Figure 7. Palm Desert subsidence area, Coachella Valley, California: *A*, location of Global Positioning System (GPS) station, continuous Global Positioning System (CGPS) station, consolidated rock, and wells overlain on the 2014–17 stacked interferogram; *B*, deformation time series for location PD1 and water-surface elevations for selected wells for 1995–2017; and *C*, deformation along Monterey Avenue since December 28, 2014. Water-surface elevation data are referenced to the National Geodetic Vertical Datum of 1929 and were provided by the Coachella Valley Water District.

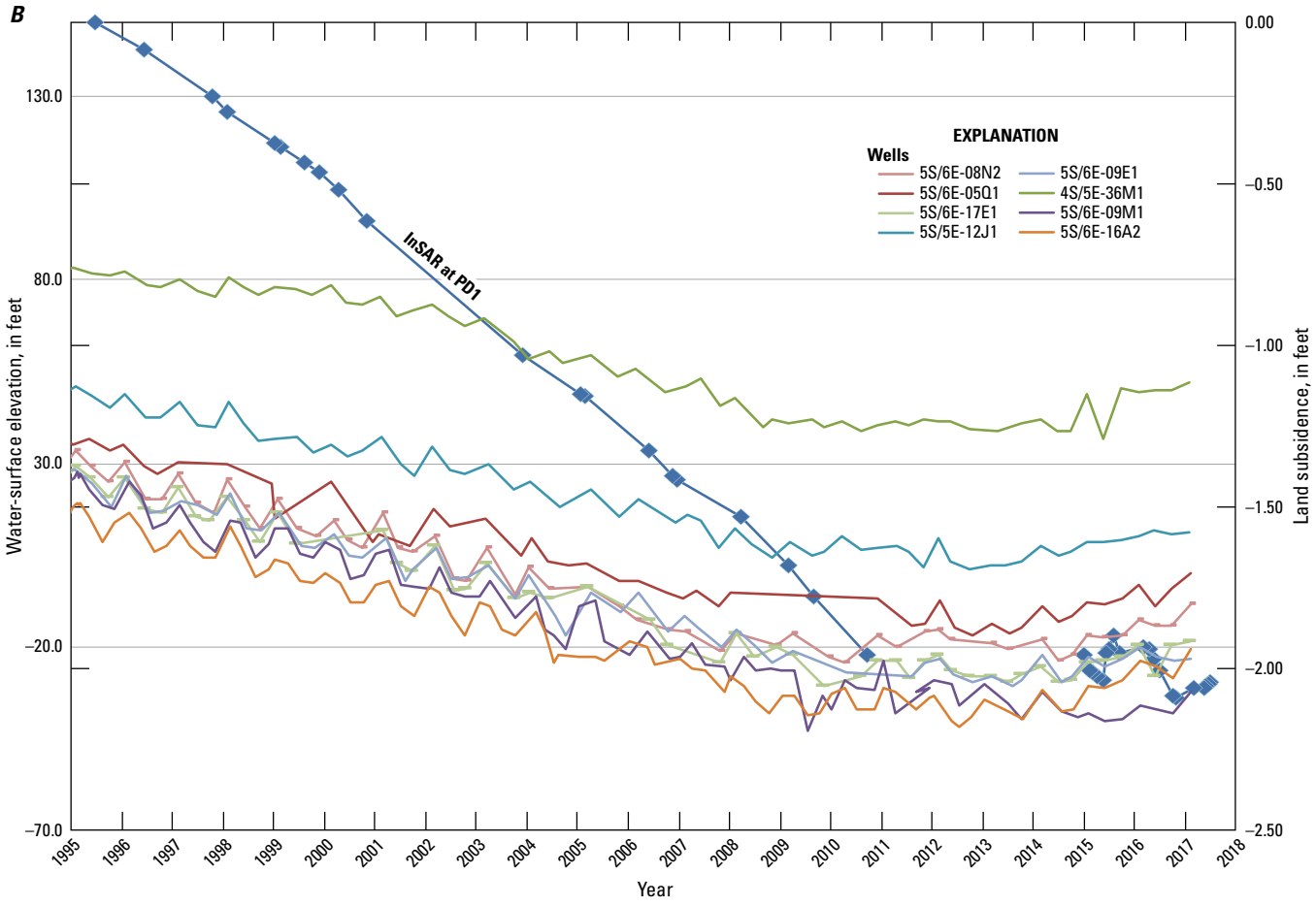

Figure 7. —Continued

A series of deformation profiles (section A–A') have been constructed for a 3.5 mi (5.6 km) stretch of Monterey Avenue in the Palm Desert area, as was done in Sneed and others (2014; fig. 7*A*). Along this profile, maximum subsidence of 0.12 ft (35 mm) was approximately 0.6 mi (1 km) north of Fred Waring Drive between December 28, 2014, and June 27, 2017, corresponding to an average rate of 0.05 ft/yr (14 mm/yr; fig. 7*C*). The location of this maximum subsidence magnitude and rate along this profile is consistent with the location of maximum subsidence during 1995–2010; however, the location subsided at about half of the rate during 2014–17 compared to 1995–2010 (Sneed and others, 2014; figs. 7*A*, 7*C*).

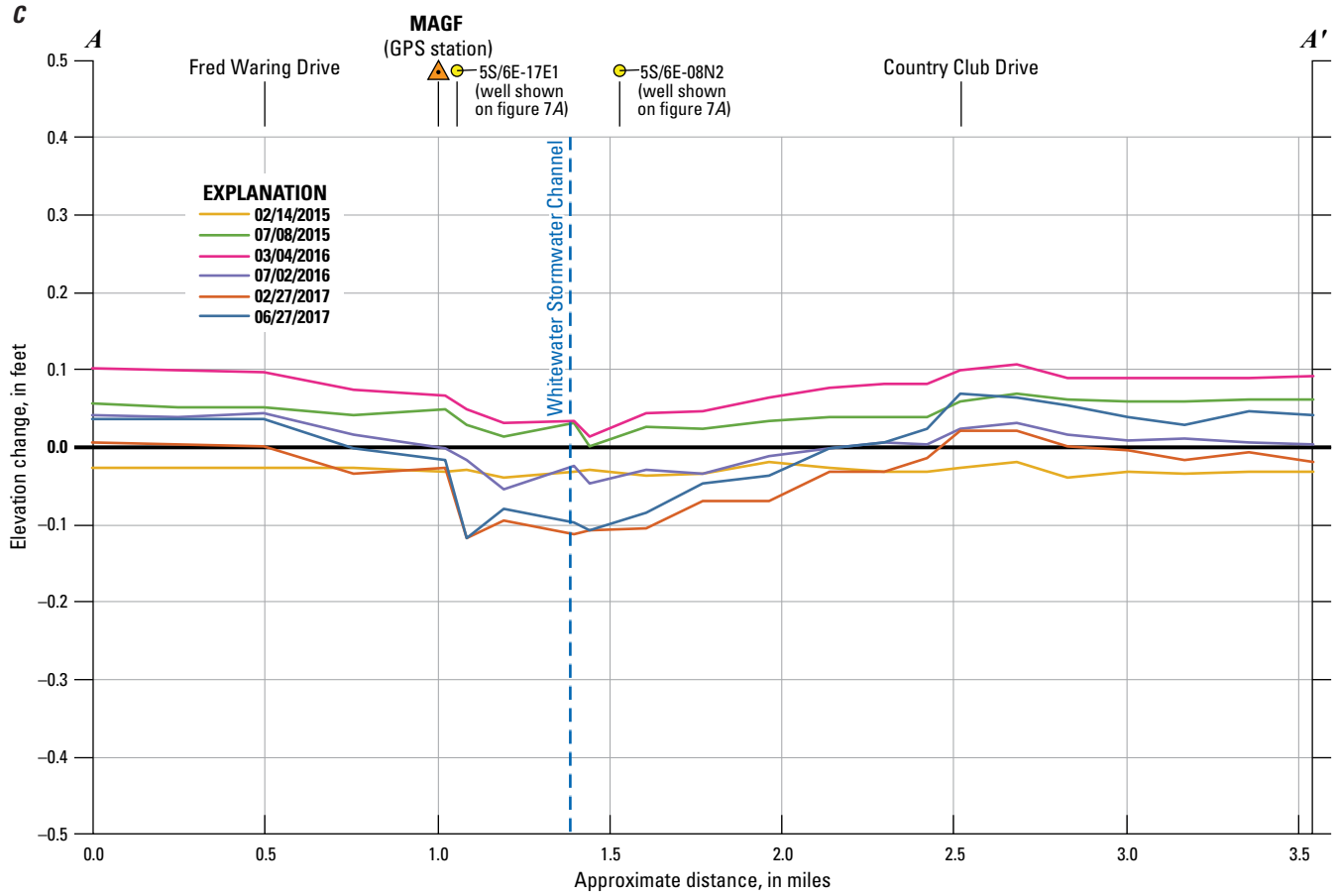

Figure 7. —Continued

Indian Wells Area

Interferograms for the Indian Wells area show subtle subsidence features near the areas described by Sneed and others (2014) that they termed the west bowl, east bowl, and 3rd bowl (fig. 8*A*). The west bowl is centered approximately 0.3 mi (0.5 km) south of Hwy 111 and 0.1 mi (0.2 km) east of Eldorado Drive and is elongated northwest–southeast. The east bowl is centered about 0.3 mi (0.5 km) south of Hwy 111 and about 0.9 mi (1.4 km) east of the west bowl and is approximately circular. The 3rd bowl is centered about 0.4 mi (0.6 km) south of Hwy 111, nearly coalesces with the east bowl, and is elongated northwest–southeast. Together, the three bowls make up an area of about 3 mi^2 (8 km^2). Although these features were prevalent in 2009–12 interferograms generated from TerraSAR-X SAR data (appendix figs. 1.1 and 1.2), the subsidence features are much less prevalent or even absent in 2014–17 interferograms generated from Sentinel-1A SAR data (appendix figs. 1.3–1.24) and in the resulting stacked interferogram for 2014–17 (figs. 5*A*, 8*A*). Additionally, the interferograms show notable apparent subsidence in an area to the north of these bowls, centered on a golf course between the Whitewater Stormwater Channel and Fred Waring Drive. The apparent deformation in this area probably is not actual deformation, however, but instead is a manifestation of spatial decorrelation in several Sentinel-1A interferograms used in the stacked interferogram. Decorrelation also is present in TerraSAR-X interferograms, and thus neither satellite's data could be interpreted to indicate land-surface deformation in this area. The extent of subsidence during 2009–12 terminated abruptly on the northeast edges of all three bowls, as discussed in Sneed and others (2014). The abrupt termination of subsidence extent was not evident in 2014–17 interferograms, likely because the subsidence magnitudes were too small to discern an abrupt termination from the C-band InSAR results.

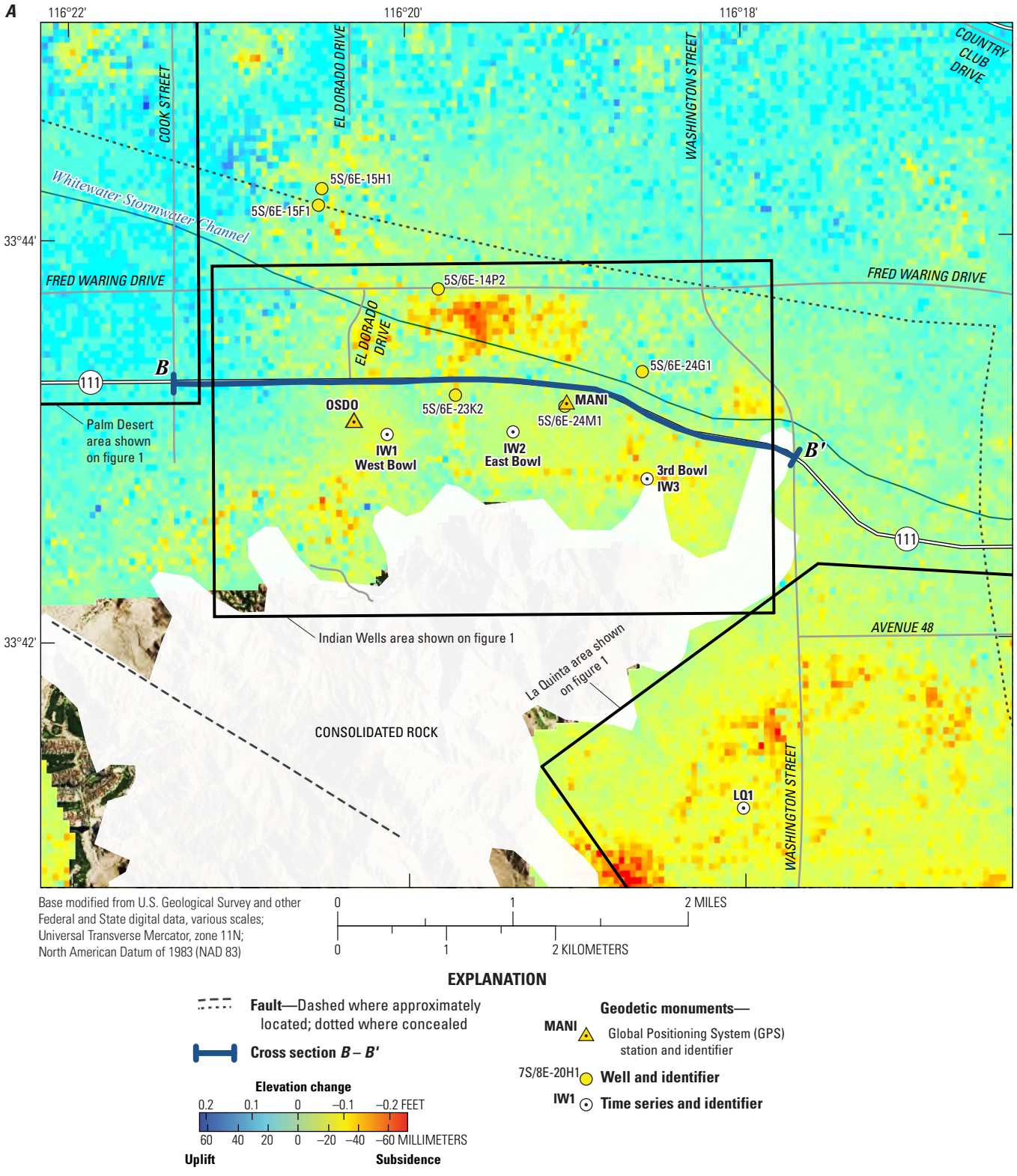

Figure 8. Indian Wells subsidence area, Coachella Valley, California: *A*, location of Global Positioning System (GPS) stations, consolidated rock, and wells overlain on the 2014–17 stacked interferogram; *B*, deformation time series for locations IW1, IW2, and IW3 and water-surface elevations for selected wells for 1995–2017; and *C*, deformation along Highway 111 since December 28, 2014. Note, the apparent subsidence between Whitewater Stormwater Channel and Fred Waring Drive in part *A* is likely not actual subsidence, but instead is a manifestation of spatial decorrelation in interferograms used to generate this image. Water-surface elevation data are referenced to the National Geodetic Vertical Datum of 1929 and were provided by the Coachella Valley Water District.

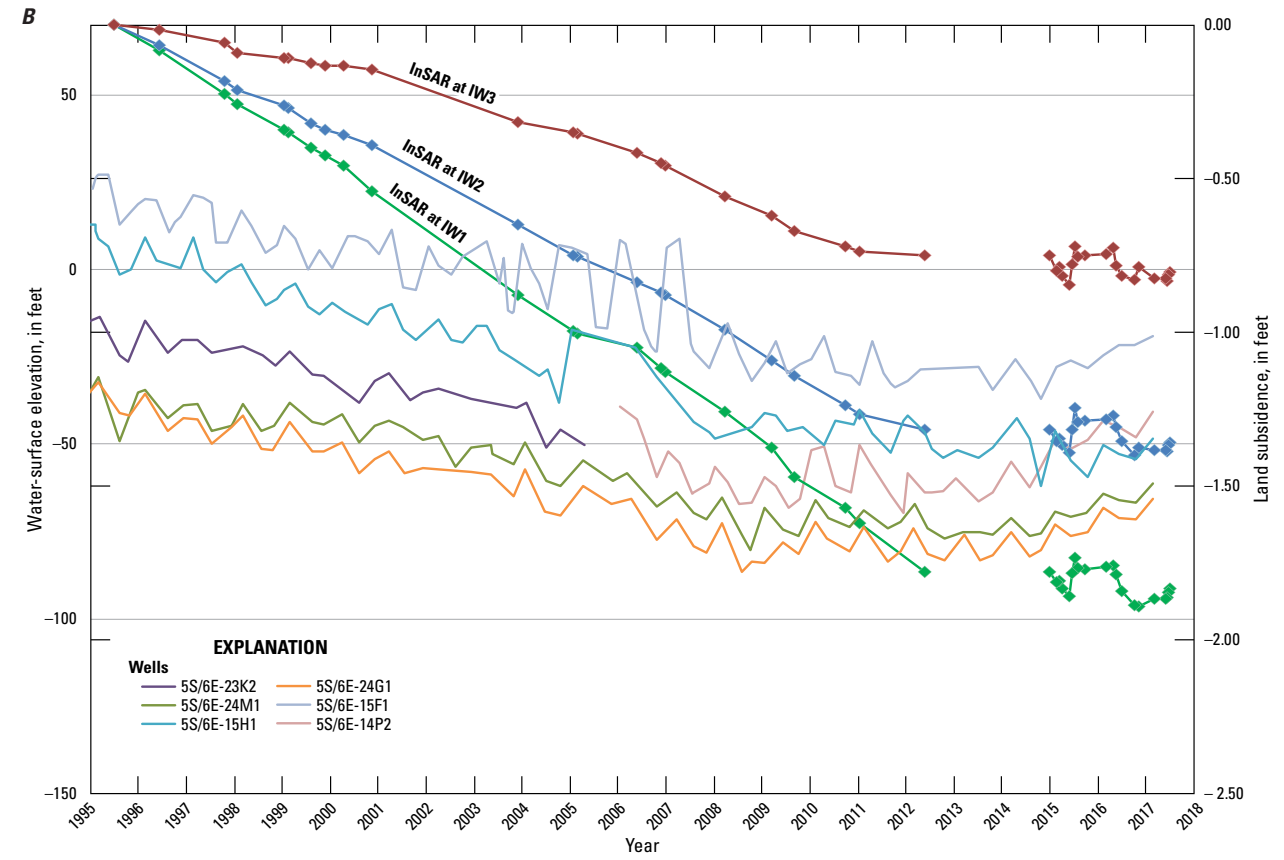

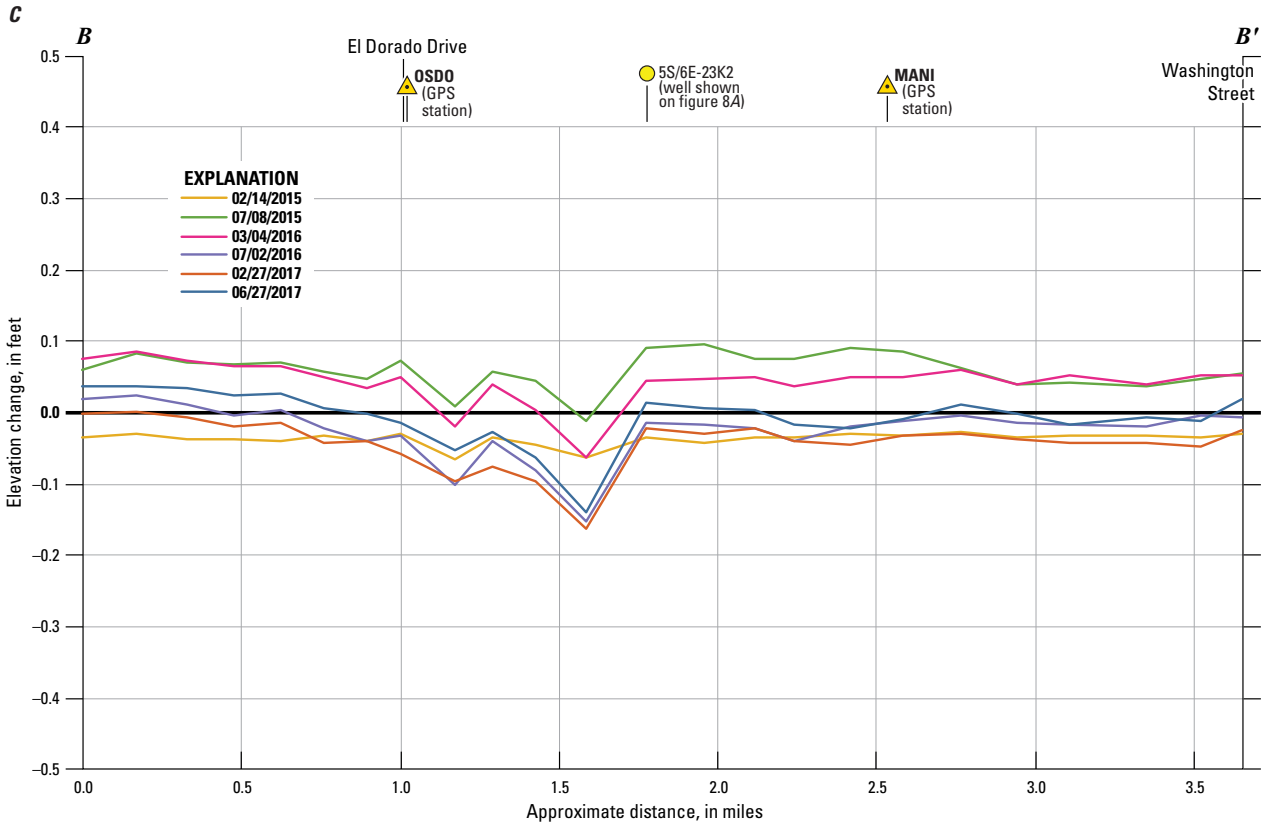

Figure 8. —Continued

Deformation time series were constructed for the previously identified locations in Sneed and others (2014) using TerraSAR-X InSAR results for July 2009 to May 2012 (appendix figs. 1.1 and 1.2) and Sentinel-1A InSAR results for December 2014 to June 2017 (appendix figs. 1.3–1.24; IW1, IW2, and IW3 in figs. 8*A,* 8*B*). To temporally align these results with results presented in Sneed and others (2014), the first interferogram used for the time series (July 28, 2009–January 7, 2011; appendix fig. 1.1) was adjusted by removing the subsidence estimated for July 28, 2009–September 19, 2010, to correspond to the last date (September 19, 2010) for which results are presented in Sneed and others (2014). The time series for September 19, 2010–May 16, 2012, combined with the time series for December 28, 2014–June 27, 2017, indicates periods of both subsidence and uplift, resulting in net subsidence. The subsidence magnitudes are 0.26 ft (79 mm), 0.12 ft (36 mm), and 0.09 ft (26 mm) for IW1, IW2, and IW3, respectively, during 2010–17 (fig. 8*B*). Using an average subsidence rate for a selected location in each bowl for 1995–10 and for 2014–17 indicates that the subsidence rate at IW1 in the west bowl decreased from 0.11 ft/yr to 0.02 ft/yr (34 mm/yr to 7 mm/yr); the subsidence rate at IW2 in the east bowl decreased from 0.09 to 0.02 ft/yr (26 mm/yr to 5 mm/yr); and the subsidence rate at IW3 in the 3rd bowl decreased from 0.05 to 0.02 ft/yr (16 mm/yr to 7 mm/yr). The InSAR analysis indicates that the 2014–17 subsidence rates for IW1 and IW2 were substantially less than the 2010–12 subsidence rates, and the subsidence rates for IW3 were similar during 2014–17 and 2010–12. Furthermore, the 2010–12 subsidence rates generally were less than the 1995–2010 rates, indicating a trend of slowing subsidence (Sneed and others, 2014).

A series of deformation profiles (section B–B') have been constructed for a 3.7 mi (5.9 km) stretch of California Highway 111 in the Indian Wells area, as was done in Sneed and others (2014; figs. 8*A,* 8*C*). Maximum subsidence along this profile of 0.14 ft (43 mm) was approximately 0.6 mi (1 km) east of Eldorado Dr. between December 28, 2014, and June 27, 2017 (fig. 8*C*), corresponding to a maximum rate of 0.06 ft/yr (17 mm/yr). The location of this maximum subsidence magnitude was about 0.7 mi (1.1 km) east of the location of maximum subsidence along this stretch during 1995–2010, but the subsidence rate was similar to the maximum rate computed for 1995–2010 (Sneed and others, 2014).

La Quinta Area Including Parts of the Coachella Branch of the All-American Canal

The La Quinta area is the largest of the three subsidence areas discussed this report, extending about 5 mi (8 km) northwest to southeast and extending from the Santa Rosa Mountains on the west to an agriculturally active center of the Coachella Valley. Similar to the Palm Desert and Indian Wells areas, InSAR analysis indicated more subtle subsidence features in the La Quinta area than those reported in Sneed and others (2014), making the eastern extent of the area ambiguous. The maximum subsidence in the La Quinta area during December 28, 2014–June 27, 2017, was about 0.26 ft (80 mm) at several locations (figs. 5*A,* 9*A*). The most rapidly subsiding part of the La Quinta subsidence area was approximately 13.5 mi^2 (35 km^2) and generally bounded by Avenue 48 on the north, Avenue 58 on the south, Santa Rosa Mountains on the west, and Monroe Street on the east.

Deformation time series were constructed for the five previously identified locations in Sneed and others (2014) using TerraSAR-X InSAR results for July 2009 to May 2012 (appendix figs. 1.1 and 1.2) and Sentinel-1A InSAR results for December 2014 to June 2017 (appendix figs. 1.3–1.24; locations LQ1–5 in fig. 9*B*). To temporally align these results with results presented in Sneed and others (2014), the first interferogram of the time series (July 28, 2009–January 7, 2011, appendix fig. 1.1) was adjusted by removing the subsidence estimated for July 28, 2009–September 19, 2010, to correspond to the last date (September 19, 2010) for which results are presented in Sneed and others (2014). Time series at the five selected locations interpreted in Sneed and others (2014) show periods of subsidence and uplift, resulting in net subsidence ranging from about 0.05 ft (15 mm) to about 0.20 ft (61 mm) at four locations (LQ1, LQ2, LQ3, and LQ4) and nearly no change at the fifth location (LQ5) during 2010–17 (fig. 9*B*). The InSAR analysis indicates that the 2014–17 subsidence rates generally were less than, or similar to, the 2010–12 subsidence rates, and the 2010–12 subsidence rates were substantially less than the 1995–2010 subsidence rates, indicating a trend of slowing subsidence (Sneed and others, 2014). Using an average subsidence rate for each of the five locations for 1995–2010 and for 2014–17 indicates that the LQ1, LQ2, LQ3, and LQ4 subsidence rates decreased from as much as about 0.13 ft/yr (40 mm/yr) to less than 0.04 ft/yr (12 mm/yr) from 1995–2010 to 2014–17, and subsidence rates at LQ5 decreased from about 0.05 ft/yr (15 mm/yr) to about 0.01 ft/yr (3 mm/yr) from 1995–2010 to 2014–17.

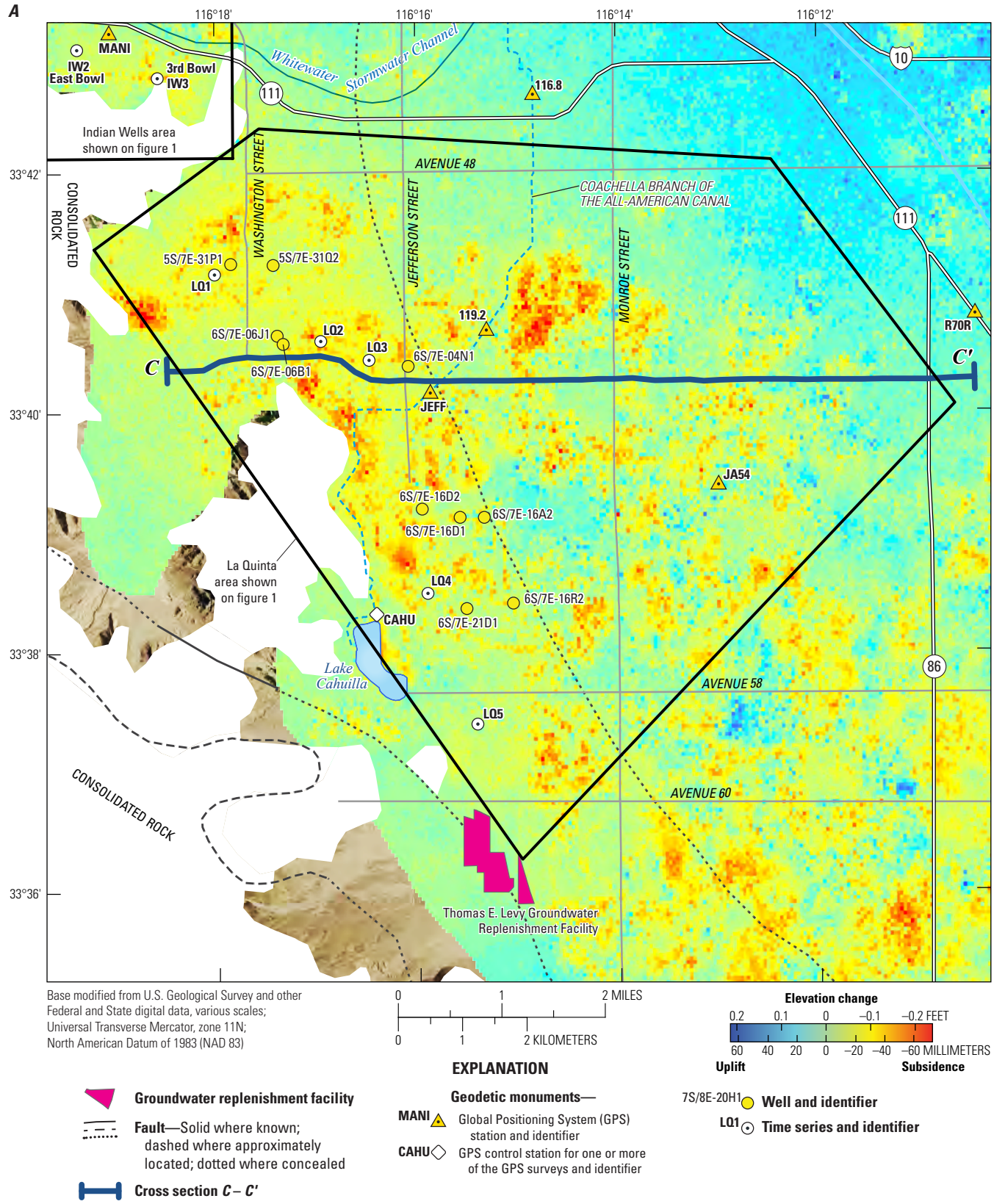

Figure 9. La Quinta subsidence area, Coachella Valley, California: *A*, location of Global Positioning System (GPS) stations, consolidated rock, and wells overlain on the 2014–17 stacked interferogram; *B*, deformation time series for locations LQ1, LQ2, LQ3, LQ4, and LQ5 and water-surface elevations for selected wells for 1995–2017; and *C*, deformation along Avenue 52 since December 28, 2014. Water-surface elevation data are referenced to the National Geodetic Vertical Datum of 1929 and were provided by the Coachella Valley Water District.

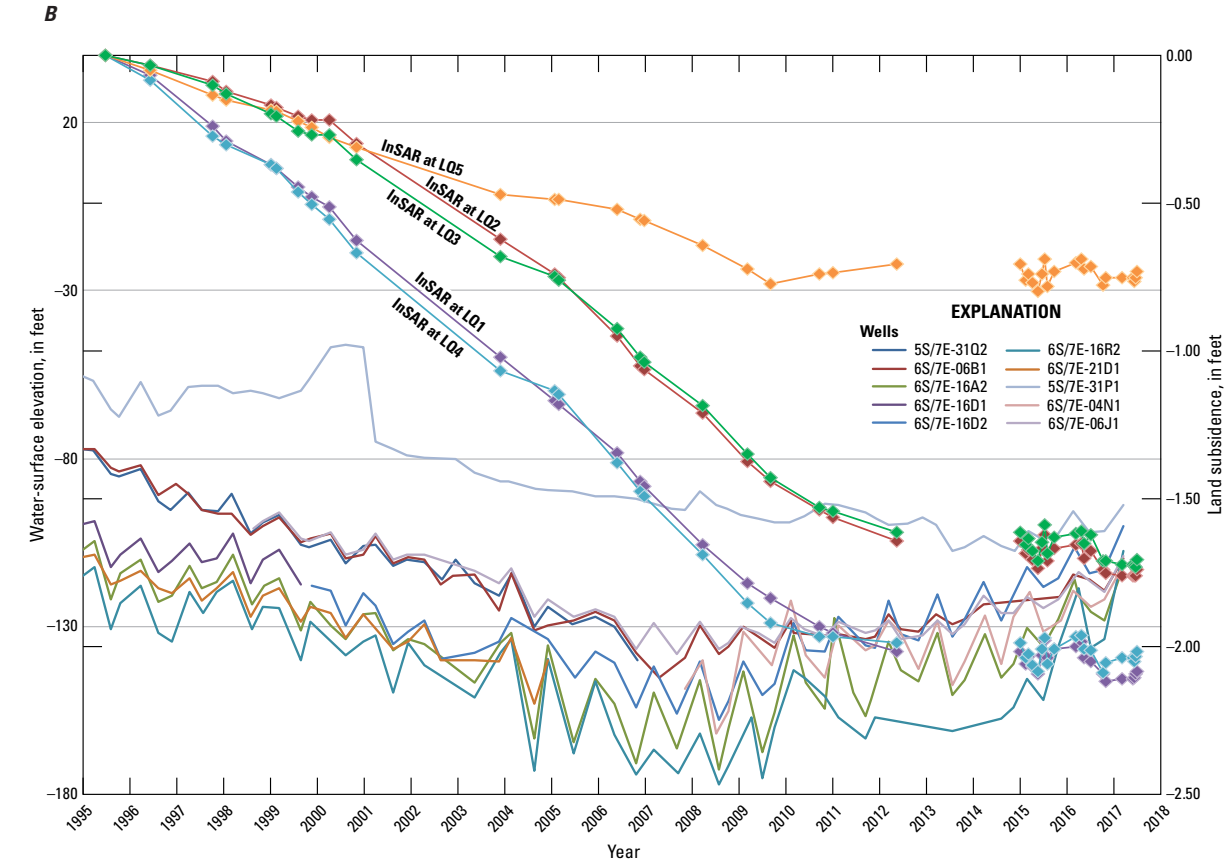

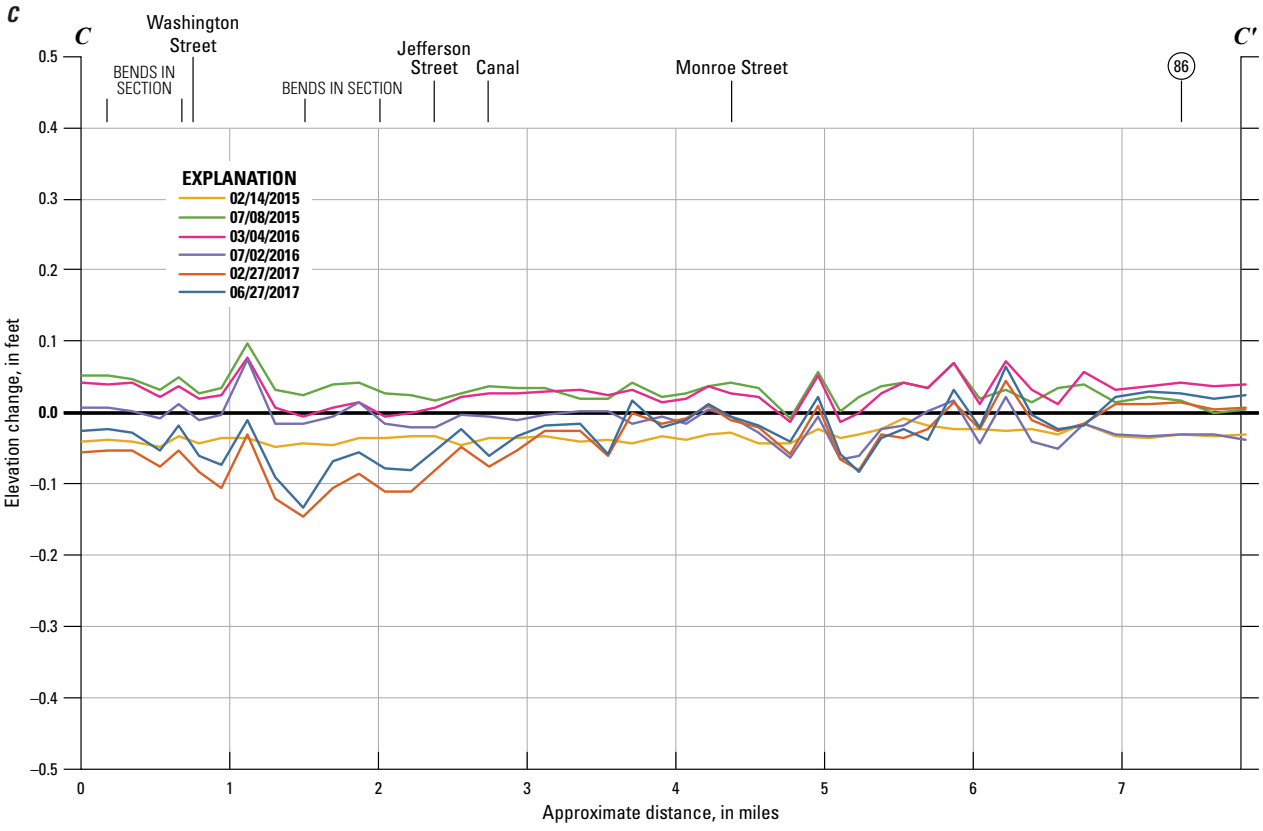

Figure 9. —Continued

A series of deformation profiles (section C–C') have been constructed for a 7.8 mi (12.6 km) stretch of Avenue 52 in the La Quinta area, as was done in Sneed and others (2014; figs. 9*A*, 9*C*). Maximum subsidence of 0.13 ft (41 mm) was approximately 0.9 mi (1.4 km) west of Jefferson St. between December 28, 2014, and June 27, 2017 (fig. 9*C*), corresponding to a maximum rate of 0.05 ft/yr (16 mm/yr). The location of this maximum subsidence magnitude was about 0.5 mi (0.8 km) west of the location of maximum subsidence during 1995–2010, and the subsidence rate for the recent period was about half the subsidence rate during 1995–2010 (Sneed and others, 2014; figs. 9*A*, 9*C*).

Long-term subsidence along the Coachella branch of the All-American Canal was analyzed in detail because subsidence had caused sags in the canal that adversely affected flow, loss of freeboard, and misalignment of the water surface and the concrete liner in some areas (Steve Bigley, Coachella Valley Water District, oral commun., 2013). These problems prompted the CVWD to reroute a section of the canal during 2014–15. The effects of a sag in a channel are increased flow velocity in the upstream end, decreased velocity in the middle, and loss of flow velocity immediately downstream of the sag. If the sag is sufficiently deep, the height of the channel banks at the sag might not be sufficient to raise the water surface in the canal enough to maintain flow velocity downstream of the subsided reach. Reduced flow velocity reduces the volume of water that can be delivered through the canal.

A series of deformation profiles, consisting of 41 selected pixels covering about 27 mi (43 km) of the canal upstream from Lake Cahuilla, have been constructed to analyze the differential subsidence along the canal, as was done in Sneed and others (2014; fig. 10*A*, 10*B*). InSAR results for December 28, 2014, to June 27, 2017, indicate subsidence of as much as 0.25 ft (78 mm) along the 5.6 mi (9 km) reach upstream of Lake Cahuilla; results for the next 19.3 mi (31 km) upstream indicate as much as about 0.07 ft (22 mm) of uplift; results for the final 1.9 mi (3 km) indicate about 0.03 ft (8 mm) of subsidence (fig. 10). The maximum subsidence of 0.25 ft (78 mm) during 2014–17 was just south of the 90-degree bend in the canal about 2.5 mi (4 km) upstream from Lake Cahuilla, corresponding to a maximum rate of 0.1 ft/yr (31 mm/yr). The location of this maximum subsidence was about 0.3 mi (0.5 km) downstream from the location of maximum subsidence during 1995–2010, and the rate was about the same (Sneed and others, 2014).

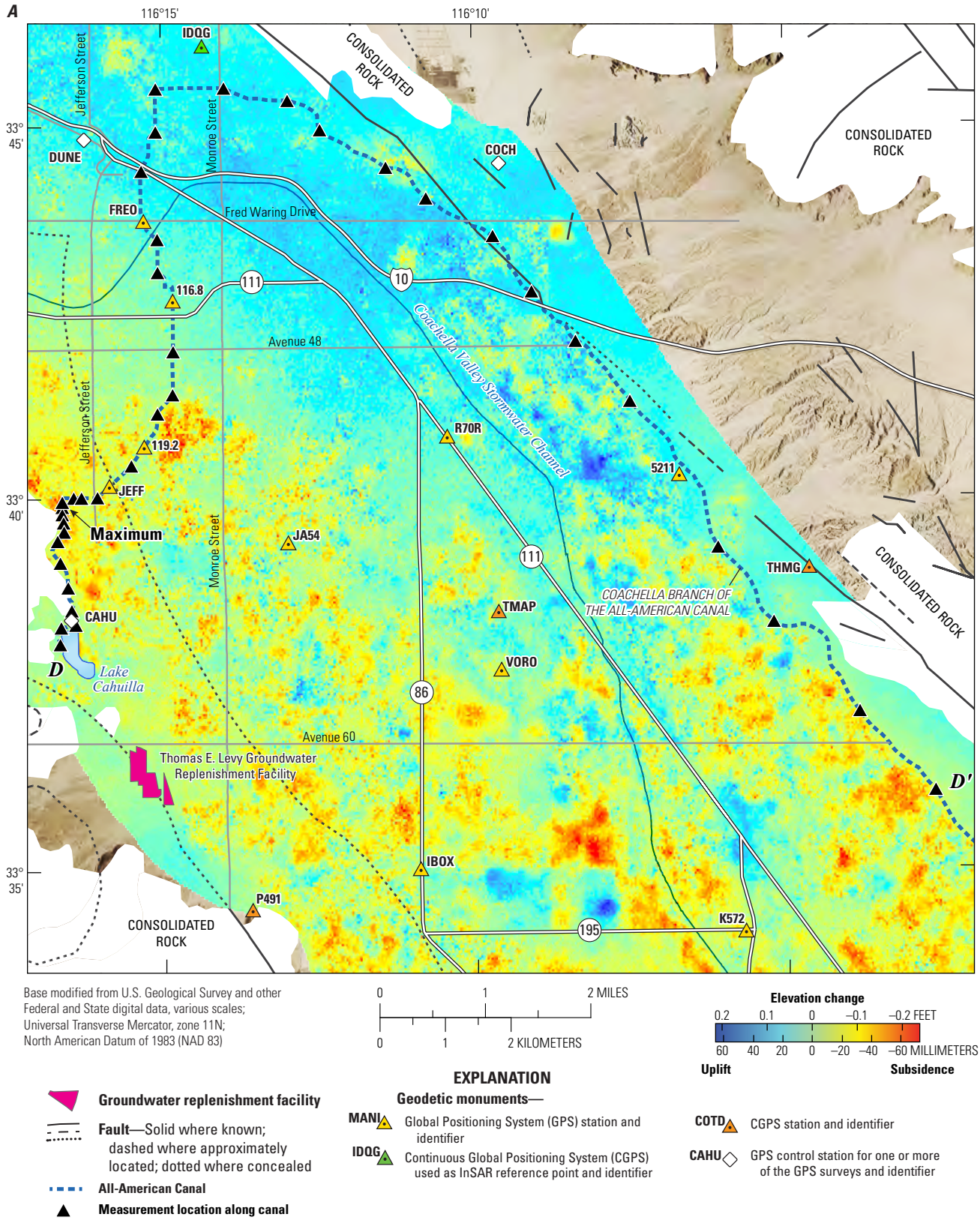

Figure 10. Coachella branch of the All-American Canal, Coachella Valley, California: *A*, location of 41 measurement locations, 13 Global Positioning System (GPS) stations, 4 continuous Global Positioning System (CGPS) stations, faults, and consolidated rock, overlain on the 2014–17 stacked interferogram; and *B*, deformation derived from the 41 locations along the canal since December 28, 2014.

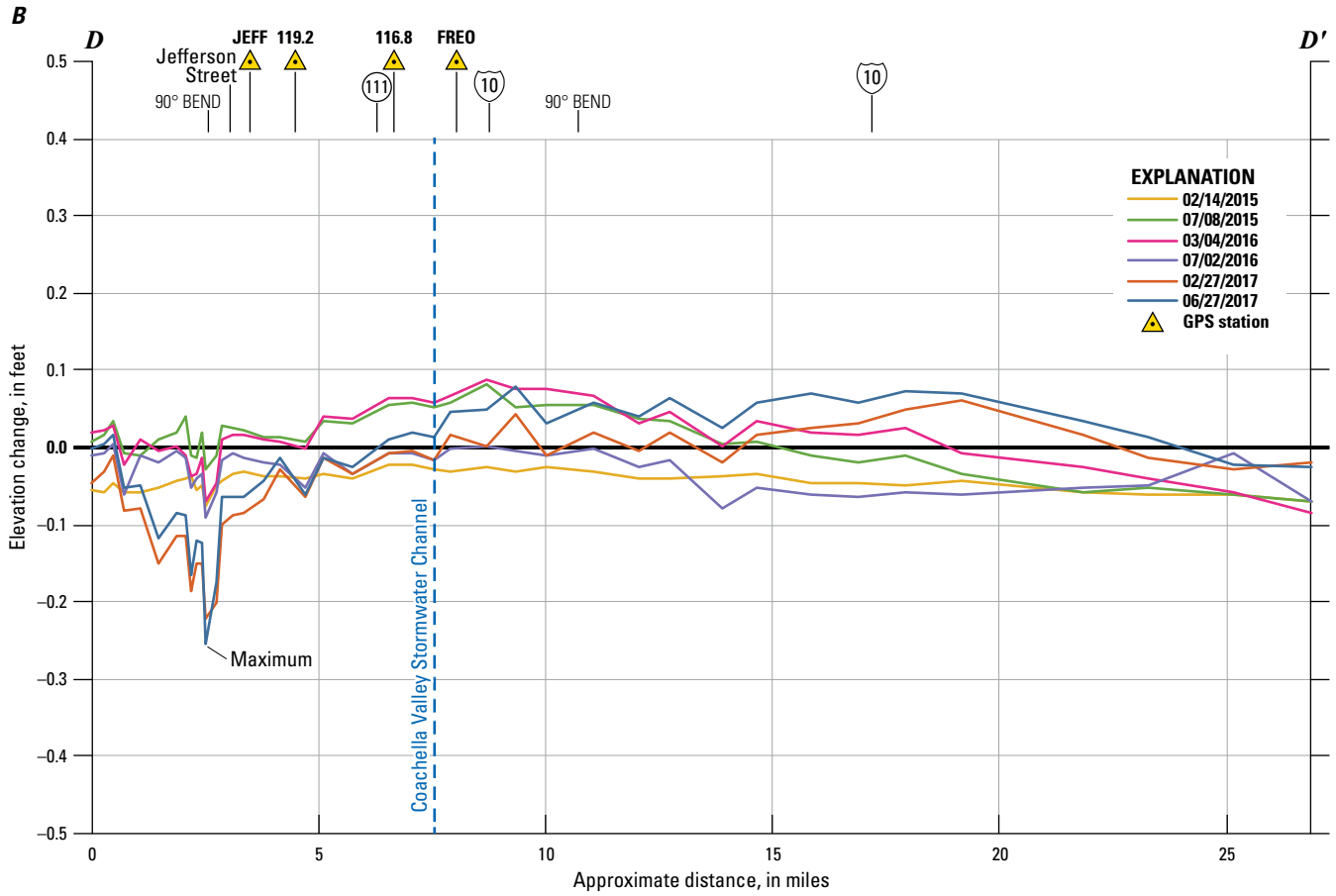

Figure 10. —Continued

Comparison of Global Positioning System Surveys and Interferometric Synthetic Aperture Radar Results

Subsidence magnitudes derived from GPS surveys and InSAR measurements were compared for the 13 geodetic monuments included in the area covered by TerraSAR-X data processed for this study (116.8, 119.2, CAHU, DUNE, FREO, IBOX, JA54, JEFF, JOHN, MANI, OSDO, R70R, and VORO; fig. 11). GPS and InSAR measurements were not compared at the other 11 monuments (5211, C101, COCH, DEEP, G70, K572, K70, MAGF, P572, PAIN, and TOR2) because they were not covered by TerraSAR-X data processed for this study. The coverage by TerraSAR-X was important for comparison because Sentinel-1A data only overlap the GPS survey data results for about 9 months (December 2014–September 2015), whereas TerraSAR-X data overlap the GPS survey data results for about 21 months (August 2010–May 2012). Total coverage for the two satellites is 30 months, or 2.5 years. The large data gap between the two satellite datasets—May 16, 2012, to December 28, 2014 (2.6 years)—is about half of the period represented by the GPS survey data (5.1 years). Consequently, if deformation rates were steady during these 5.1 years, then it would be expected that the InSAR-derived deformation magnitudes would be about half of the GPS-derived deformation magnitudes. As already discussed in this report, however, the rates computed from InSAR data indicated that deformation rates were not steady—subsidence rates generally decreased from 2010–12 to 2014–17.

Magnitudes of GPS-derived elevation changes at the monuments are given in table 1. Magnitudes of elevation changes from InSAR data at GPS monuments for August 25, 2010–September 18, 2015, were determined to closely correspond with the timing of the GPS surveys (August 25, 2010–September 30, 2015). Because August 25, 2010, was not a SAR acquisition date, however, no interferograms are available for that date. To compensate for this temporal mismatch and to enable a better comparison between the deformation magnitudes obtained from the InSAR and GPS Survey analyses, the linear estimate of the potential deformation between July 28, 2009, and August 25, 2010 (393 days), was subtracted from the interferogram for the longer period (528 days, July 28, 2009–January 7, 2011).

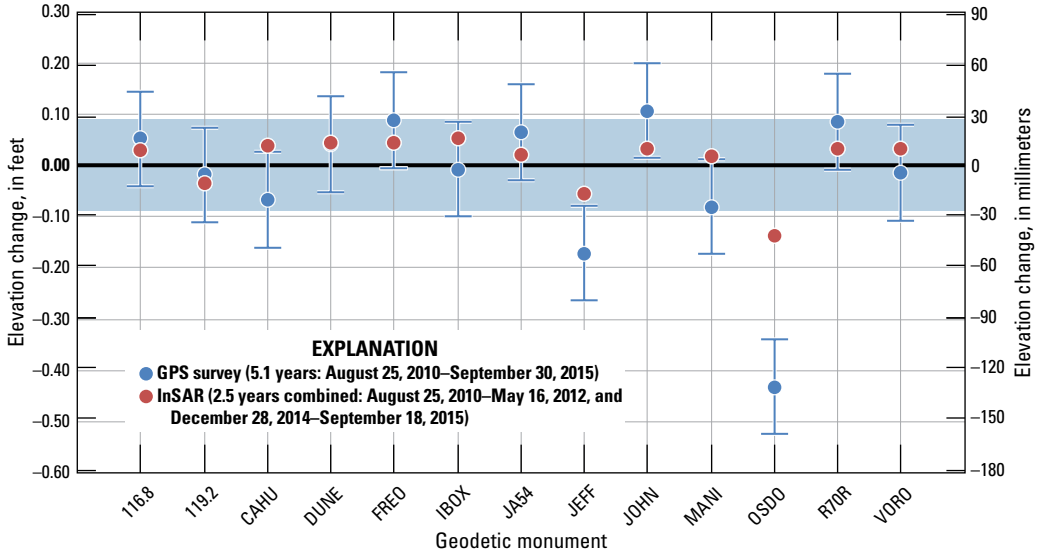

Figure 11. Comparison of elevation change from Global Positioning System (GPS) surveys and interferometric synthetic aperture radar image analysis for 13 geodetic monuments during 2010–15, Coachella Valley, California. The elevation-change uncertainty associated with the GPS surveys in 2010 and 2015 (±0.09 ft or ±28 mm) is represented by the error bars, and the blue shaded area indicates stability during 2010–15 according to the GPS survey results (that is, the elevation change was less than ±0.09 ft or ±28 mm).

Of the 13 monuments for which measurements were compared, the GPS results indicated that 10 monuments were stable (change was within the expected error of the GPS survey results, which was ±0.09 ft or ±28 mm) and that 3 deformed between 2010 and 2015—stations JEFF and OSDO subsided, whereas JOHN uplifted. The InSAR results for the 10 stable monuments fell within, or nearly within, the expected error of the GPS results, indicating strong agreement (fig. 11). As expected, more subsidence was measured at JEFF and OSDO using the 5.1-year GPS record than the 2.5-year InSAR record, and more uplift was measured at JOHN using the 5.1-year GPS record than the 2.5-year InSAR record (fig. 11). At JEFF, GPS results indicated 0.17 ft (52 mm) of subsidence, and InSAR results indicated 0.06 ft (17 mm) of subsidence. At OSDO, GPS results indicated 0.43 ft (132 mm) of subsidence, and InSAR results indicated 0.14 ft (42 mm) of subsidence. At JOHN, GPS results indicated 0.11 ft (33 mm) of uplift, and InSAR results indicated 0.03 ft (10 mm) of uplift. These results show that InSAR-derived magnitudes were about one-third of the GPS-derived magnitudes, indicating good agreement considering (1) the InSAR measurements represent about half the time span that the GPS measurements represent; (2) the subsidence rates decreased during 2010–15; (3) the expected error of the InSAR measurements (±0.05 ft or ±15 mm); and (4) the expected error in the GPS data (±0.09 ft or ±28 mm; fig. 11).

Groundwater Levels

The three sections of this report that follow describe groundwater levels throughout the Coachella Valley, near GPS stations, and in the three subsidence areas detected by InSAR. Groundwater-level data were provided by the CVWD.

Groundwater Levels Throughout the Coachella Valley

Groundwater levels throughout the Coachella Valley, from near the Whitewater River Groundwater Replenishment Facility in the north to the Salton Sea in the south, generally fluctuated seasonally or in response to recharge operations and were stable or rose annually since about 2010 (fig. 12). The valley-wide stabilization and recovery of groundwater levels marks a reversal in decades-long trends of decline that brought groundwater levels to historical low levels in about 2010. This stabilization and recovery correspond to the timing of various surface-water and conservation projects implemented by the CVWD to increase recharge or reduce reliance on groundwater (figs. 13, 14). The multi-pronged water-resource management approach includes agricultural and urban (recreational, residential, and commercial) water users in the Coachella Valley.

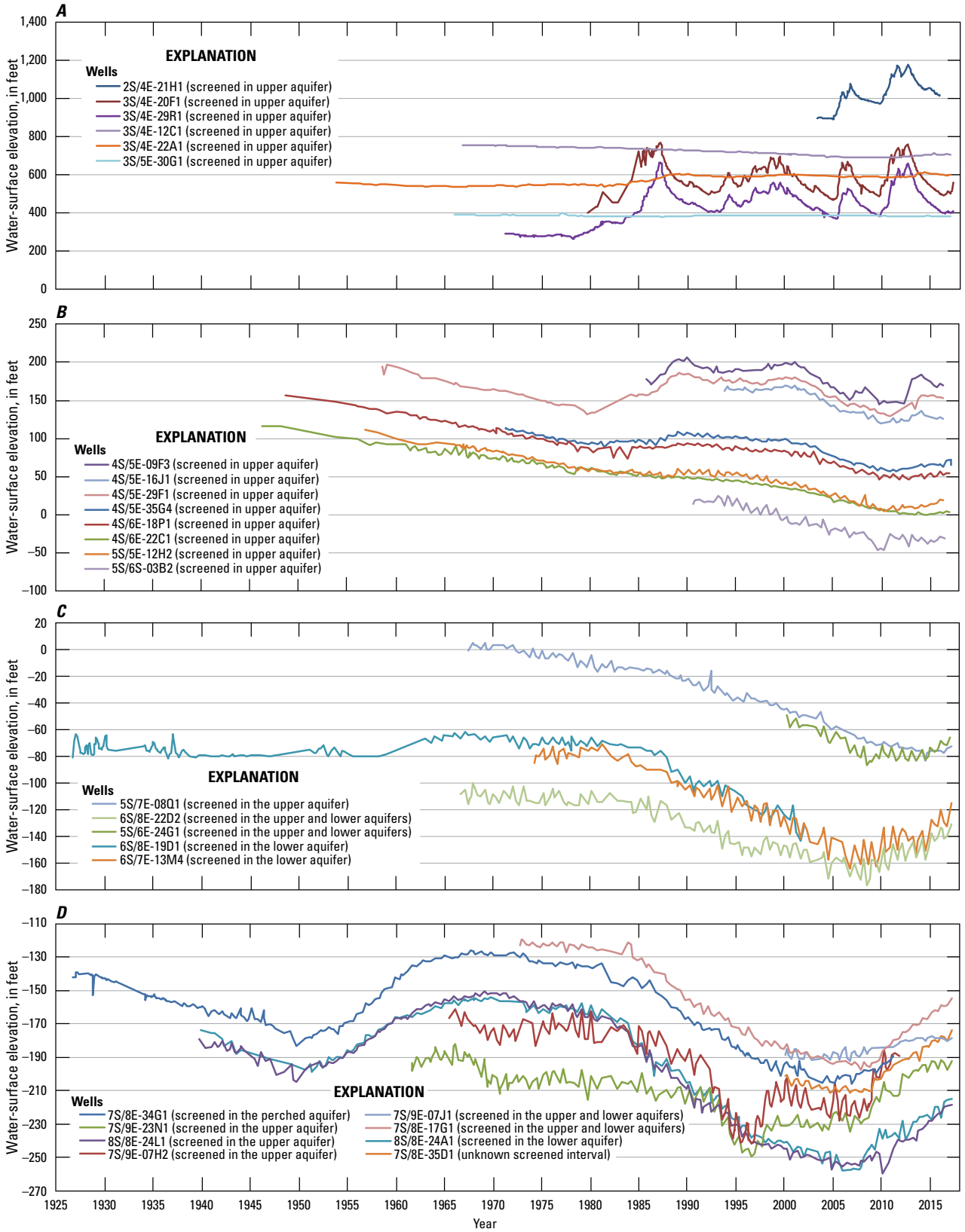

Figure 12. Water-surface elevations in Coachella Valley, California, 1925–2017, for wells in *A*, the northern part of the valley; *B*, the north-central part of the valley; *C*, the south-central part of the valley; and *D*, the southern part of the valley. See figure 5*A* for locations of wells. Water-surface elevation data are referenced to the National Geodetic Vertical Datum of 1929 and were provided by the Coachella Valley Water District.

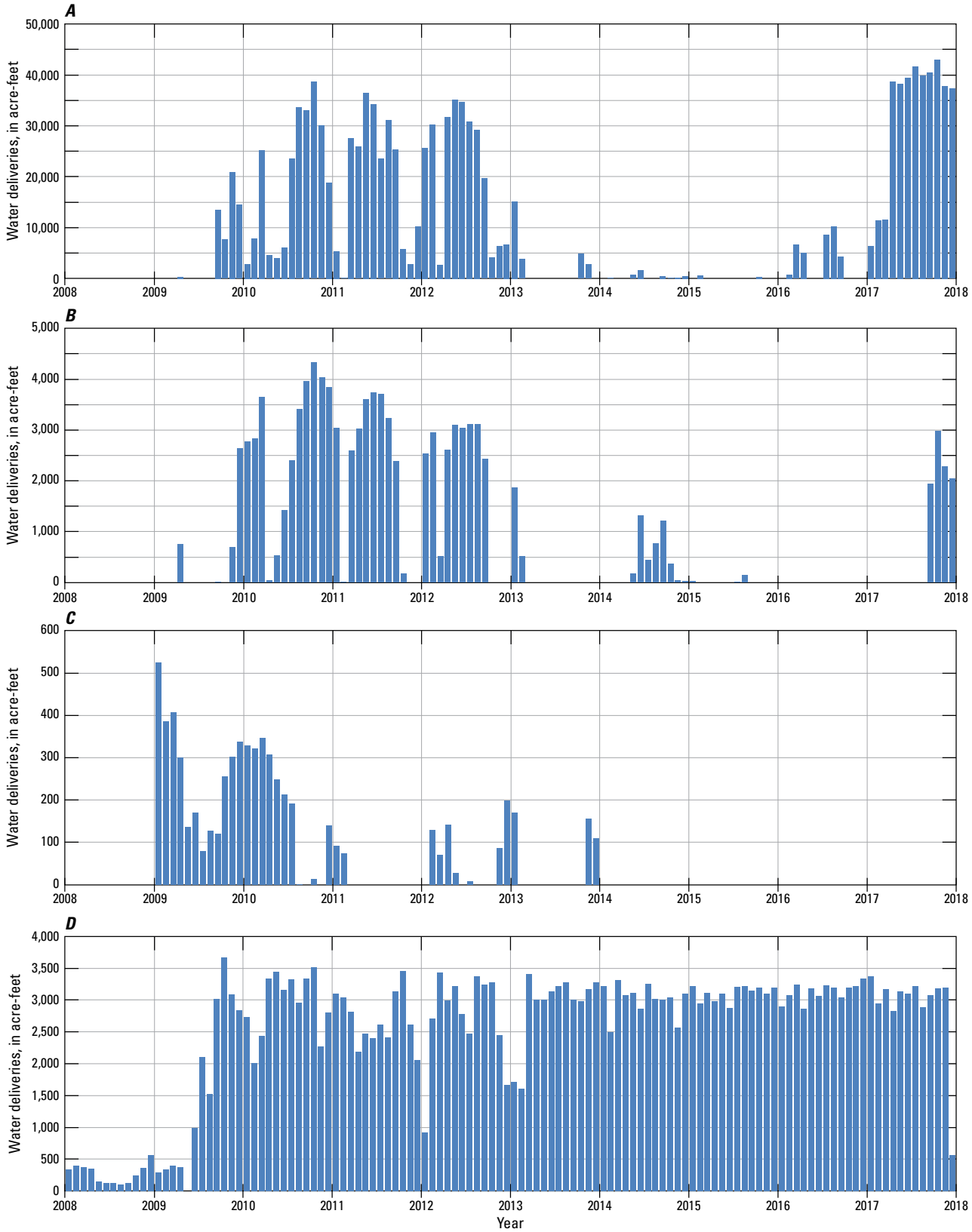

Figure 13. Water deliveries to groundwater replenishment facilities in Coachella Valley, California, 2008–17, for *A*, Whitewater River Groundwater Replenishment Facility; *B*, Mission Creek Groundwater Replenishment Facility; *C*, Pilot Martinez Canyon Groundwater Replenishment Facility; and, *D*, Thomas E. Levy Groundwater Replenishment Facility. See figure 5*A* for locations of groundwater replenishment facilities.

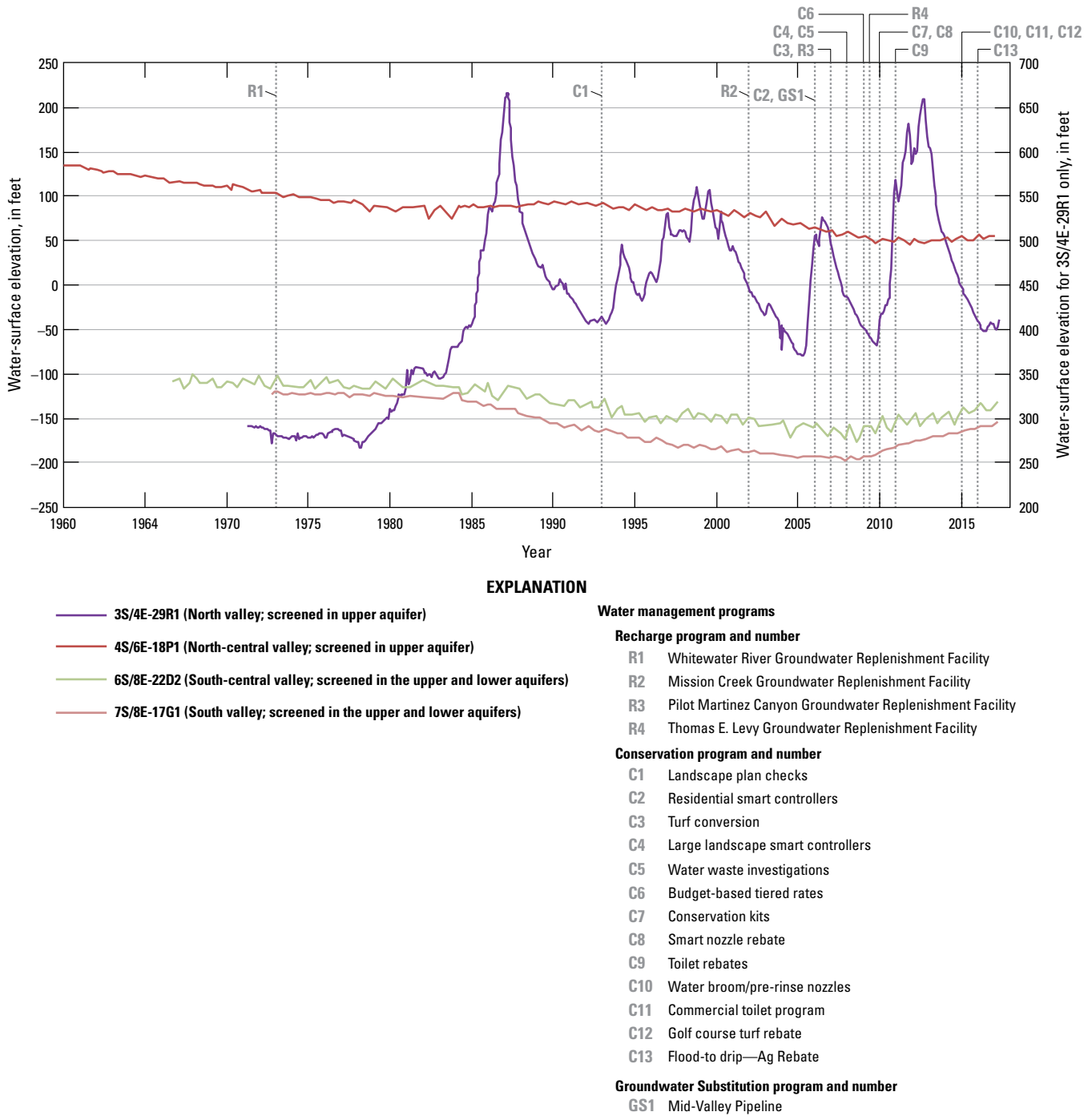

Figure 14. Water-surface elevations for representative wells in the northern, north-central, south-central, and southern parts of Coachella Valley, California, and implementation timeline of managed aquifer-recharge, conservation, and groundwater-substitution programs, 1960–2017. See figure 5*A* for locations of wells. Water-surface elevation data are referenced to the National Geodetic Vertical Datum of 1929. Water-surface elevation data and implementation timeline of water-management programs were provided by the Coachella Valley Water District.

In the largely unpopulated northernmost areas of the Coachella Valley, north of Palm Springs (fig. 1), recharge operations at the Whitewater River and Mission Creek Groundwater Replenishment Facilities (figs. 5*A*, 13*A*, 13*B*) had marked effects on groundwater levels in wells near the facilities as early as the 1980s (2S/4E-21H1, 3S/4E-20F1, and 3S/4E-29R1 in fig. 12*A*; 3S/4E-29R1 in fig. 14). Groundwater levels in wells farther away were less affected because of the greater distance; because they were not hydrologically downgradient; or because they were otherwise hydrologically disconnected, such as by groundwater-flow barriers including faults (3S/4E-12C1, 3S/4E-22A1, and 3S/5E-30G1 in fig. 12*A*; fig. 5*A*). Relatively small amounts of water were delivered to these two facilities during 2013–16 compared to 2010–12 and 2017 (fig. 13*A*, 13*B*), which is reflected in the lower groundwater levels (3S/4E-29R1; fig. 14).

In the more urbanized part of the valley stretching from Palm Springs to La Quinta and Coachella, the groundwater-level responses to recharge operations were less, and the seasonal and longer term trends were more obvious (figs. 12*B*, 12*C*, 4S/6E-18P1, and 6S/8E-22D2 in fig. 14). Although seasonal fluctuations are evident in the groundwater-level records throughout this area, an important feature is the recovery of groundwater levels starting about 2010, after decades of decline that had brought groundwater levels to their lowest levels. Such largely urbanized areas are where many of the conservation programs that have been implemented by the CVWD are expected to be more commonly adopted, such as the golf course turf rebate (starting in 2015), residential and large landscape smart controllers (starting in 2006 and 2008, respectively), nozzle and toilet rebates (starting in 2010 and 2011, respectively), and turf conversion (starting in 2007; Ivory Reyburn, Coachella Valley Water District, written commun., 2017). The implementation of budget-based, tiered rates in 2009 most closely coincides with the reversal of long-term groundwater-level decline in the area. In addition, many new connections from golf courses, resorts, and other businesses to the Mid-Valley Pipeline Project since 2006 resulted in surface and recycled water substitution for groundwater.

In the largely rural southernmost area of the Coachella Valley, south of La Quinta and Coachella, groundwater-level seasonal fluctuations were superimposed on long-term trends of declines and recoveries since the 1920s (fig. 12*D*). By about 2010, the groundwater level in many wells was at the lowest recorded level. Since 2010, however, groundwater levels have recovered markedly—even more than the recovery in areas to the north. The implementation of substantially increased recharge operations at the Thomas E. Levy Groundwater Replenishment Facility starting in 2009 coincided with the abrupt reversal of long-term groundwater-level declines in the area (figs. 12*D*, 13*D*; 7S/8E-17G1 in fig. 14). The volume of water delivered and the proximity and hydrologic connection from monitored wells to this groundwater replenishment facility, as well as the local aquifer-system structure and composition, influenced the timing and magnitude of these groundwater-level rises (figs. 12*D*, 13*D*). Unlike recharge operations at the Whitewater River and Mission Creek Groundwater Replenishment Facilities, water deliveries at the Thomas E. Levy Groundwater Replenishment Facility began in earnest in 2009 and were fairly stable during 2010–17 (figs. 13*A*, 13*B*, 13*D*). The Pilot Martinez Canyon Groundwater Replenishment Facility has recharged substantially smaller volumes of water compared to the other replenishment facilities and has not been operated since 2013 (fig. 13*C*). This rural, southernmost area of the valley is where the flood-to-drip agricultural rebate conservation program was implemented by the CVWD starting in 2016 that has since been discontinued.

Groundwater Levels Near Global Positioning System (GPS) Stations

Groundwater levels in wells near GPS stations that subsided, were stable, or uplifted between 2010 and 2015 generally showed seasonal fluctuations superimposed on longer term stability or increase (figs. 3, 4). The stability or increase generally was preceded by decades of decline. In the southern part of the geodetic network, where uplift was measured (near K572, JOHN, P572, and TOR2; fig. 3), groundwater levels generally increased by about 5–30 ft (1.5–9 m) between 2010 and 2015 (figs. 4*R*, 4*S*, 4*V*, 4*X*). Water-level increases in this area tended to be larger and started sooner than in other areas of the geodetic network. These larger groundwater-level increases are associated with increased recharge at the Thomas E. Levy Groundwater Replenishment Facility starting in mid-2009 (fig. 13*D*). In the northwestern area of the geodetic network, where subsidence was measured at three monuments (MAGF, OSDO, and JEFF; fig. 3), groundwater-level increases were more modest and started later (after about 2013) than in other areas of the network (figs. 4*C*, 4*F*, 4*L*). In the northeastern, central, and southeastern areas of the geodetic network (near DUNE, COCH, FREO, MANI, 116.8, R70R, 119.2, DEEP, 5211, JA54, CAHU, VORO, PAIN, IBOX, C101, K70, and G70; fig. 3), where land-surface elevations were fairly stable, groundwater levels generally showed seasonal fluctuations superimposed on longer term groundwater-level stability and recovery during 2010–15 (figs. 4*A*, 4*B*, 4*D*, 4*E*, 4*G*–4*K*, 4*M*–4*Q*, 4*T*–4*U*, 4*W*).

Groundwater Levels in the Three Subsidence Areas Detected by InSAR

Three areas (Palm Desert, Indian Wells, and La Quinta) had substantial subsidence prior to 2010 and much smaller subsidence magnitudes during 2010–17, as measured using InSAR. These areas and other localized areas in the southern Coachella Valley were in or near areas where groundwater pumping generally caused seasonal groundwater-level fluctuations and longer term groundwater-level declines prior to 2010 (figs. 7*B,* 8*B,* 9*B,* 12*C,* 12*D*). After about 2010 when the lowest water levels were recorded, however, most groundwater levels near Palm Desert (fig. 7*B*), Indian Wells (fig. 8*B*), La Quinta (fig. 9*B*), and in areas to the south (figs. 12*C*, 12*D*) showed water-level stability or recovery.

Relation of Land Subsidence and Groundwater Levels

Throughout much of the Coachella Valley, groundwater-level recoveries during 2010–17 coincided with uplift or substantially reduced subsidence rates. In the mostly rural northern parts of the valley, fluctuations in groundwater levels were driven partly by recharge operations at the Whitewater River and Mission Creek Groundwater Replenishment Facilities (figs. 13*A*, 13*B*) and partly by other anthropogenic and natural processes. Groundwater-level changes from late 2014 to mid-2017 corresponded to the InSAR results shown in figure 5*A* and were varied. Some wells indicated groundwater-level rise, while other wells indicated stability or decline. During 2010–17, most groundwater levels remained above historical lows (for example, 2S/4E-21H1, 3S/4E-20F1, and 3S/4E-29R1 in figure 12*A*). The small magnitude of land-surface uplift measured between 2014 and 2017 (as much as 0.20 ft or 60 mm) is consistent with elastic expansion of an unconsolidated aquifer system where groundwater levels have risen. If some depth intervals of the Coachella Valley aquifer system compacted in response to groundwater-level decline, then the compaction rate in these depth intervals was outpaced by the expansion rate in other depth intervals of the aquifer system.

In the more urbanized areas of the valley stretching from Palm Springs to La Quinta and Coachella, groundwater-level response to recharge operations at the Whitewater River Groundwater Replenishment Facility was muted, and seasonal and longer term trends in groundwater-levels and land-surface deformation became more prevalent (figs. 4*A–I*, 4*K–M*, 7*B,* 8*B,* 12*B*). Southward of La Quinta and Coachella, the land use becomes more rural, and the effects of recharge operations at the Thomas E. Levy Groundwater Replenishment Facility are shown superimposed on the seasonal and longer term trends in groundwater-levels and land-surface deformation (figs. 4*O*, 4*Q–V*, 4*X*, 5*A,* 12*C,* 12*D,* 13*D*). These recharge operations appear to have had a marked effect on groundwater levels and associated aquifer-system deformation.

Subsidence and declining groundwater levels throughout the southern Coachella Valley were simultaneous prior to about 2010. Reduced subsidence rates or uplift and recovering groundwater levels throughout the valley were simultaneous after about 2010. These observations indicate that deformation of the aquifer system caused by groundwater-level changes likely is causing subsidence and uplift. Although aquifer-system deformation likely is the cause of the observed land-surface elevation changes, tectonically induced vertical, crustal movements in the region also could have played a role. Because of the localized character of the subsidence signals, however, which are typical of subsidence caused by localized pumping, and because the CGPS stations on the margins of the valley (fig. 1) that were used for the GPS network adjustments were fairly stable between 1996 and 2015, vertical, crustal movement probably did not contribute much to the elevation changes measured at other geodetic monuments in the network or measured using InSAR elsewhere in the valley.

Between 1995 and 2010, groundwater levels fluctuated seasonally and declined annually in association with fairly steady rates of land subsidence in some areas, regardless of season. Thick aquitards in the Palm Desert, Indian Wells, and the northern part of the La Quinta area cause residual compaction that could be a substantial part of total compaction in these areas (Sneed and others, 2014). Since 2010, groundwater levels have fluctuated seasonally and recovered annually in these areas and were associated with periods of uplift and of subsidence, which resulted in net subsidence. The subsidence rates have not only slowed since 2010, but generally slowed throughout 2010–17. Net subsidence during a period of groundwater-level recovery likely is a result of an imbalance between the elastic expansion of the coarser grained aquifers and thin, quickly equilibrating aquitards and the ongoing, residual compaction of the thick, slowly draining aquitards. This mixed mechanical response of the aquifer system indicates that the stresses causing compaction of the thicker aquitards are not represented by the measured stresses (water levels). Because of the impedance of groundwater flow in the aquitards, hydraulic head in the aquifers may not have changed throughout a significant part of the thicker aquitards. If this is the case, subsidence rates are expected to slow asymptotically if groundwater levels continue to recover or stabilize.

Future Monitoring

Monitoring in the Coachella Valley is a proven way to track groundwater levels and land subsidence or uplift. The CVWD has been, and continues to be, involved in several agreements and projects that increase recharge or reduce reliance on groundwater. Continued monitoring could track the effect these management actions have on the aquifer system. Colorado River water allocations are changing. Complex water transfers to implement the Quantification Settlement Agreement are ongoing. Mitigation measures including budget-based tiered rates, managed aquifer-recharge projects, and groundwater substitution for irrigation primarily for golf courses by the Mid-Valley Pipeline Project are being instituted, all of which decrease the reliance on groundwater (Coachella Valley Water District, 2012). Phase 1 of the Palm Desert Groundwater Replenishment Facility, which consists of recharge ponds along the Whitewater Stormwater Channel in Palm Desert, began recharge operations in early 2019, with the management goal of mitigating the continued, albeit slowed, groundwater-level declines and associated subsidence in the Palm Desert and Indian Wells areas (Coachella Valley Water District, 2019). Phase 2 of the Palm Desert Groundwater Replenishment Facility involves construction of additional recharge ponds in the Whitewater Stormwater Channel in Palm Desert (Coachella Valley Water District, 2017).

The GPS surveys at 5-year intervals have been, and are expected to continue to be, an adequate frequency to track land-surface elevation changes at fixed-station locations, allowing sufficient time for meaningful changes to be detected, considering the expected error (±0.09 ft or ±28 mm) when comparing GPS results from repeat surveys. A GPS survey in or about 2020 could clarify the initial effects of the Palm Desert Groundwater Replenishment Facility actions, additional conversions from groundwater to canal water (largely golf courses), and other new water-management strategies. Processing of spatially detailed InSAR-derived maps of ground displacements, however, could continue annually, or more frequently depending on data availability, to assess land-surface deformation between the GPS surveys. Because InSAR-detected areas of subsidence overlap the GPS network, GPS network monitoring could provide validation of InSAR measurements, as in this study.

The frequency of groundwater-level measurements in the Coachella Valley could be increased to define changes better throughout the year. The wells used for measurements generally have long or multiple screens, such that the groundwater-level measurements represent a composite of groundwater levels throughout a large thickness of the aquifer system. Increasing the measurement frequency of groundwater levels in wells, and especially in piezometers, which are wells constructed with short screens and small diameters for monitoring purposes, would substantially improve analysis of the relation between changes in groundwater levels and land-surface elevations. In concert with more frequent groundwater-level measurements, frequent high-resolution measurements of aquifer-system compaction from borehole extensometers would improve the analysis of aquifer-system responses to groundwater-level changes. Information from paired extensometer and well sites would be useful for delineating depth intervals of compaction and estimating aquifer-system properties that govern groundwater flow and land subsidence. This information could be useful for constraining a numerical model of groundwater flow and aquifer-system compaction that could help quantify relations among groundwater levels, subsidence, and other geologic processes and could simulate future aquifer-system compaction and resultant land subsidence for various water-management scenarios.

Summary

Groundwater has been a major source of agricultural, recreational, municipal, and domestic water supply in the Coachella Valley since the early 1920s. Groundwater levels declined throughout the Coachella Valley from the 1920s until 1949. In 1949, the importation of surface water from the Colorado River to the southern Coachella Valley began, resulting in decreased pumping and recovery of groundwater levels in some areas. In the 1970s, the demand for water in the Coachella Valley had increased to the point that groundwater levels again declined in response to increased pumping, except in some northern areas of the valley near the Whitewater River Groundwater Replenishment Facility (fig. 12). By about 2010, however, when many groundwater levels were at historical lows, the decades-long trend of declines stopped, and groundwater levels began to stabilize or recover. The valley-wide stabilization and recovery of groundwater levels corresponded to the timing of various surface-water management and conservation projects implemented by the Coachella Valley Water District (CVWD) to increase recharge or reduce reliance on groundwater (figs. 13, 14).

During the mid-1990s when groundwater levels had been declining for decades, concerns were raised that the declines could cause subsidence. As a result, the U.S. Geological Survey and the CVWD began a series of cooperative studies to determine the location, extent, and magnitude of subsidence in the southern Coachella Valley. Results of the first study indicated that the land surface had subsided about 0.5 feet (ft) or 150 millimeters (mm) between 1930 and 1996 (Ikehara and others, 1997). Results of the next several studies, covering 1993–2010, indicated as much as about 2 ft (600 mm) of local subsidence along the west side of the valley in and near the communities of Palm Desert, Indian Wells, and La Quinta, and smaller magnitudes were measured throughout the southern Coachella Valley (Sneed and others, 2014). Beginning in about 2010, however, groundwater conditions had begun to change—groundwater levels began to stabilize or recover, and land subsidence stopped or slowed substantially almost everywhere in the southern Coachella Valley. Additionally, the northern Coachella Valley was included in this latest study. This report presents the results and interpretations of the Global Positioning System (GPS) data collected at geodetic monuments in the southern Coachella Valley during surveys in 2010 and 2015 and shows detailed maps of vertical land-surface changes detected by analyzing interferometric synthetic aperture radar (InSAR) data collected throughout the Coachella Valley from 2010 to 2017. Groundwater levels for 2010–17 also were examined and compared with the GPS measurements and the InSAR-generated maps to determine if the vertical changes in land surface could be related to the changes in groundwater levels.

The GPS measurements have been useful for determining elevation changes at specific locations, and InSAR measurements have been more useful for determining elevation changes for the entire valley. The GPS measurements taken at 24 geodetic monuments in August 2010 and September 2015 indicated that the land-surface elevation was stable at 17 monuments but changed at 7 monuments during those 5 years (table 1). Subsidence ranged 0.17–0.43 ±0.09 ft (52–132 ±28 mm) at three monuments, and uplift ranged 0.11–0.18 ±0.09 ft (33–54 ±28 mm) at four monuments between 2010 and 2015. At two of the monuments that subsided, the subsidence rates had decreased between 2010 and 2015 from those computed between 2005 and 2010 (figs. 4*C*, 4*F*). Data prior to 2010 were not available for the third monument that subsided; thus, its 2010–15 subsidence rate could not be compared to an earlier period (fig. 4*L*). At three monuments that uplifted between 2010 and 2015, data collected in 2005 and 2010 indicated stability (figs. 4*R*, 4*S*, 4*V*). Data prior to 2010 were not available for the fourth monument that uplifted; thus, its 2010–15 uplift rate could not be compared to an earlier period (fig. 4*X*).

The InSAR analyses for December 28, 2014–June 27, 2017, indicated that land surfaces uplifted as much as 0.20 ft (60 mm) near the Whitewater River Groundwater Replenishment Facility and subsided as much as about 0.26 ft (80 mm) in the La Quinta area and by lesser magnitudes in Palm Desert, Indian Wells, and other localized areas in the largely rural southern Coachella Valley (figs. 5–10). All three of these urban areas were identified in previous reports covering periods during 1993–2010 (Sneed and others, 2014). The comparison of 2014–17 subsidence rates with those derived for that earlier period, however, generally indicates a substantial slowing of subsidence. The InSAR analyses indicated that the northern Coachella Valley generally was stable or uplifted during 2014–17.

Water levels in wells near the subsiding monuments, in and near the three subsiding areas shown by InSAR and throughout the valley, generally indicate seasonal fluctuations and longer-term stability or rising groundwater levels since about 2010 (figs. 4, 7*B,* 8*B,* 9*B,* 12). The rising groundwater levels mark a reversal in the trend of groundwater-level declines during the preceding decades (fig. 12). Groundwater-level recoveries previously were observed beginning in about 2009 for parts of the La Quinta area and were associated with increased recharge operations at the Thomas E. Levy Groundwater Replenishment Facility and decreased pumping (Sneed and others, 2014; figs. 13, 14). Continued valley-wide stabilization and recovery of groundwater levels since then clearly marks a reversal in a decades-long trend of declines that brought many groundwater levels to historical lows in about 2010. This important change likely is a result of the combined effects of various projects designed and implemented by the CVWD to increase recharge and reduce groundwater pumping (figs. 13, 14). This trend reversal provides insights into aquifer-system mechanics. Although many areas have stopped subsiding and some have even uplifted, the few areas that did subside during 2010–17, albeit at a slower rate, indicate a mixed aquifer-system response. Subsidence when groundwater levels are stable or recovering indicates potential residual compaction in thicker aquitards. At the same time, coarser grained materials and thinner aquitards might have expanded as groundwater levels recovered.

Groundwater conditions in the Coachella Valley—including some of the historically most overdrafted areas—have improved markedly since about 2010. The valley-wide stabilization and recovery of groundwater levels, and the reduced rates or cessation of subsidence, corresponded to the timing of various surface-water and water-conservation projects implemented by the CVWD to increase recharge or to reduce reliance on groundwater (figs. 13, 14). The multi-pronged water-resource management approach includes agricultural and urban (recreational, residential, and commercial) water users of the Coachella Valley. Colorado River and recycled water have been substituted for groundwater for some agricultural, golf course, and other non-potable water uses. Conservation programs including smart controllers, nozzle and toilet rebates, turf conversion, and budget-based tiered rates largely target urban water use, but golf-course turf rebates and flood-to-drip rebates include golf course and agricultural water users as well. Colorado River and State Water Project water have been recharged to the groundwater basin through managed groundwater replenishment facilities, and a new groundwater replenishment facility in Palm Desert has recently (2019) begun operations. Continued monitoring could track the effects that management actions based on these programs and projects have on the aquifer system. Future monitoring also would help inform the CVWD and others about the effects of future mitigation measures, as has been done using the results of previous studies.

References Cited

Ajala, R., Persaud, P., Stock, J.M., Fuis, G.S., Hole, J.A., Goldman, M., and Scheirer, D., 2019, Three-dimensional basin and fault structure from a detailed seismic velocity model of Coachella Valley, Southern California: Journal of Geophysical Research—Solid Earth, v. 124, no. 5, p. 4728–4750, https://doi.org/10.1029/2018JB016260.

Atwater, T., 1970, Implications of plate tectonics for the Cenozoic tectonic evolution of western North America: Geological Society of America Bulletin, v. 81, no. 12, p. 3513–3536, https://doi.org/10.1130/0016-7606(1970)81[3513:IOPTFT]2.0.CO;2.

Bawden, G.W., Sneed, M., Stork, S.V., and Galloway, D.L., 2003, Measuring human-induced land subsidence from space: U.S. Geological Survey Fact Sheet 069–03, 4 p., https://doi.org/10.3133/fs06903.

California Department of Water Resources, 1964, Coachella Valley investigation: California Department of Water Resources Bulletin 108, 145 p.

California Department of Water Resources, 1979, Coachella Valley area well standards investigation: Los Angeles, California Department of Water Resources, Southern District, 40 p.

Coachella Valley Water District, 2012, Coachella Valley water management plan 2010 update, final report: Coachella Valley Water District, 286 p., accessed February 12, 2020, at http://www.cvwd.org/DocumentCenter/View/1321/Coachella-Valley-Water-Management-Plan-Final-Report-PDF?bidId=.

Coachella Valley Water District, 2017, Palm Desert groundwater replenishment project draft environmental impact report SCH#2017041072: Coachella Valley Water District, accessed April 7, 2020, at http://www.cvwd.org/ArchiveCenter/ViewFile/Item/638.

Coachella Valley Water District, 2019, CVWD celebrates replenishment milestone: Coachella Valley Water District, accessed April 7, 2020, at https://www.cvwd.org/CivicAlerts.aspx?AID=283.

Coachella Valley Water District, undated, Quantification settlement agreement—Water for the future: Coachella Valley Water District, accessed February 11, 2020, at http://waterforthefuture.org/.

Crowell, B.W., Bock, Y., Sandwell, D.T., and Fialko, Y., 2013, Geodetic investigation into the deformation of the Salton Trough: Journal of Geophysical Research—Solid Earth, v. 118, no. 9, p. 5030–5039, https://doi.org/10.1002/jgrb.50347.

Fuis, G.S., and Mooney, W.D., 1990, Lithospheric structure and tectonics from seismic-refraction and other data, chap. 8 *of* Wallace, R.E., ed., The San Andreas Fault System, California: U.S. Geological Survey Professional Paper 1515, p. 207–236, https://doi.org/10.3133/pp1515.

Galloway, D.L., Jones, D.R., and Ingebritsen, S.E., 1999, Land subsidence in the United States: U.S. Geological Survey Circular 1182, 177 p., https://doi.org/10.3133/cir1182.

Goldstein, R.M., and Werner, C.L., 1998, Radar interferogram filtering for geophysical applications: Geophysical Research Letters, v. 25, no. 21, p. 4035–4038, https://doi.org/10.1029/1998GL900033.

Hanson, R.T., 1989, Aquifer-system compaction, Tucson Basin and Avra Valley, Arizona: U.S. Geological Survey Water-Resources Investigations Report 88–4172, 69 p., https://doi.org/10.3133/wri884172.

Holzer, T.L., 1984, Ground failure induced by ground-water withdrawal from unconsolidated sediment: Reviews in Engineering Geology, v. 6, p. 67–106, https://doi.org/10.1130/REG6-p67.

Holzer, T.L., 1998, The history of the aquifer-drainage model, *in* Borchers, J., ed., Land subsidence—Case studies and current research, Proceedings of the Dr. Joseph F. Poland Symposium on Land Subsidence: Association of Engineering Geologists Special Publication 8, p. 7–12.

Ikehara, M.E., Predmore, S.K., and Swope, D.J., 1997, Geodetic network to evaluate historical elevation changes and to monitor land subsidence in Lower Coachella Valley, California, 1996: U.S. Geological Survey Water-Resources Investigations Report 97–4237, scale 1:63,000, 1 sheet [folded in envelope], https://doi.org/10.3133/wri974237.

Ireland R.L., Poland, J.F., and Riley, F.S., 1984, Land subsidence in the San Joaquin Valley, California, as of 1980: U.S. Geological Survey Professional Paper 437–I, 93 p., https://doi.org/10.3133/pp437I.

Langbein, J., 2008, Noise in GPS displacement measurements from Southern California and Southern Nevada: Journal of Geophysical Research, v. 113, no. B5, 12 p., https://doi.org/10.1029/2007JB005247.

Leake, S.A., and Prudic, D.E., 1991, Documentation of a computer program to simulate aquifer-system compaction using the modular finite-difference ground-water flow model: U.S. Geological Survey Techniques of Water-Resources Investigations, book 6, chap A2, 68 p., https://doi.org/10.3133/twri06A2.

Martin, P., ed., 2011, with contributions by Brandt, J., Catchings, R.D., Christensen, A.H., Flint, A.L., Gandhok, G., Goldman, M.R., Halford, K.J., Langenheim, V.E., Martin, P., Rymer, M.J., Schroeder, R.A., Smith, G.A., and Sneed, M., The source, discharge, and chemical characteristics of water from Agua Caliente Spring, Palm Springs, California: U.S. Geological Survey Scientific Investigations Report 2011–5156, 106 p., https://doi.org/10.3133/sir20115156.

McKibben, M.A., 1993, The Salton Trough rift, *in* Reynolds, R.E., and Reynolds, J., eds., Ashes, faults, and basins: San Bernardino County Museum Association Special Publication v. 93–1, p. 76–80.

Meinzer, O.E., 1928, Compressibility and elasticity of artesian aquifers: Economic Geology, v. 23, no. 3, p. 263–291, https://doi.org/10.2113/gsecongeo.23.3.263.

Meltzner, A.J., Rockwell, T.K., and Owen, L.A., 2006, Recent and long-term behavior of the Brawley Fault Zone, Imperial Valley, California—An escalation in slip rate?: Bulletin of the Seismological Society of America, v. 96, no. 6, p. 2304–2328, https://doi.org/10.1785/0120050233.

Phillips, S.P., Carlson, C.S., Metzger, L.F., Howle, J.F., Galloway, D.L., Sneed, M., Ikehara, M.E., Hudnut, K.W., and King, N.E., 2003, Analysis of tests of subsurface injection, storage, and recovery of freshwater in Lancaster, Antelope Valley, California: U.S. Geological Survey Water-Resources Investigations Report 03–4061, 122 p., https://doi.org/10.3133/wri034061.

Poland, J.F., ed., 1984, Guidebook to studies of land subsidence due to ground-water withdrawal, v. 40 of UNESCO Studies and Reports in Hydrology: Paris, France, United Nations Educational, Scientific and Cultural Organization, 305 p., 5 appendixes.

PRISM Climate Group, 2015, Precipitation data from PRISM data: PRISM Climate Group, Oregon State University, accessed February 11, 2020, at http://www.prism.oregonstate.edu/.

Riley, F.S., 1998, Mechanics of aquifer systems—The scientific legacy of Joseph F. Poland, *in* Borchers, J., ed., Land subsidence—Case studies and current research, Proceedings of the Dr. Joseph F. Poland Symposium on Land subsidence: Association of Engineering Geologists Special Publication 8, p. 13–27.

Scripps Orbit and Permanent Array Center, 2017, ftp (file transfer protocol) website, Scripps Orbit and Permanent Array Center, accessed September 10, 2017, at ftp://garner.ucsd.edu/.

Shen, Z., King, R.W., Agnew, D.C., Wang, M., Herring, T.A., Dong, D., and Fang, P., 2011, A unified analysis of crustal motion in Southern California, 1970–2004—The SCEC Crustal Motion Map: Journal of Geophysical Research, v. 116, no. B11, 19 p., https://doi.org/10.1029/2011JB008549.

Sneed, M., 2020, Global Positioning System survey data for 2015 and interferometric synthetic aperture radar data for 1995–2017, Coachella Valley, Riverside County, California: U.S. Geological Survey data release, https://doi.org/10.5066/P9B35CNL.

Sneed, M., and Brandt, J.T., 2007, Detection and measurement of land subsidence using global positioning system and interferometric synthetic aperture radar, Coachella Valley, California, 1996–2005: U.S. Geological Survey Scientific Investigations Report 2007–5251, v. 2.0, 31 p., https://doi.org/10.3133/sir20075251.

Sneed, M., and Galloway, D.L., 2000, Aquifer-system compaction and land subsidence—Measurements, analyses, and simulations—the Holly site: U.S. Geological Survey Water-Resources Investigations Report 00–4015, 65 p., https://doi.org/10.3133/wri20004015.

Sneed, M., Ikehara, M.E., Galloway, D.L., and Amelung, F., 2001, Detection and measurement of land subsidence using global positioning system and interferometric synthetic aperture radar, Coachella Valley, California, 1996–98: U.S. Geological Survey Water-Resources Investigations Report 01–4193, 26 p., https://doi.org/10.3133/wri014193.

Sneed, M., Stork, S.V., and Ikehara, M.E., 2002, Detection and measurement of land subsidence using global positioning system and interferometric synthetic aperture radar, Coachella Valley, California, 1998–2000: U.S. Geological Survey Water-Resources Investigations Report 02–4239, 29 p., https://doi.org/10.3133/wri024239.

Sneed, M., Brandt, J., and Solt, M., 2013, Land subsidence along the Delta-Mendota Canal in the northern part of the San Joaquin Valley, California, 2003–10: U.S. Geological Survey Scientific Investigations Report 2013–5142, 86 p., https://doi.org/10.3133/sir20135142.

Sneed, M., Brandt, J.T., and Solt, M., 2014, Land subsidence, groundwater levels, and geology in the Coachella Valley, California, 1993–2010: U.S. Geological Survey, Scientific Investigations Report 2014–5075, 62 p., https://doi.org/10.3133/sir20145075.

Sylvester, A.G., and Smith, R.R., 1976, Tectonic transpression and basement-controlled deformation in San Andreas Fault Zone, Salton Trough, California: The American Association of Petroleum Geologists Bulletin, v. 60, no. 12, p. 2081–2102 , https://doi.org/10.1306/C1EA3A73-16C9-11D7-8645000102C1865D.

Terzaghi, K., 1925, Principles of soil mechanics, IV—Settlement and consolidation of clay: Engineering News Record, v. 95, no. 3, p. 874–878.

Tyley, S.J., 1971, Analog model study of the ground-water basin of the upper Coachella Valley, California, U.S. Geological Survey Water Supply Paper 2027, 89 p., https://doi.org/10.3133/wsp2027.

Williams, S.D.P., Bock, Y., Fang, P., Jamason, P., Nikolaidis, R.M., Prawirodirdjo, L., Miller, M., and Johnson, D.J., 2004, Error analysis of continuous GPS position time series: Journal of Geophysical Research, v. 109, no. B3, 19 p., https://doi.org/10.1029/2003JB002741.

Zebker, H.A., Rosen, P.A., and Hensley, S., 1997, Atmospheric effects in interferometric synthetic aperture radar surface deformation and topographic maps: Journal of Geophysical Research, v. 102, no. B4, p. 7547–7563, https://doi.org/10.1029/96JB03804.

Zerbini, S., Richter, B., Negusini, M., Romagnoli, C., Simon, D., Domenichini, F., and Schwahn, W., 2001, Height and gravity variations by continuous GPS, gravity, and environmental parameter observations in the southern Po Plain, near Bologna, Italy: Earth and Planetary Science Letters, v. 192, no. 3, p. 267–279, https://doi.org/10.1016/S0012-821X(01)00445-9.

Zilkoski, D.B., D'Onofrio, J.D., and Frakes, S.J., 1997, Guidelines for establishing GPS-derived ellipsoid heights, (Standards: 2 cm and 5 cm) version 4.3: Silver Spring, Md., National Geodetic Survey, 10 p., 3 appendices.

Appendix 1. Interferometric Synthetic Aperture Radar Interferograms, Coachella Valley, California

See table 2 for a list of these interferograms.

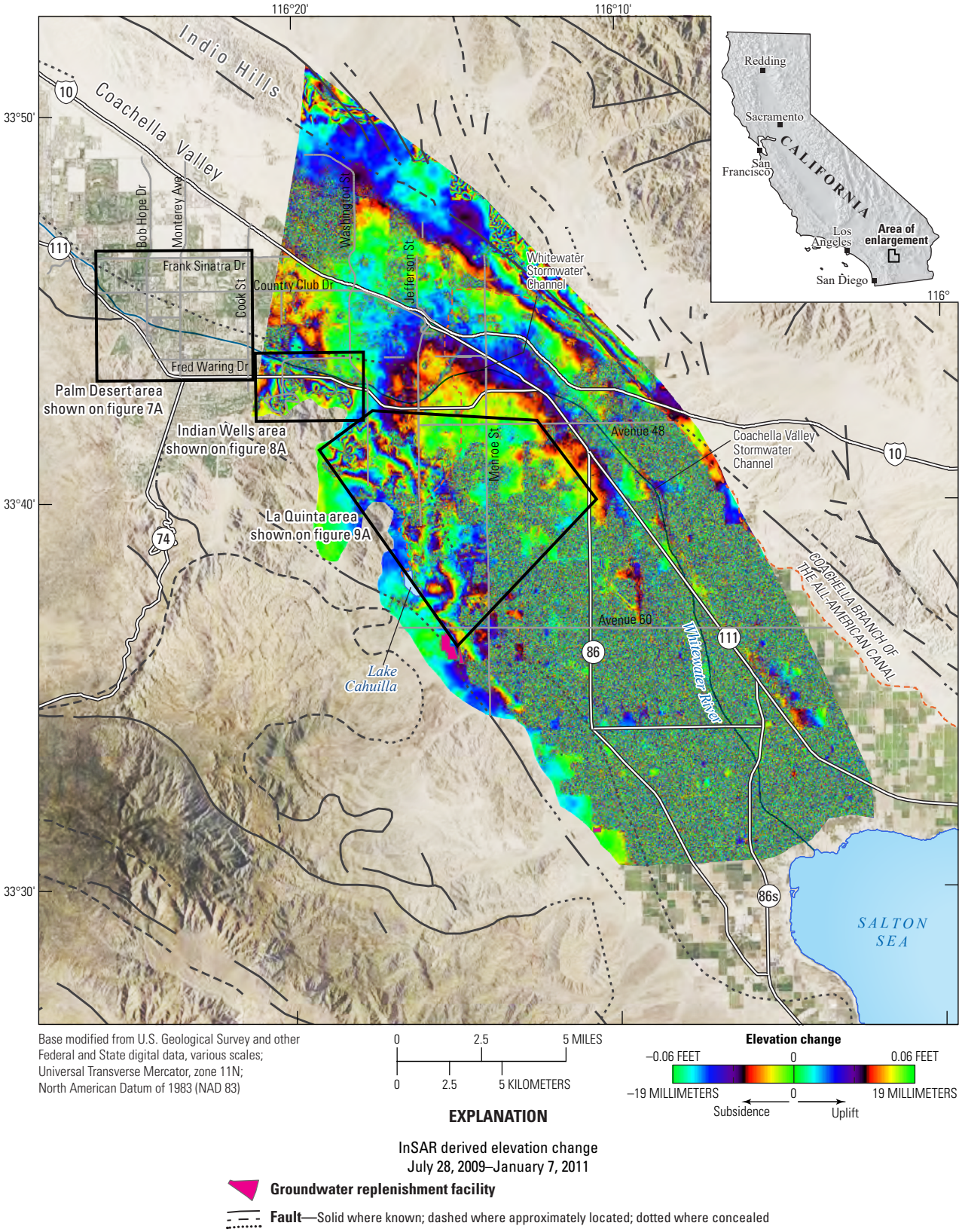
116°20'
116°10'
116°
33°50'
33°40'
33°30'
Indio Hills
Coachella Valley
Bob Hope Dr
Monterey Ave
Washington St
Jefferson St
Frank Sinatra Dr
Country Club Dr
Cook St
Fred Waring Dr
Whitewater Stormwater Channel
Palm Desert area shown on figure 7A
Indian Wells area shown on figure 8A
La Quinta area shown on figure 9A
Monroe St
Avenue 48
Coachella Valley Stormwater Channel
Avenue 60
Lake Cahuilla
Whitewater River
COACHELLA BRANCH OF THE ALL-AMERICAN CANAL
SALTON SEA
10
111
74
86
86s
Redding
Sacramento
San Francisco
CALIFORNIA
Los Angeles
Area of enlargement
San Diego
Base modified from U.S. Geological Survey and other Federal and State digital data, various scales; Universal Transverse Mercator, zone 11N; North American Datum of 1983 (NAD 83)
0 2.5 5 MILES
0 2.5 5 KILOMETERS
Elevation change
–0.06 FEET 0 0.06 FEET
–19 MILLIMETERS 0 19 MILLIMETERS
Subsidence
Uplift
EXPLANATION
InSAR derived elevation change
July 28, 2009–January 7, 2011
Groundwater replenishment facility
Fault—Solid where known; dashed where approximately located; dotted where concealed

Figure 1.1.

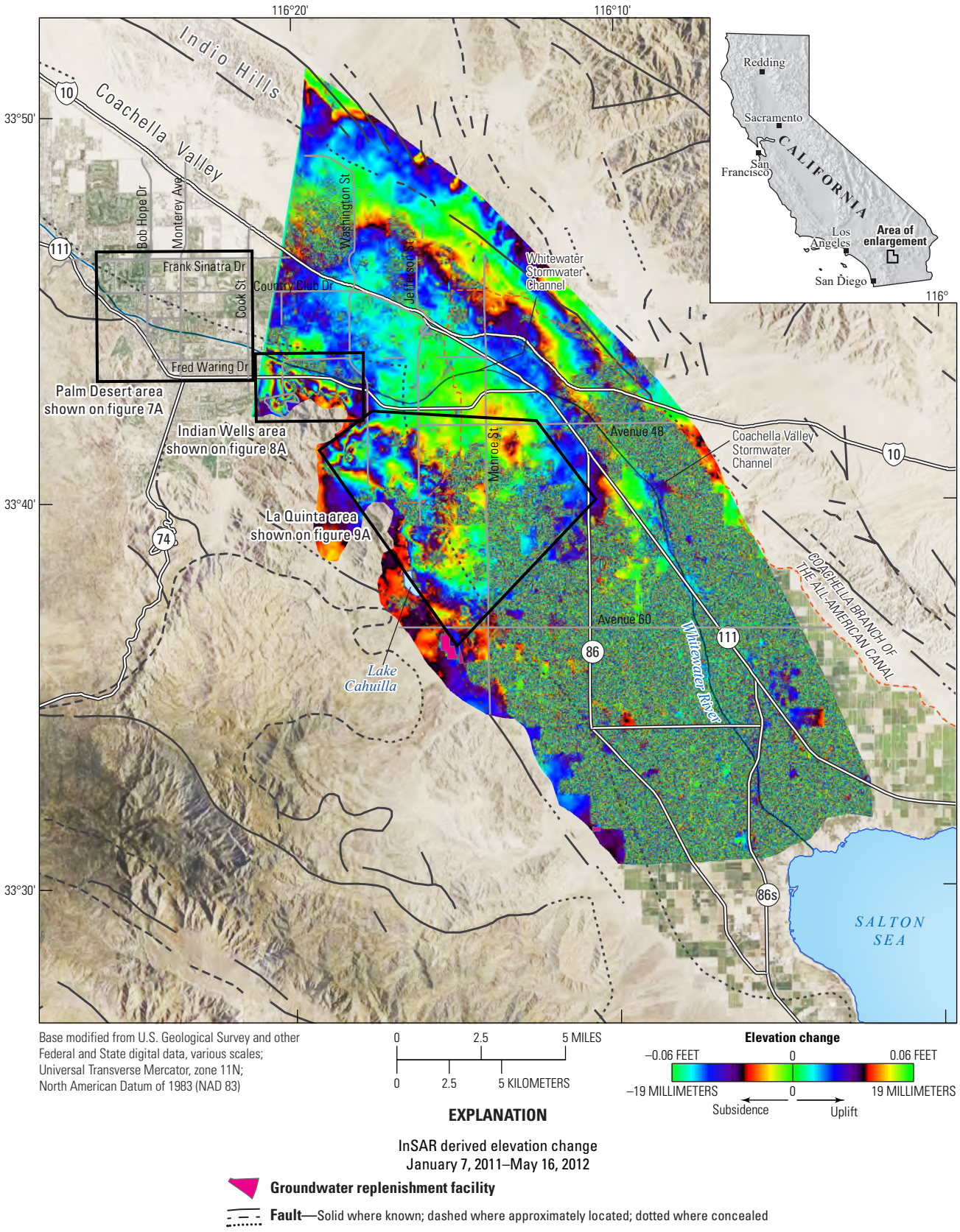
116°20'
116°10'
116°
33°50'
33°40'
33°30'
Indio Hills
Coachella Valley
Bob Hope Dr
Monterey Ave
Washington St
Jefferson St
Frank Sinatra Dr
Cook St
Country Club Dr
Fred Waring Dr
Whitewater Stormwater Channel
Palm Desert area shown on figure 7A
Indian Wells area shown on figure 8A
La Quinta area shown on figure 9A
Monroe St
Avenue 48
Coachella Valley Stormwater Channel
Avenue 60
Whitewater River
COACHELLA BRANCH OF THE ALL-AMERICAN CANAL
Lake Cahuilla
SALTON SEA
10
111
74
86
86s
Redding
Sacramento
San Francisco
CALIFORNIA
Los Angeles
Area of enlargement
San Diego
Base modified from U.S. Geological Survey and other Federal and State digital data, various scales; Universal Transverse Mercator, zone 11N; North American Datum of 1983 (NAD 83)
0 2.5 5 MILES
0 2.5 5 KILOMETERS
Elevation change
–0.06 FEET 0 0.06 FEET
–19 MILLIMETERS 0 19 MILLIMETERS
Subsidence
Uplift
EXPLANATION
InSAR derived elevation change
January 7, 2011–May 16, 2012
Groundwater replenishment facility
Fault—Solid where known; dashed where approximately located; dotted where concealed

Figure 1.2.

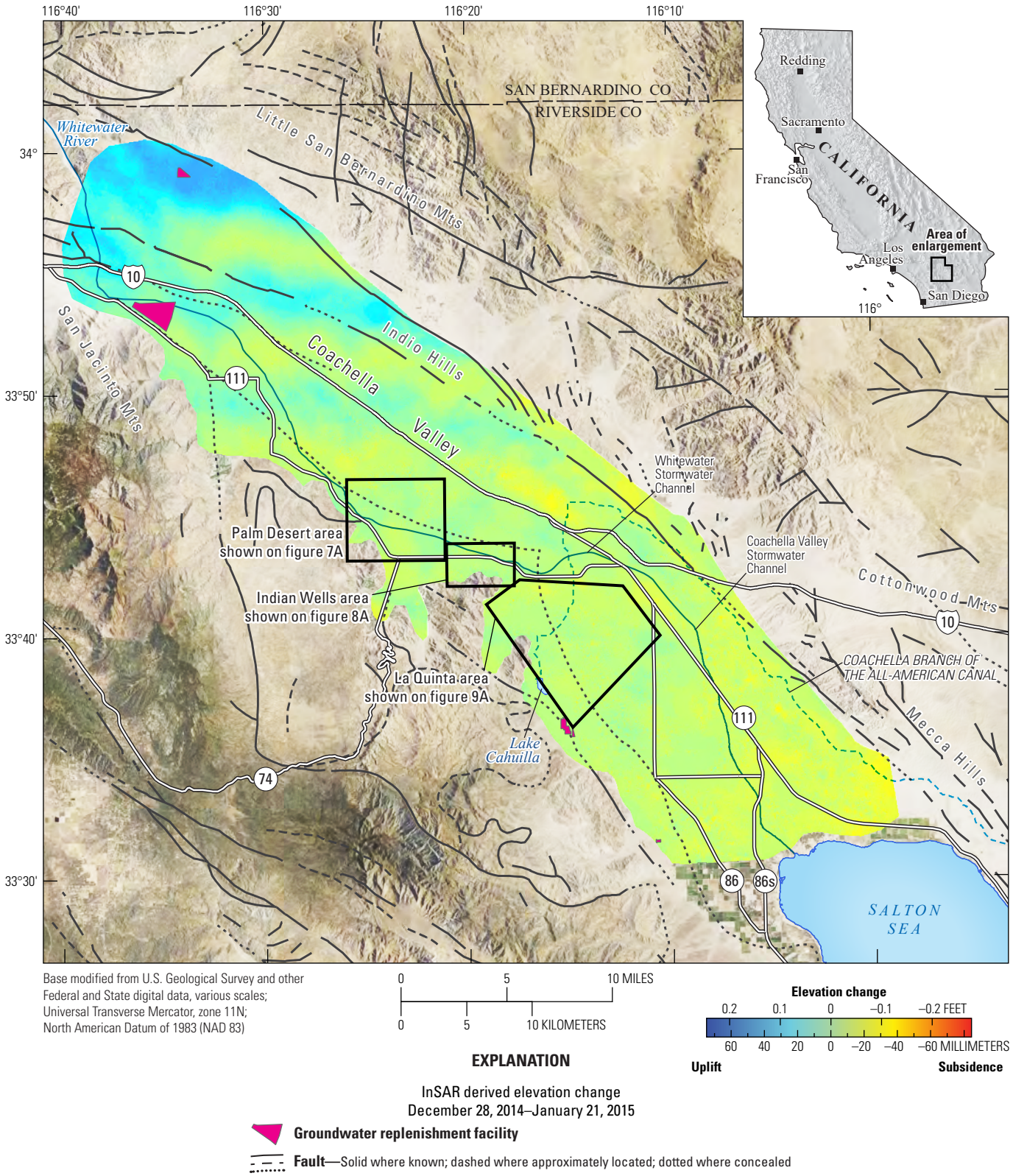
116°40'
116°30'
116°20'
116°10'
34°
33°50'
33°40'
33°30'
SAN BERNARDINO CO
RIVERSIDE CO
Whitewater River
Little San Bernardino Mts
San Jacinto Mts
Indio Hills
Coachella Valley
Whitewater Stormwater Channel
Coachella Valley Stormwater Channel
Palm Desert area shown on figure 7A
Indian Wells area shown on figure 8A
La Quinta area shown on figure 9A
Lake Cahuilla
Cottonwood Mts
COACHELLA BRANCH OF THE ALL-AMERICAN CANAL
Mecca Hills
SALTON SEA
10
111
74
86
86s
Redding
Sacramento
San Francisco
CALIFORNIA
Los Angeles
San Diego
Area of enlargement
116°
Base modified from U.S. Geological Survey and other Federal and State digital data, various scales; Universal Transverse Mercator, zone 11N; North American Datum of 1983 (NAD 83)
0 5 10 MILES
0 5 10 KILOMETERS
Elevation change
0.2 0.1 0 –0.1 –0.2 FEET
60 40 20 0 –20 –40 –60 MILLIMETERS
Uplift
Subsidence
EXPLANATION
InSAR derived elevation change
December 28, 2014–January 21, 2015
Groundwater replenishment facility
Fault—Solid where known; dashed where approximately located; dotted where concealed

Figure 1.3.

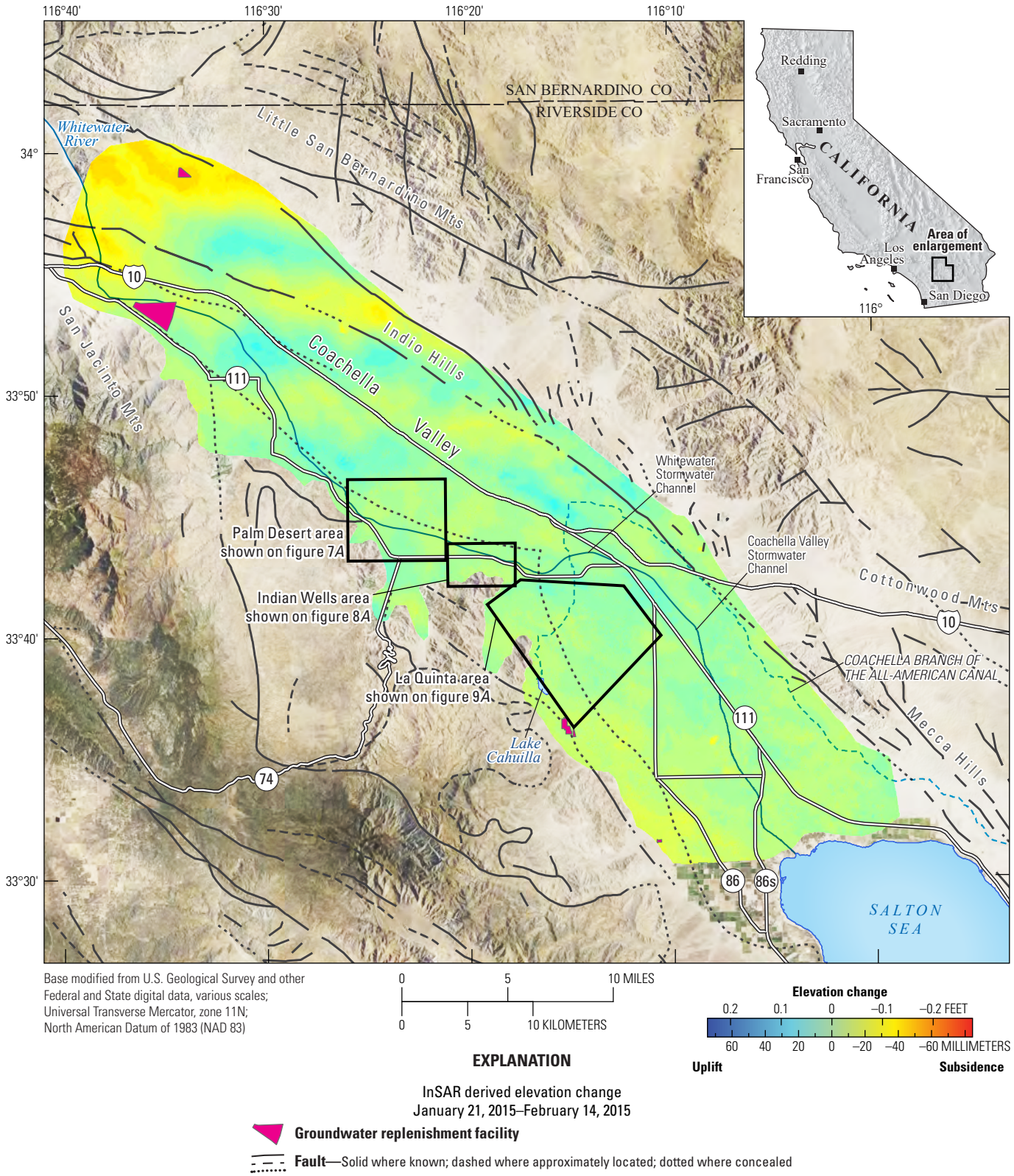
116°40'
116°30'
116°20'
116°10'
34°
33°50'
33°40'
33°30'
SAN BERNARDINO CO
RIVERSIDE CO
Whitewater River
Little San Bernardino Mts
San Jacinto Mts
Indio Hills
Coachella Valley
Whitewater Stormwater Channel
Coachella Valley Stormwater Channel
Palm Desert area shown on figure 7A
Indian Wells area shown on figure 8A
La Quinta area shown on figure 9A
Lake Cahuilla
Cottonwood Mts
COACHELLA BRANCH OF THE ALL-AMERICAN CANAL
Mecca Hills
SALTON SEA
10
111
74
86
86s
Redding
Sacramento
San Francisco
CALIFORNIA
Los Angeles
Area of enlargement
San Diego
116°
Base modified from U.S. Geological Survey and other Federal and State digital data, various scales; Universal Transverse Mercator, zone 11N; North American Datum of 1983 (NAD 83)
0 5 10 MILES
0 5 10 KILOMETERS
Elevation change
0.2 0.1 0 –0.1 –0.2 FEET
60 40 20 0 –20 –40 –60 MILLIMETERS
Uplift
Subsidence
EXPLANATION
InSAR derived elevation change
January 21, 2015–February 14, 2015
Groundwater replenishment facility
Fault—Solid where known; dashed where approximately located; dotted where concealed

Figure 1.4.

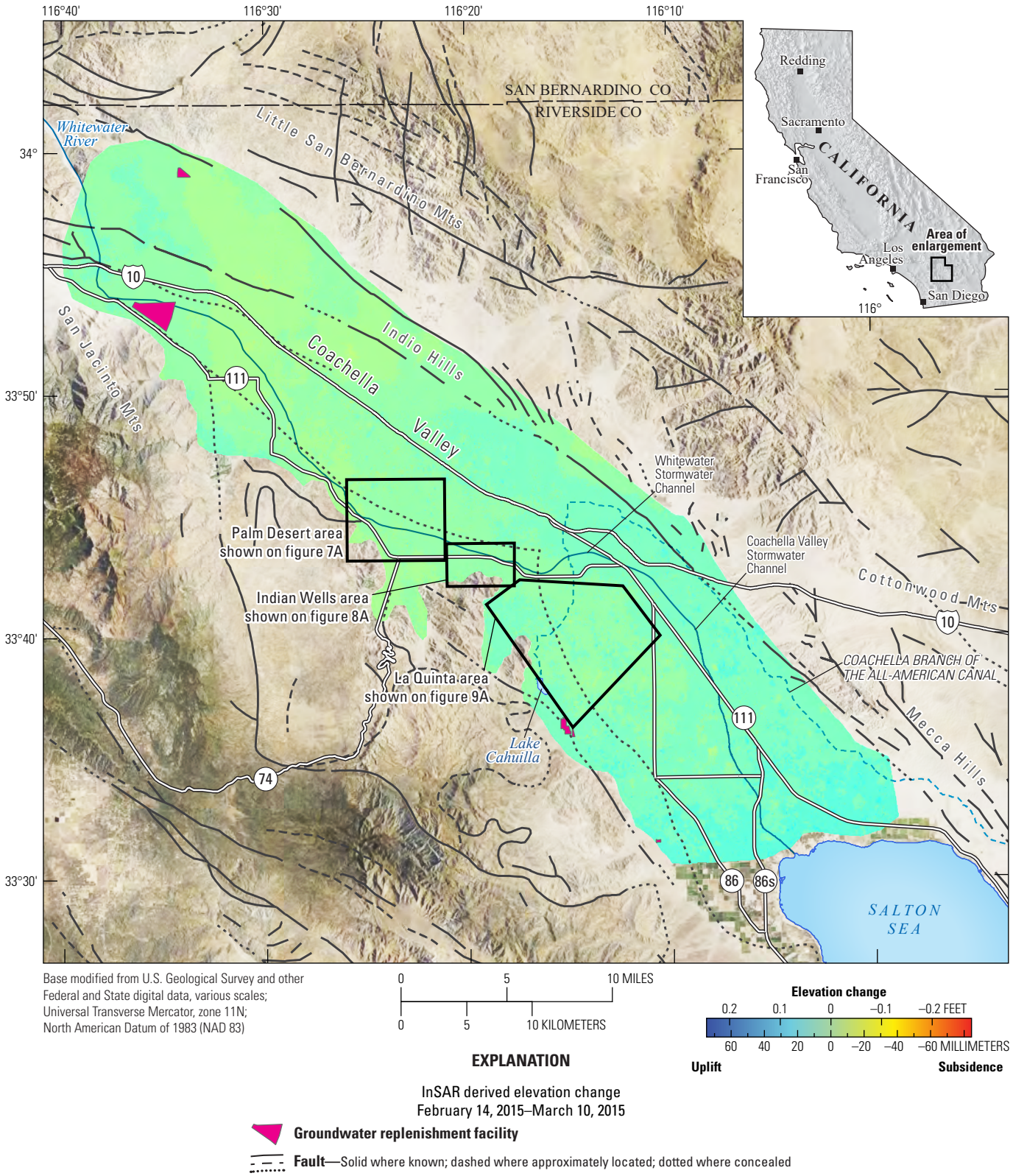
116°40'
116°30'
116°20'
116°10'
34°
33°50'
33°40'
33°30'
SAN BERNARDINO CO
RIVERSIDE CO
Whitewater River
Little San Bernardino Mts
San Jacinto Mts
Indio Hills
Coachella Valley
Whitewater Stormwater Channel
Coachella Valley Stormwater Channel
Palm Desert area shown on figure 7A
Indian Wells area shown on figure 8A
La Quinta area shown on figure 9A
Lake Cahuilla
Cottonwood Mts
COACHELLA BRANCH OF THE ALL-AMERICAN CANAL
Mecca Hills
SALTON SEA
10
111
74
86
86s
Redding
Sacramento
San Francisco
CALIFORNIA
Los Angeles
San Diego
Area of enlargement
116°
Base modified from U.S. Geological Survey and other Federal and State digital data, various scales; Universal Transverse Mercator, zone 11N; North American Datum of 1983 (NAD 83)
0 5 10 MILES
0 5 10 KILOMETERS
Elevation change
0.2 0.1 0 –0.1 –0.2 FEET
60 40 20 0 –20 –40 –60 MILLIMETERS
Uplift
Subsidence
EXPLANATION
InSAR derived elevation change
February 14, 2015–March 10, 2015
Groundwater replenishment facility
Fault—Solid where known; dashed where approximately located; dotted where concealed

Figure 1.5.

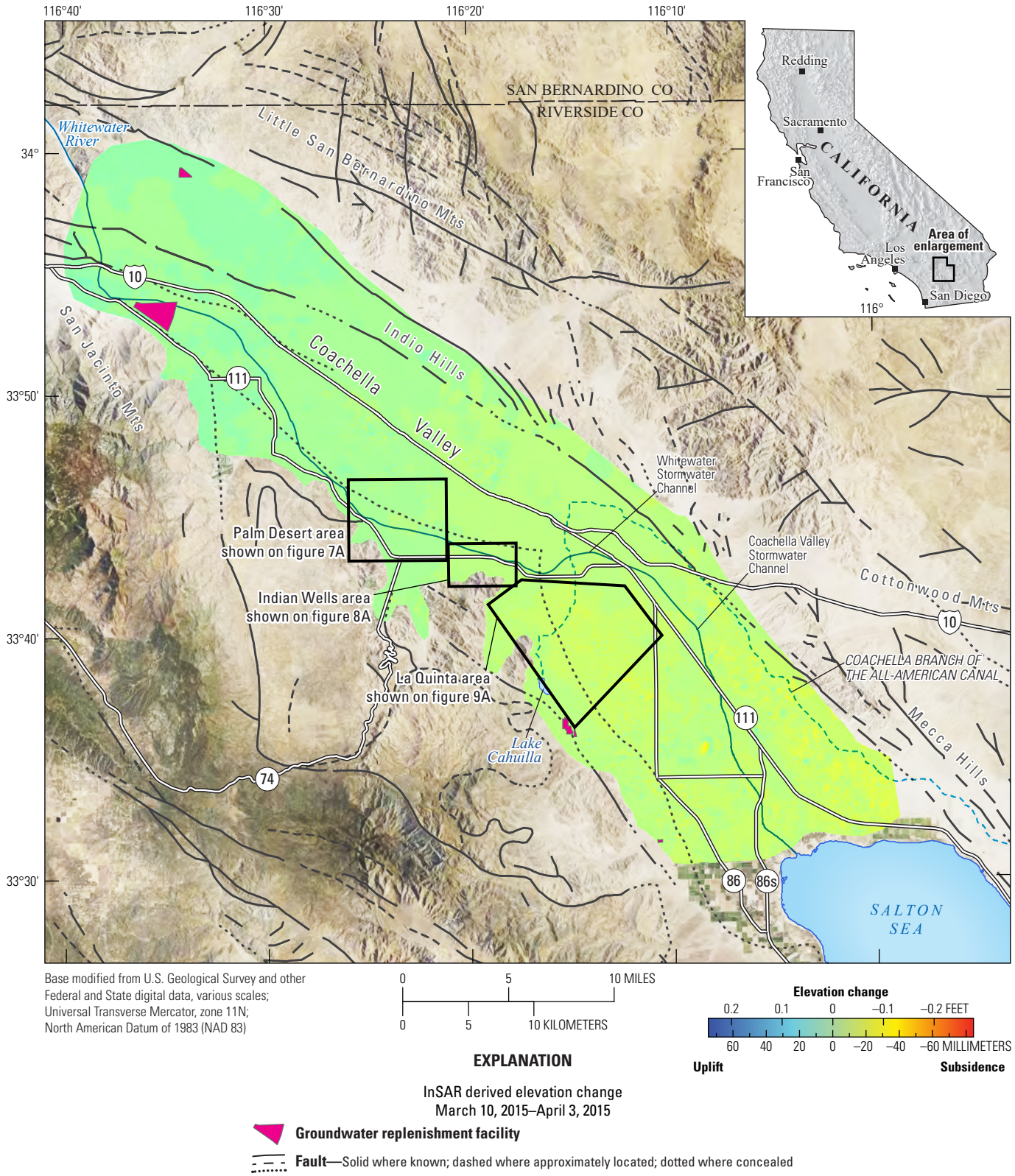
116°40'
116°30'
116°20'
116°10'
34°
33°50'
33°40'
33°30'
116°
SAN BERNARDINO CO
RIVERSIDE CO
Whitewater River
Little San Bernardino Mts
San Jacinto Mts
Indio Hills
Coachella Valley
Palm Desert area shown on figure 7A
Indian Wells area shown on figure 8A
La Quinta area shown on figure 9A
Lake Cahuilla
Whitewater Stormwater Channel
Coachella Valley Stormwater Channel
Cottonwood Mts
COACHELLA BRANCH OF THE ALL-AMERICAN CANAL
Mecca Hills
SALTON SEA
10
111
74
86
86s
Redding
Sacramento
San Francisco
CALIFORNIA
Los Angeles
Area of enlargement
San Diego
Base modified from U.S. Geological Survey and other Federal and State digital data, various scales;
Universal Transverse Mercator, zone 11N;
North American Datum of 1983 (NAD 83)
0 5 10 MILES
0 5 10 KILOMETERS
Elevation change
0.2 0.1 0 –0.1 –0.2 FEET
60 40 20 0 –20 –40 –60 MILLIMETERS
Uplift
Subsidence
EXPLANATION
InSAR derived elevation change
March 10, 2015–April 3, 2015
Groundwater replenishment facility
Fault—Solid where known; dashed where approximately located; dotted where concealed

Figure 1.6.

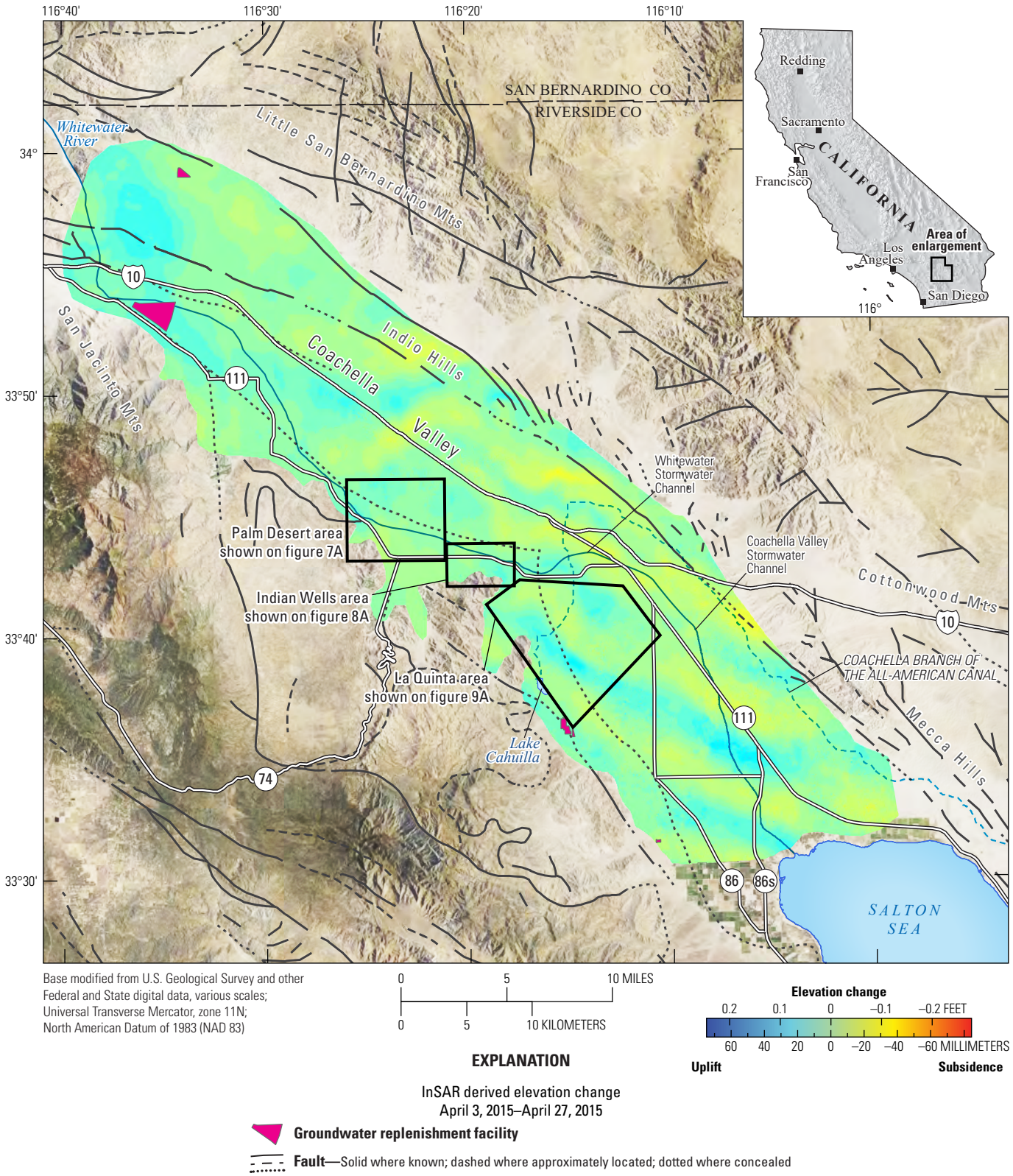
116°40'
116°30'
116°20'
116°10'
34°
33°50'
33°40'
33°30'
SAN BERNARDINO CO
RIVERSIDE CO
Whitewater River
Little San Bernardino Mts
San Jacinto Mts
Indio Hills
Coachella Valley
Whitewater Stormwater Channel
Coachella Valley Stormwater Channel
Palm Desert area shown on figure 7A
Indian Wells area shown on figure 8A
La Quinta area shown on figure 9A
Lake Cahuilla
Cottonwood Mts
COACHELLA BRANCH OF THE ALL-AMERICAN CANAL
Mecca Hills
SALTON SEA
10
111
74
86
86s
Redding
Sacramento
San Francisco
CALIFORNIA
Los Angeles
San Diego
Area of enlargement
116°
Base modified from U.S. Geological Survey and other Federal and State digital data, various scales; Universal Transverse Mercator, zone 11N; North American Datum of 1983 (NAD 83)
0 5 10 MILES
0 5 10 KILOMETERS
Elevation change
0.2 0.1 0 –0.1 –0.2 FEET
60 40 20 0 –20 –40 –60 MILLIMETERS
Uplift
Subsidence
EXPLANATION
InSAR derived elevation change
April 3, 2015–April 27, 2015
Groundwater replenishment facility
Fault—Solid where known; dashed where approximately located; dotted where concealed

Figure 1.7.

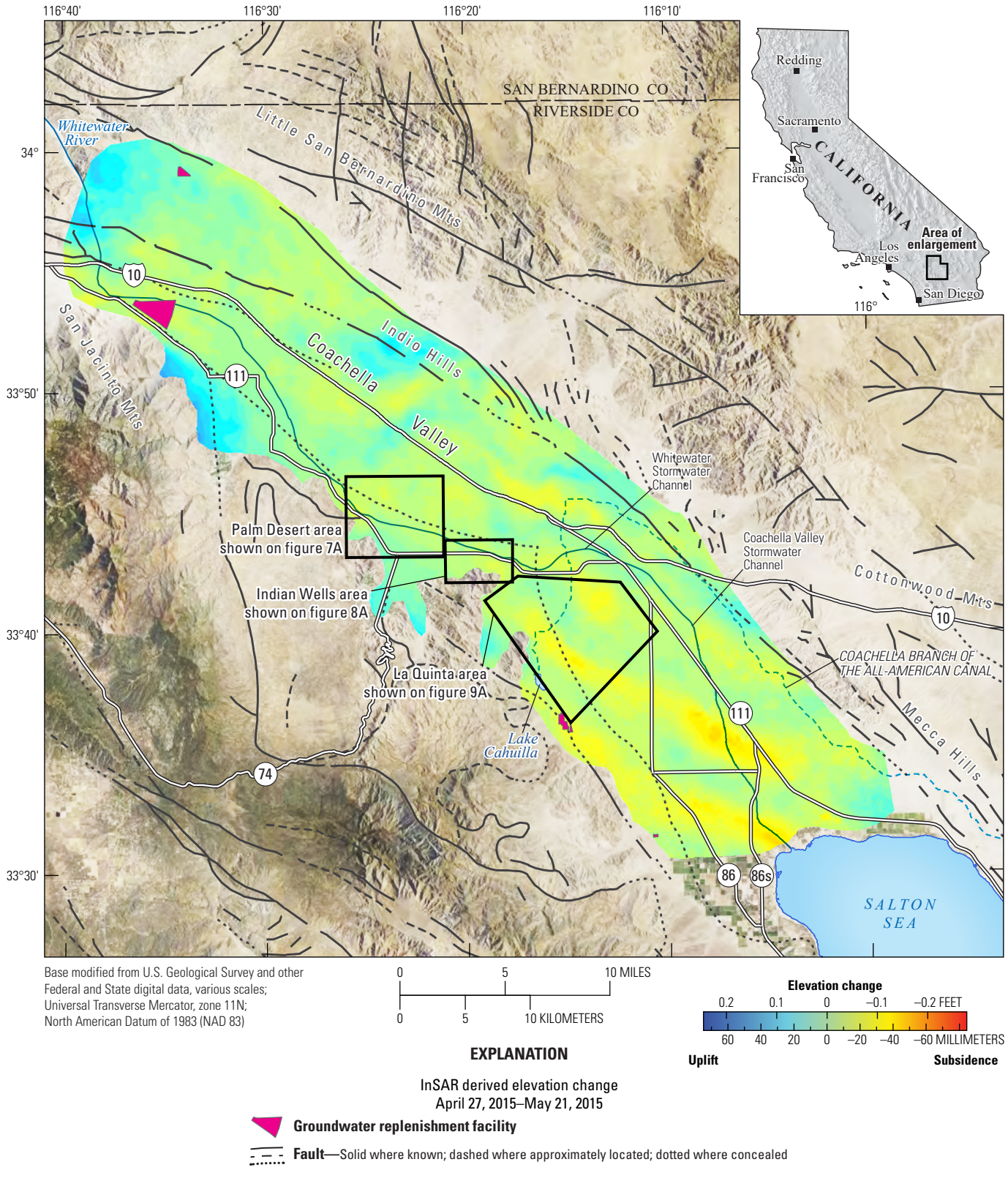
116°40'
116°30'
116°20'
116°10'
34°
33°50'
33°40'
33°30'
SAN BERNARDINO CO
RIVERSIDE CO
Whitewater River
Little San Bernardino Mts
San Jacinto Mts
Indio Hills
Coachella Valley
Whitewater Stormwater Channel
Coachella Valley Stormwater Channel
Palm Desert area shown on figure 7A
Indian Wells area shown on figure 8A
La Quinta area shown on figure 9A
Lake Cahuilla
Cottonwood Mts
COACHELLA BRANCH OF THE ALL-AMERICAN CANAL
Mecca Hills
SALTON SEA
10
111
74
86
86s
Redding
Sacramento
San Francisco
CALIFORNIA
Los Angeles
Area of enlargement
San Diego
116°
Base modified from U.S. Geological Survey and other Federal and State digital data, various scales; Universal Transverse Mercator, zone 11N; North American Datum of 1983 (NAD 83)
0 5 10 MILES
0 5 10 KILOMETERS
Elevation change
0.2 0.1 0 –0.1 –0.2 FEET
60 40 20 0 –20 –40 –60 MILLIMETERS
Uplift
Subsidence
EXPLANATION
InSAR derived elevation change
April 27, 2015–May 21, 2015
Groundwater replenishment facility
Fault—Solid where known; dashed where approximately located; dotted where concealed

Figure 1.8.

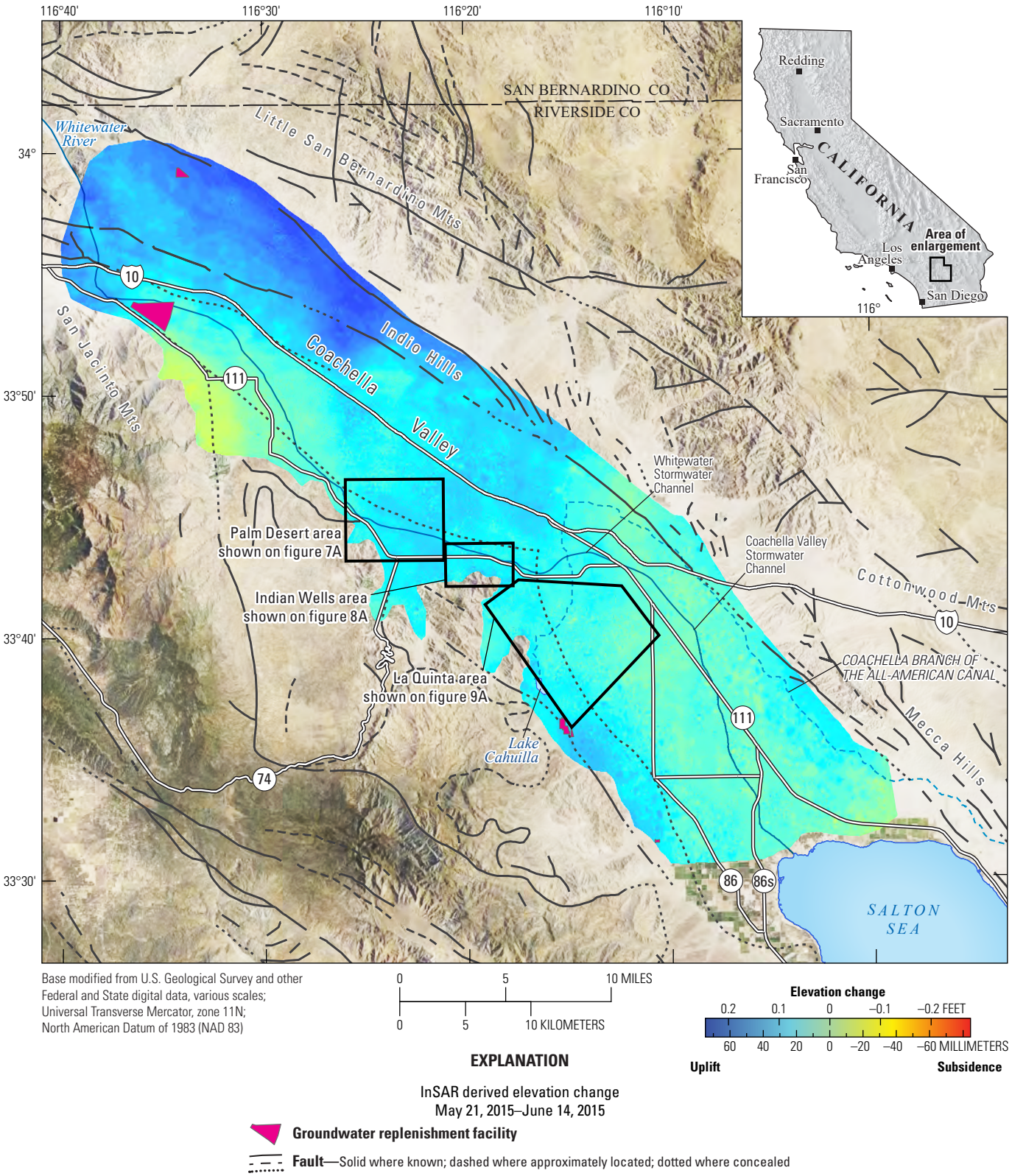
116°40'
116°30'
116°20'
116°10'
34°
33°50'
33°40'
33°30'
SAN BERNARDINO CO
RIVERSIDE CO
Whitewater River
Little San Bernardino Mts
San Jacinto Mts
Indio Hills
Coachella Valley
Whitewater Stormwater Channel
Coachella Valley Stormwater Channel
Palm Desert area shown on figure 7A
Indian Wells area shown on figure 8A
La Quinta area shown on figure 9A
Lake Cahuilla
Cottonwood Mts
COACHELLA BRANCH OF THE ALL-AMERICAN CANAL
Mecca Hills
SALTON SEA
10
111
74
86
86s
Redding
Sacramento
San Francisco
CALIFORNIA
Los Angeles
San Diego
Area of enlargement
116°
Base modified from U.S. Geological Survey and other Federal and State digital data, various scales; Universal Transverse Mercator, zone 11N; North American Datum of 1983 (NAD 83)
0 5 10 MILES
0 5 10 KILOMETERS
Elevation change
0.2 0.1 0 –0.1 –0.2 FEET
60 40 20 0 –20 –40 –60 MILLIMETERS
Uplift
Subsidence
EXPLANATION
InSAR derived elevation change
May 21, 2015–June 14, 2015
Groundwater replenishment facility
Fault—Solid where known; dashed where approximately located; dotted where concealed

Figure 1.9.

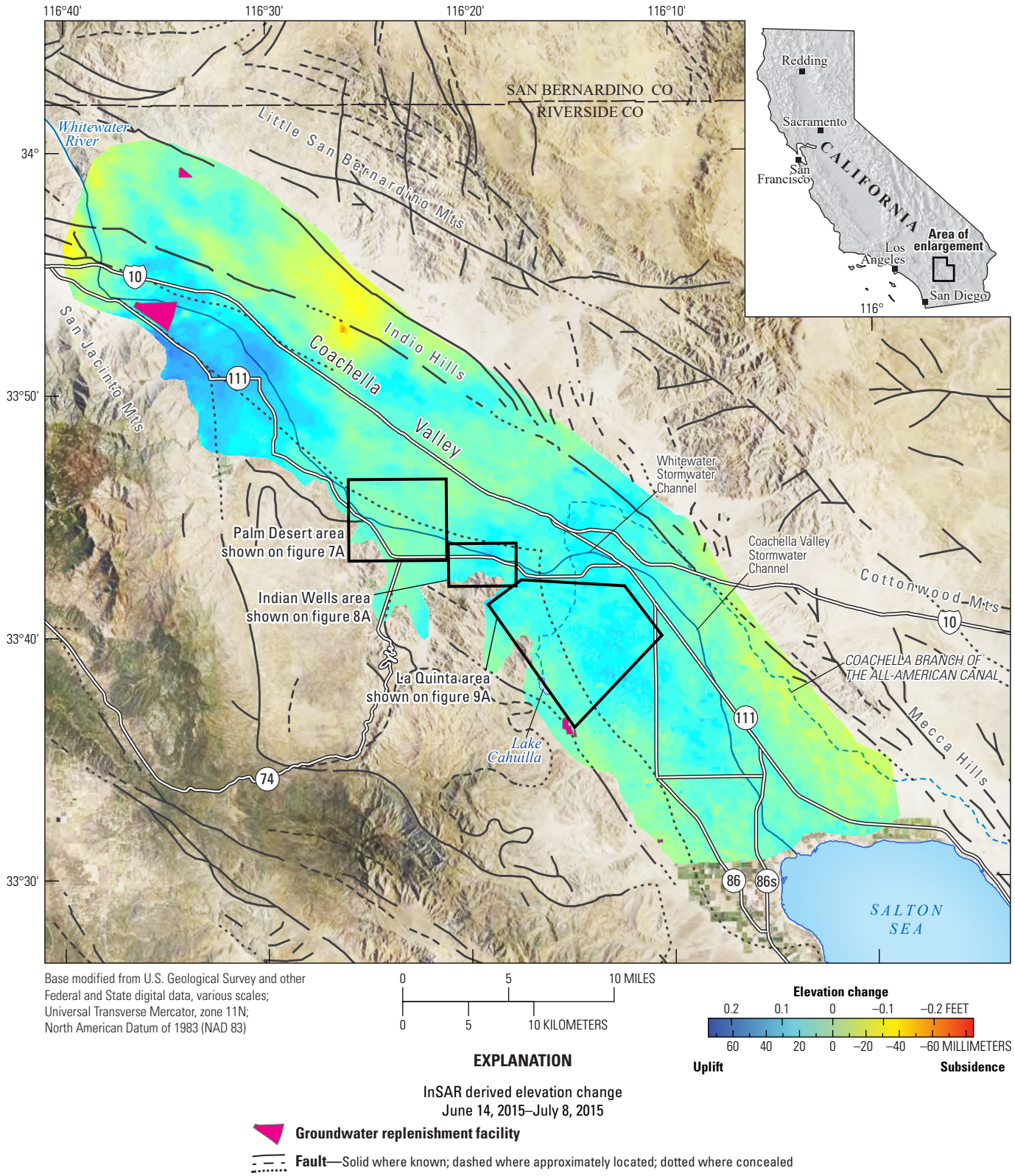
116°40'
116°30'
116°20'
116°10'
34°
33°50'
33°40'
33°30'
116°
SAN BERNARDINO CO
RIVERSIDE CO
Whitewater River
Little San Bernardino Mts
San Jacinto Mts
Indio Hills
Coachella Valley
Palm Desert area shown on figure 7A
Indian Wells area shown on figure 8A
La Quinta area shown on figure 9A
Whitewater Stormwater Channel
Coachella Valley Stormwater Channel
Cottonwood Mts
COACHELLA BRANCH OF THE ALL-AMERICAN CANAL
Mecca Hills
Lake Cahuilla
SALTON SEA
10
111
74
86
86s
Redding
Sacramento
San Francisco
CALIFORNIA
Los Angeles
Area of enlargement
San Diego
Base modified from U.S. Geological Survey and other Federal and State digital data, various scales; Universal Transverse Mercator, zone 11N; North American Datum of 1983 (NAD 83)
0 5 10 MILES
0 5 10 KILOMETERS
Elevation change
0.2 0.1 0 –0.1 –0.2 FEET
60 40 20 0 –20 –40 –60 MILLIMETERS
Uplift
Subsidence
EXPLANATION
InSAR derived elevation change
June 14, 2015–July 8, 2015
Groundwater replenishment facility
Fault—Solid where known; dashed where approximately located; dotted where concealed

Figure 1.10.

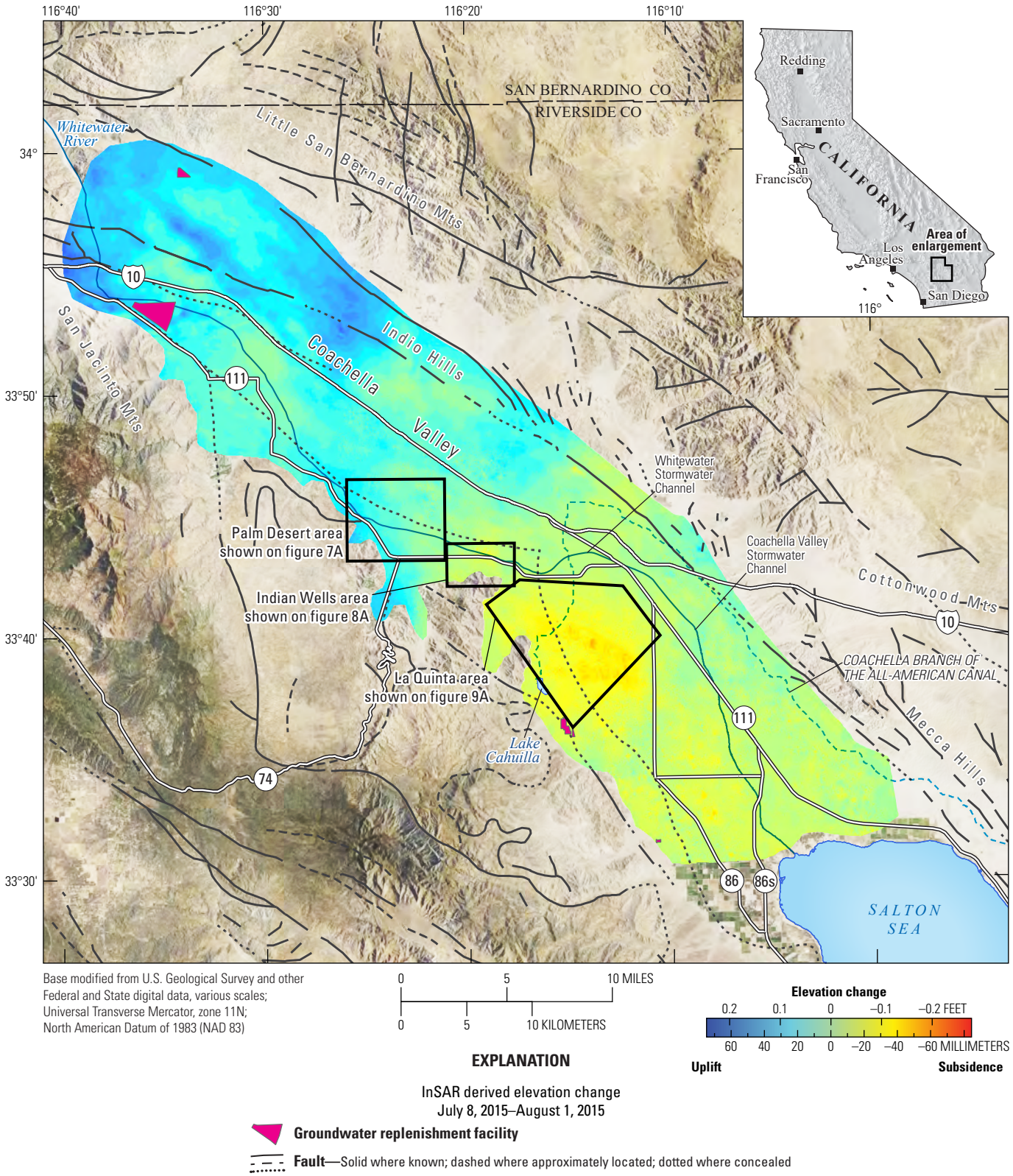
116°40'
116°30'
116°20'
116°10'
34°
33°50'
33°40'
33°30'
SAN BERNARDINO CO
RIVERSIDE CO
Whitewater River
Little San Bernardino Mts
San Jacinto Mts
Indio Hills
Coachella Valley
Whitewater Stormwater Channel
Coachella Valley Stormwater Channel
Palm Desert area shown on figure 7A
Indian Wells area shown on figure 8A
La Quinta area shown on figure 9A
Lake Cahuilla
Cottonwood Mts
COACHELLA BRANCH OF THE ALL-AMERICAN CANAL
Mecca Hills
SALTON SEA
10
111
74
86
86s
Redding
Sacramento
San Francisco
CALIFORNIA
Los Angeles
San Diego
Area of enlargement
116°
Base modified from U.S. Geological Survey and other Federal and State digital data, various scales; Universal Transverse Mercator, zone 11N; North American Datum of 1983 (NAD 83)
0 5 10 MILES
0 5 10 KILOMETERS
Elevation change
0.2 0.1 0 –0.1 –0.2 FEET
60 40 20 0 –20 –40 –60 MILLIMETERS
Uplift
Subsidence
EXPLANATION
InSAR derived elevation change
July 8, 2015–August 1, 2015
Groundwater replenishment facility
Fault—Solid where known; dashed where approximately located; dotted where concealed

Figure 1.11.

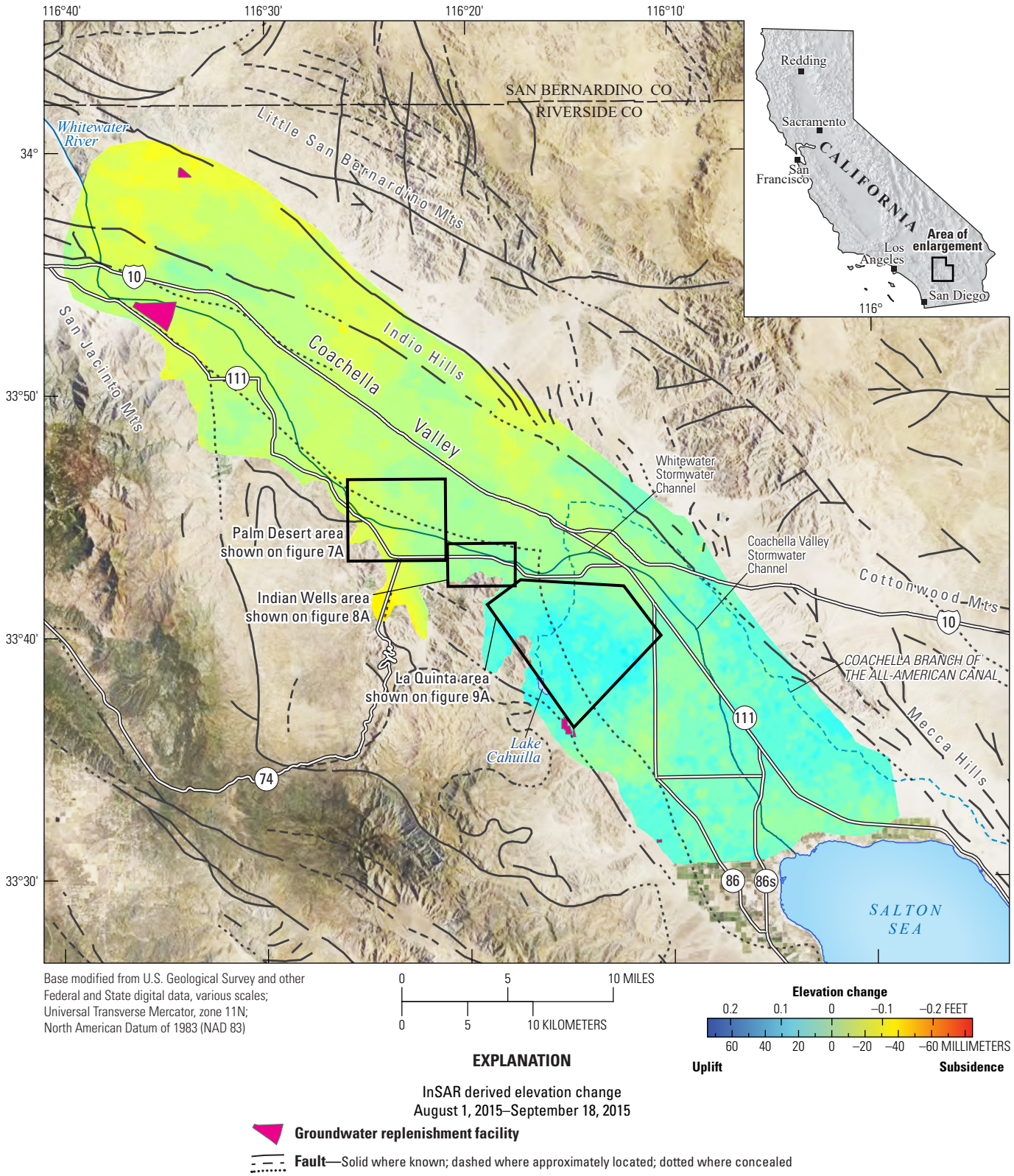
116°40'
116°30'
116°20'
116°10'
34°
33°50'
33°40'
33°30'
SAN BERNARDINO CO
RIVERSIDE CO
Whitewater River
Little San Bernardino Mts
San Jacinto Mts
Indio Hills
Coachella Valley
Palm Desert area shown on figure 7A
Indian Wells area shown on figure 8A
La Quinta area shown on figure 9A
Lake Cahuilla
Whitewater Stormwater Channel
Coachella Valley Stormwater Channel
Cottonwood Mts
COACHELLA BRANCH OF THE ALL-AMERICAN CANAL
Mecca Hills
SALTON SEA
10
111
74
86
86s
Redding
Sacramento
San Francisco
CALIFORNIA
Los Angeles
Area of enlargement
San Diego
116°
Base modified from U.S. Geological Survey and other Federal and State digital data, various scales;
Universal Transverse Mercator, zone 11N;
North American Datum of 1983 (NAD 83)
0 5 10 MILES
0 5 10 KILOMETERS
Elevation change
0.2 0.1 0 –0.1 –0.2 FEET
60 40 20 0 –20 –40 –60 MILLIMETERS
Uplift
Subsidence
EXPLANATION
InSAR derived elevation change
August 1, 2015–September 18, 2015
Groundwater replenishment facility
Fault—Solid where known; dashed where approximately located; dotted where concealed

Figure 1.12.

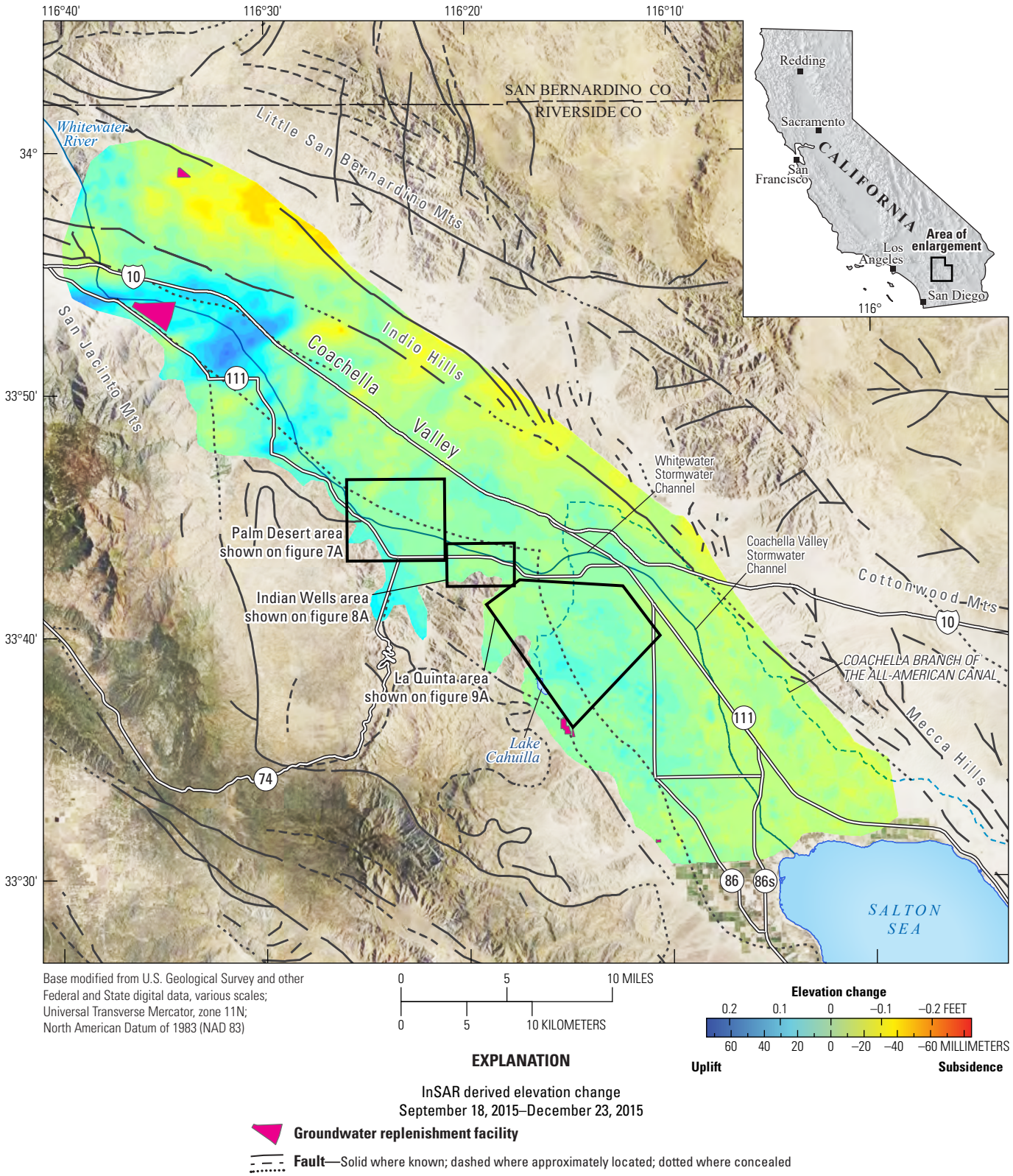
116°40'
116°30'
116°20'
116°10'
34°
33°50'
33°40'
33°30'
SAN BERNARDINO CO
RIVERSIDE CO
Whitewater River
Little San Bernardino Mts
San Jacinto Mts
Indio Hills
Coachella Valley
Whitewater Stormwater Channel
Coachella Valley Stormwater Channel
Palm Desert area shown on figure 7A
Indian Wells area shown on figure 8A
La Quinta area shown on figure 9A
Lake Cahuilla
Cottonwood Mts
COACHELLA BRANCH OF THE ALL-AMERICAN CANAL
Mecca Hills
SALTON SEA
10
111
74
86
86s
Redding
Sacramento
San Francisco
CALIFORNIA
Los Angeles
Area of enlargement
San Diego
116°
Base modified from U.S. Geological Survey and other Federal and State digital data, various scales; Universal Transverse Mercator, zone 11N; North American Datum of 1983 (NAD 83)
0 5 10 MILES
0 5 10 KILOMETERS
Elevation change
0.2 0.1 0 –0.1 –0.2 FEET
60 40 20 0 –20 –40 –60 MILLIMETERS
Uplift
Subsidence
EXPLANATION
InSAR derived elevation change
September 18, 2015–December 23, 2015
Groundwater replenishment facility
Fault—Solid where known; dashed where approximately located; dotted where concealed

Figure 1.13.

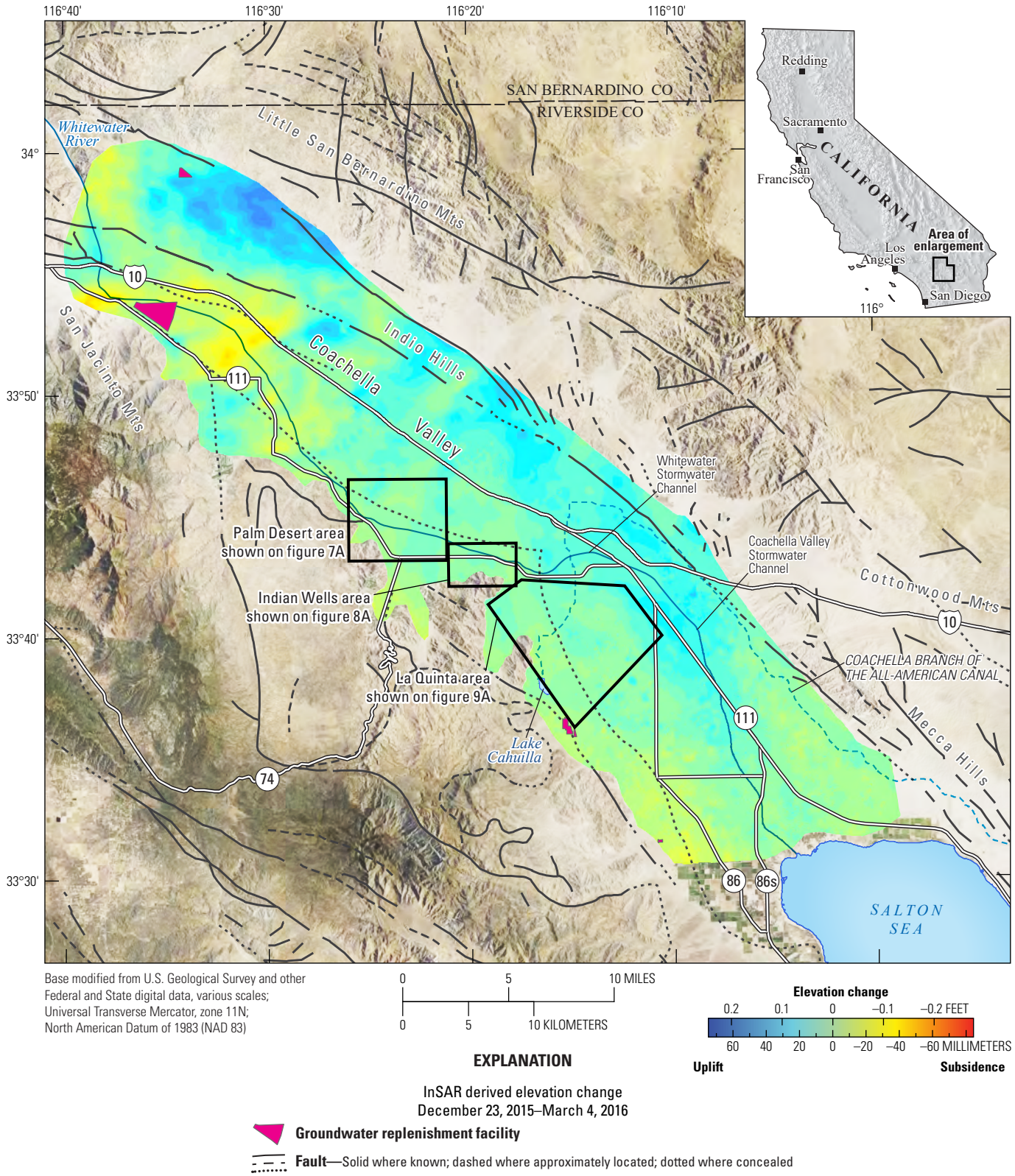
116°40'
116°30'
116°20'
116°10'
34°
33°50'
33°40'
33°30'
SAN BERNARDINO CO
RIVERSIDE CO
Whitewater River
Little San Bernardino Mts
San Jacinto Mts
Indio Hills
Coachella Valley
Palm Desert area shown on figure 7A
Indian Wells area shown on figure 8A
La Quinta area shown on figure 9A
Lake Cahuilla
Whitewater Stormwater Channel
Coachella Valley Stormwater Channel
Cottonwood Mts
COACHELLA BRANCH OF THE ALL-AMERICAN CANAL
Mecca Hills
SALTON SEA
10
111
74
86
86s
Redding
Sacramento
San Francisco
CALIFORNIA
Los Angeles
Area of enlargement
San Diego
116°
Base modified from U.S. Geological Survey and other Federal and State digital data, various scales; Universal Transverse Mercator, zone 11N; North American Datum of 1983 (NAD 83)
0 5 10 MILES
0 5 10 KILOMETERS
Elevation change
0.2 0.1 0 –0.1 –0.2 FEET
60 40 20 0 –20 –40 –60 MILLIMETERS
Uplift
Subsidence
EXPLANATION
InSAR derived elevation change
December 23, 2015–March 4, 2016
Groundwater replenishment facility
Fault—Solid where known; dashed where approximately located; dotted where concealed

Figure 1.14.

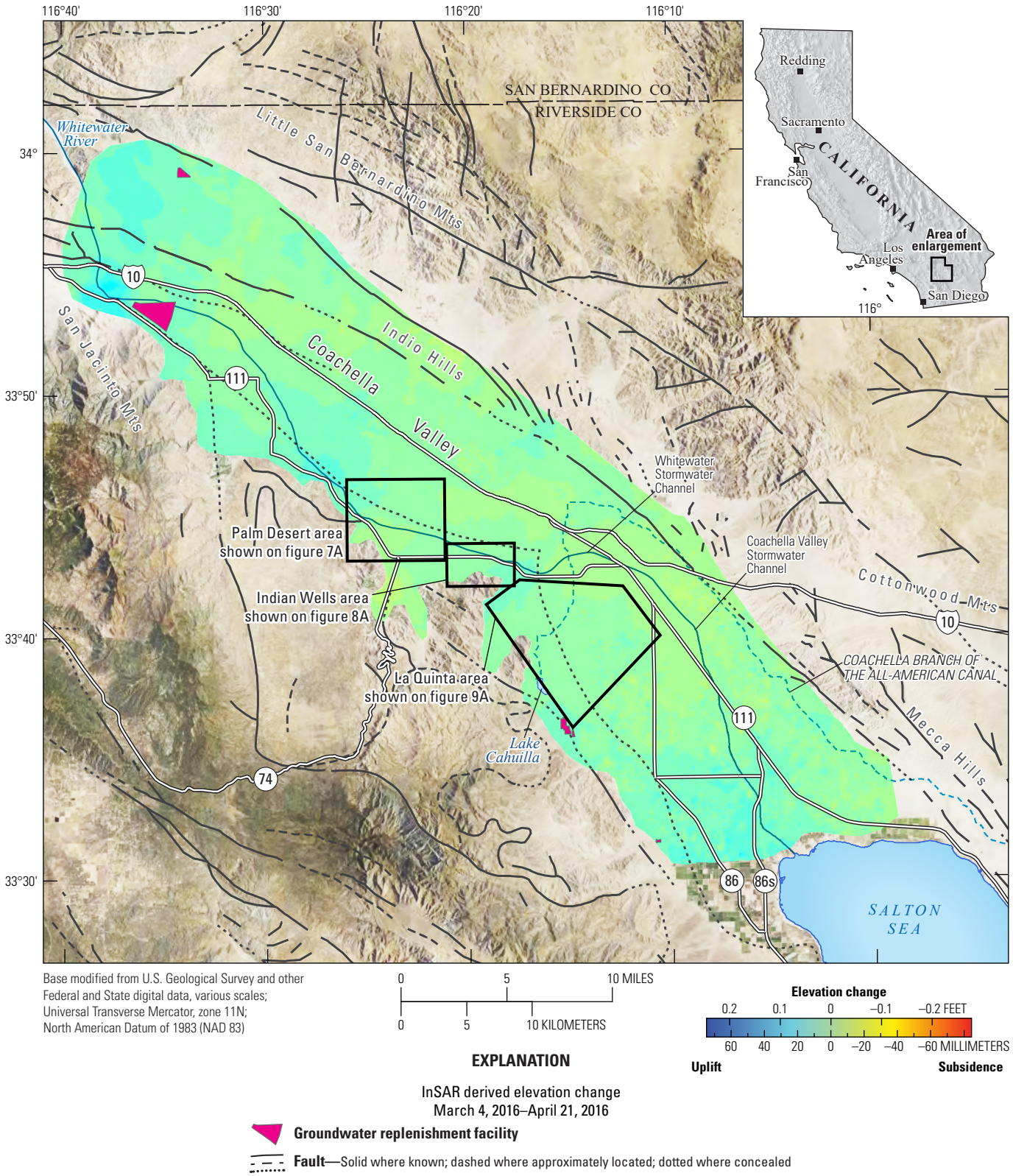
116°40'
116°30'
116°20'
116°10'
34°
33°50'
33°40'
33°30'
SAN BERNARDINO CO
RIVERSIDE CO
Whitewater River
Little San Bernardino Mts
San Jacinto Mts
Indio Hills
Coachella Valley
Whitewater Stormwater Channel
Coachella Valley Stormwater Channel
Palm Desert area shown on figure 7A
Indian Wells area shown on figure 8A
La Quinta area shown on figure 9A
Lake Cahuilla
Cottonwood Mts
COACHELLA BRANCH OF THE ALL-AMERICAN CANAL
Mecca Hills
SALTON SEA
10
111
74
86
86s
Redding
Sacramento
San Francisco
CALIFORNIA
Los Angeles
San Diego
Area of enlargement
116°
Base modified from U.S. Geological Survey and other Federal and State digital data, various scales; Universal Transverse Mercator, zone 11N; North American Datum of 1983 (NAD 83)
0 5 10 MILES
0 5 10 KILOMETERS
Elevation change
0.2 0.1 0 –0.1 –0.2 FEET
60 40 20 0 –20 –40 –60 MILLIMETERS
Uplift
Subsidence
EXPLANATION
InSAR derived elevation change
March 4, 2016–April 21, 2016
Groundwater replenishment facility
Fault—Solid where known; dashed where approximately located; dotted where concealed

Figure 1.15.

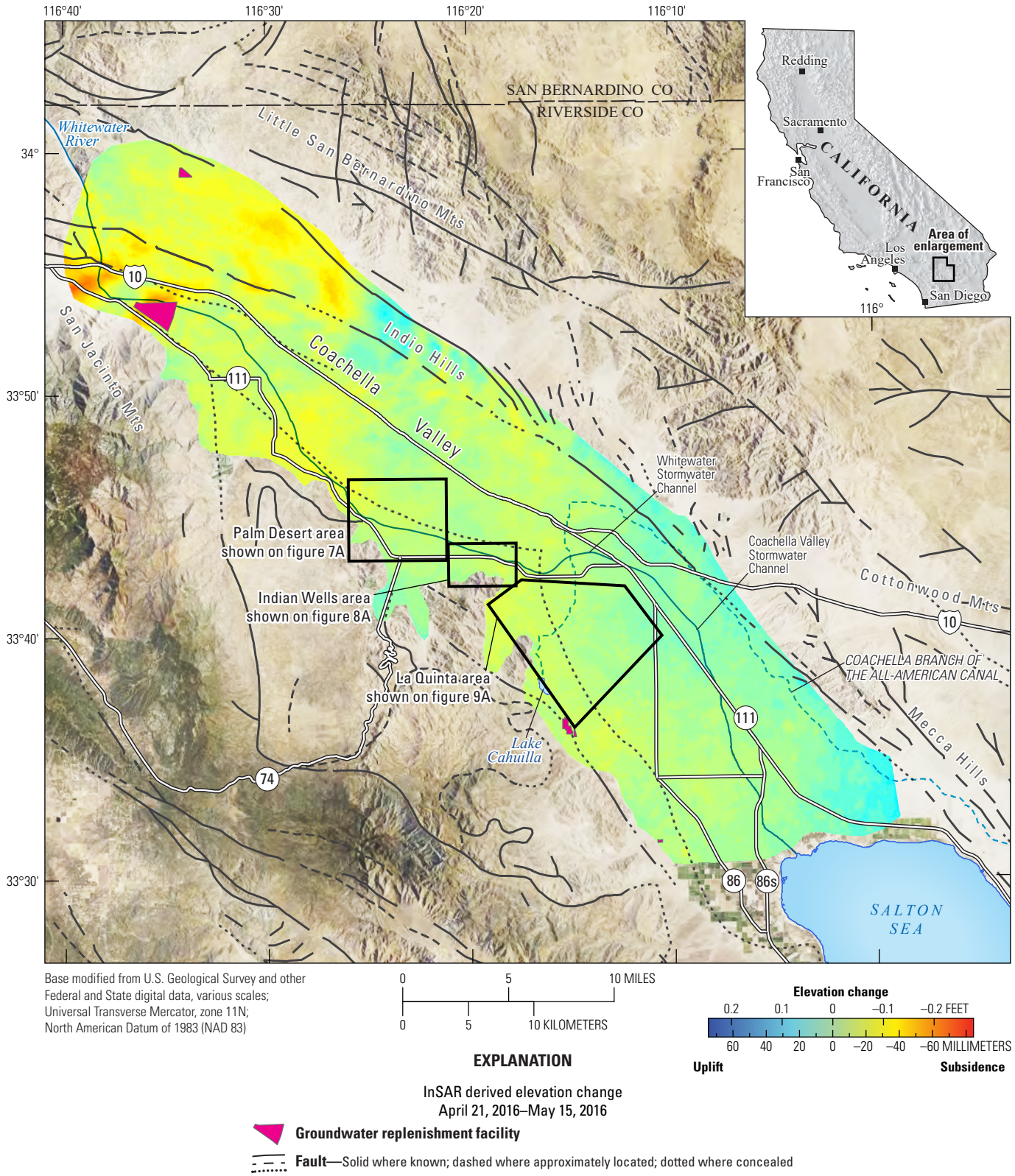
116°40'
116°30'
116°20'
116°10'
34°
33°50'
33°40'
33°30'
SAN BERNARDINO CO
RIVERSIDE CO
Whitewater River
Little San Bernardino Mts
San Jacinto Mts
Indio Hills
Coachella Valley
Whitewater Stormwater Channel
Coachella Valley Stormwater Channel
Palm Desert area shown on figure 7A
Indian Wells area shown on figure 8A
La Quinta area shown on figure 9A
Lake Cahuilla
Cottonwood Mts
COACHELLA BRANCH OF THE ALL-AMERICAN CANAL
Mecca Hills
SALTON SEA
10
111
74
86
86s
Redding
Sacramento
San Francisco
CALIFORNIA
Los Angeles
Area of enlargement
San Diego
116°
Base modified from U.S. Geological Survey and other Federal and State digital data, various scales; Universal Transverse Mercator, zone 11N; North American Datum of 1983 (NAD 83)
0 5 10 MILES
0 5 10 KILOMETERS
Elevation change
0.2 0.1 0 –0.1 –0.2 FEET
60 40 20 0 –20 –40 –60 MILLIMETERS
Uplift
Subsidence
EXPLANATION
InSAR derived elevation change
April 21, 2016–May 15, 2016
Groundwater replenishment facility
Fault—Solid where known; dashed where approximately located; dotted where concealed

Figure 1.16.

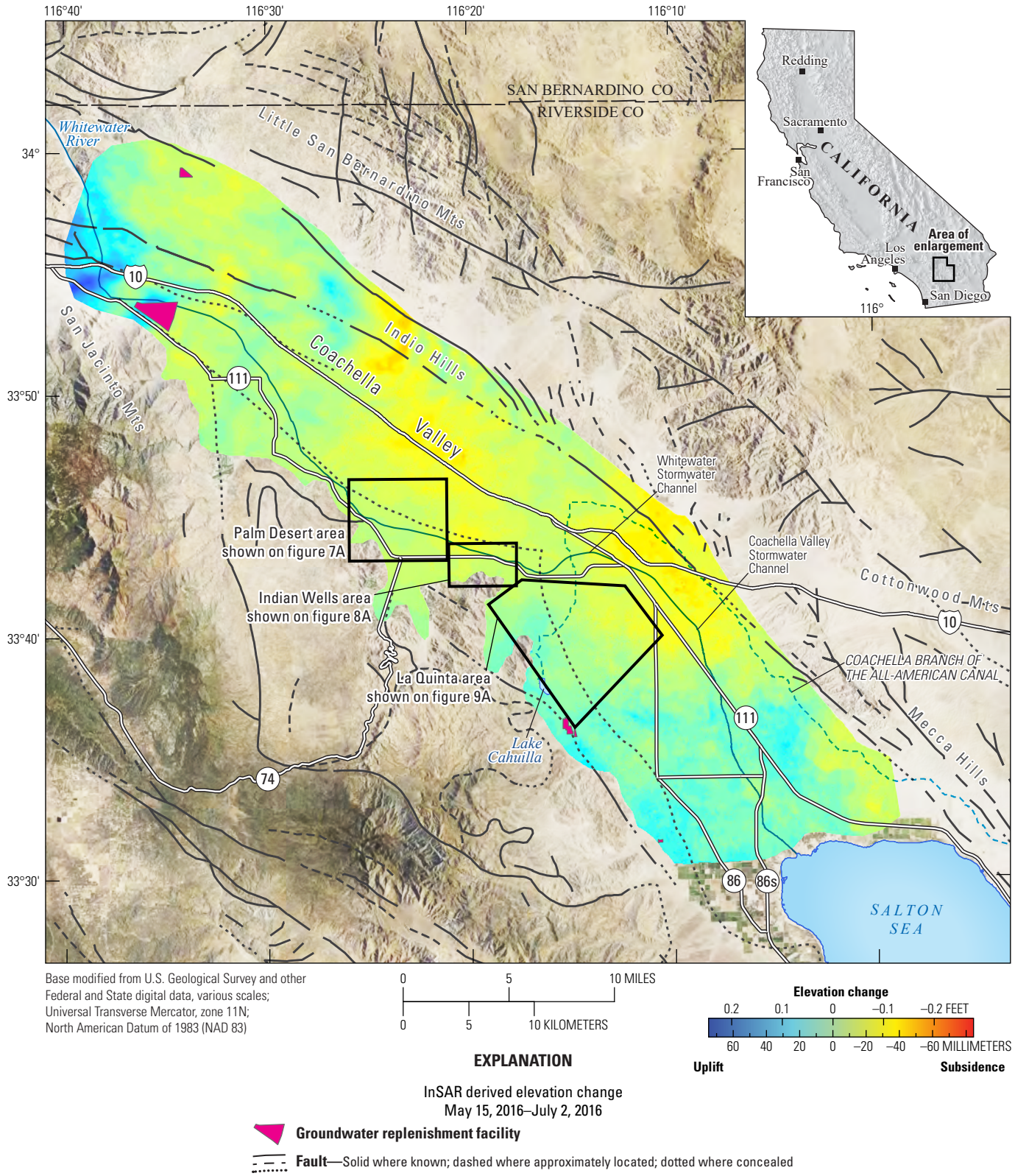
116°40'
116°30'
116°20'
116°10'
34°
33°50'
33°40'
33°30'
SAN BERNARDINO CO
RIVERSIDE CO
Whitewater River
Little San Bernardino Mts
San Jacinto Mts
Indio Hills
Coachella Valley
Whitewater Stormwater Channel
Coachella Valley Stormwater Channel
Palm Desert area shown on figure 7A
Indian Wells area shown on figure 8A
La Quinta area shown on figure 9A
Lake Cahuilla
Cottonwood Mts
COACHELLA BRANCH OF THE ALL-AMERICAN CANAL
Mecca Hills
SALTON SEA
10
111
74
86
86s
Redding
Sacramento
San Francisco
CALIFORNIA
Los Angeles
Area of enlargement
San Diego
116°
Base modified from U.S. Geological Survey and other Federal and State digital data, various scales; Universal Transverse Mercator, zone 11N; North American Datum of 1983 (NAD 83)
0 5 10 MILES
0 5 10 KILOMETERS
Elevation change
0.2 0.1 0 –0.1 –0.2 FEET
60 40 20 0 –20 –40 –60 MILLIMETERS
Uplift
Subsidence
EXPLANATION
InSAR derived elevation change
May 15, 2016–July 2, 2016
Groundwater replenishment facility
Fault—Solid where known; dashed where approximately located; dotted where concealed

Figure 1.17.

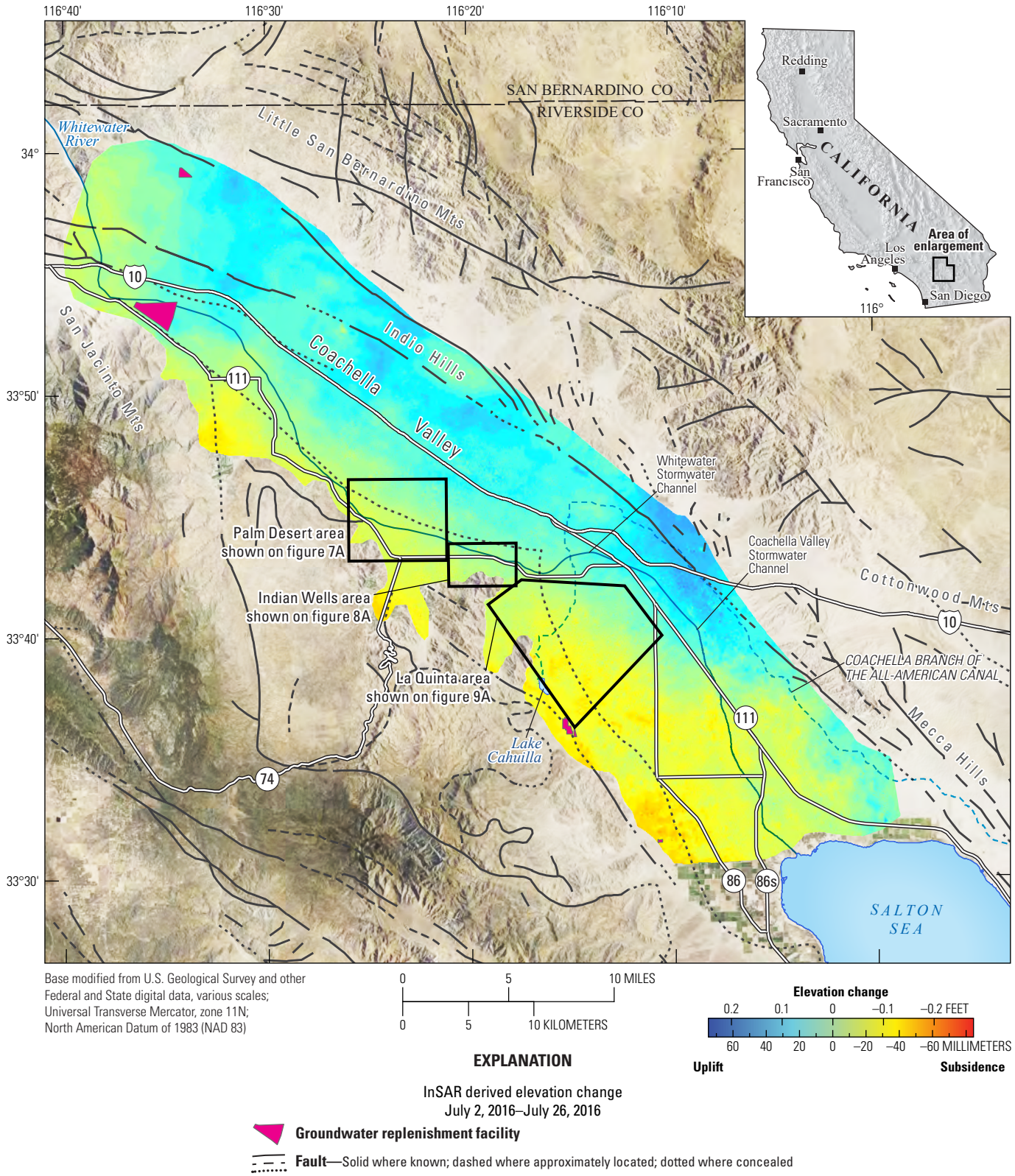
116°40'
116°30'
116°20'
116°10'
34°
33°50'
33°40'
33°30'
SAN BERNARDINO CO
RIVERSIDE CO
Whitewater River
Little San Bernardino Mts
San Jacinto Mts
Indio Hills
Coachella Valley
Palm Desert area shown on figure 7A
Indian Wells area shown on figure 8A
La Quinta area shown on figure 9A
Lake Cahuilla
Whitewater Stormwater Channel
Coachella Valley Stormwater Channel
Cottonwood Mts
COACHELLA BRANCH OF THE ALL-AMERICAN CANAL
Mecca Hills
SALTON SEA
10
111
74
86
86s
Redding
Sacramento
San Francisco
CALIFORNIA
Area of enlargement
Los Angeles
San Diego
116°
Base modified from U.S. Geological Survey and other Federal and State digital data, various scales; Universal Transverse Mercator, zone 11N; North American Datum of 1983 (NAD 83)
0 5 10 MILES
0 5 10 KILOMETERS
Elevation change
0.2 0.1 0 –0.1 –0.2 FEET
60 40 20 0 –20 –40 –60 MILLIMETERS
Uplift
Subsidence
EXPLANATION
InSAR derived elevation change
July 2, 2016–July 26, 2016
Groundwater replenishment facility
Fault—Solid where known; dashed where approximately located; dotted where concealed

Figure 1.18.

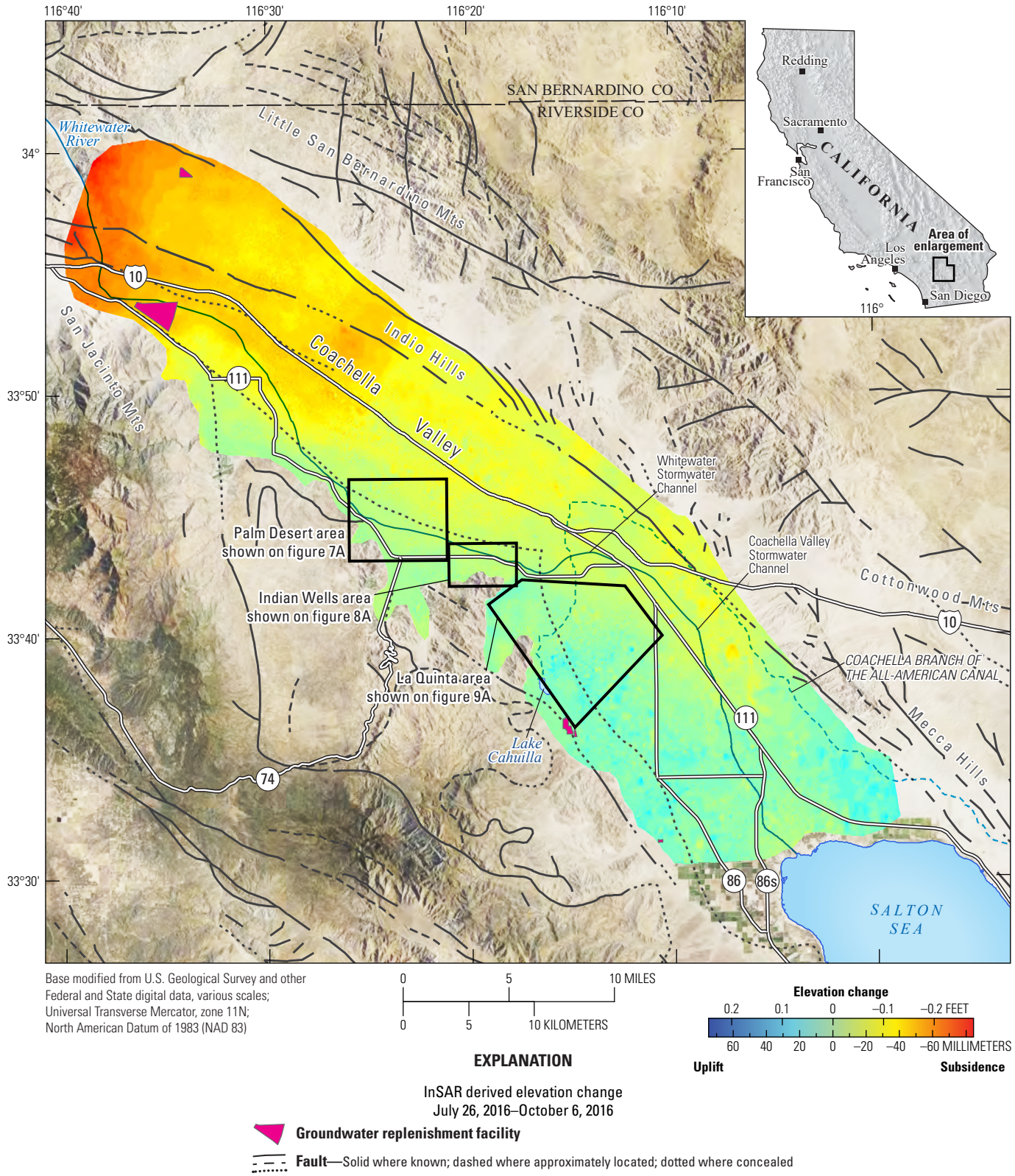
116°40'
116°30'
116°20'
116°10'
34°
33°50'
33°40'
33°30'
SAN BERNARDINO CO
RIVERSIDE CO
Whitewater River
Little San Bernardino Mts
San Jacinto Mts
Indio Hills
Coachella Valley
Whitewater Stormwater Channel
Coachella Valley Stormwater Channel
Palm Desert area shown on figure 7A
Indian Wells area shown on figure 8A
La Quinta area shown on figure 9A
Lake Cahuilla
Cottonwood Mts
COACHELLA BRANCH OF THE ALL-AMERICAN CANAL
Mecca Hills
SALTON SEA
10
111
74
86
86s
Redding
Sacramento
San Francisco
CALIFORNIA
Los Angeles
Area of enlargement
San Diego
116°
Base modified from U.S. Geological Survey and other Federal and State digital data, various scales; Universal Transverse Mercator, zone 11N; North American Datum of 1983 (NAD 83)
0 5 10 MILES
0 5 10 KILOMETERS
Elevation change
0.2 0.1 0 –0.1 –0.2 FEET
60 40 20 0 –20 –40 –60 MILLIMETERS
Uplift
Subsidence
EXPLANATION
InSAR derived elevation change
July 26, 2016–October 6, 2016
Groundwater replenishment facility
Fault—Solid where known; dashed where approximately located; dotted where concealed

Figure 1.19.

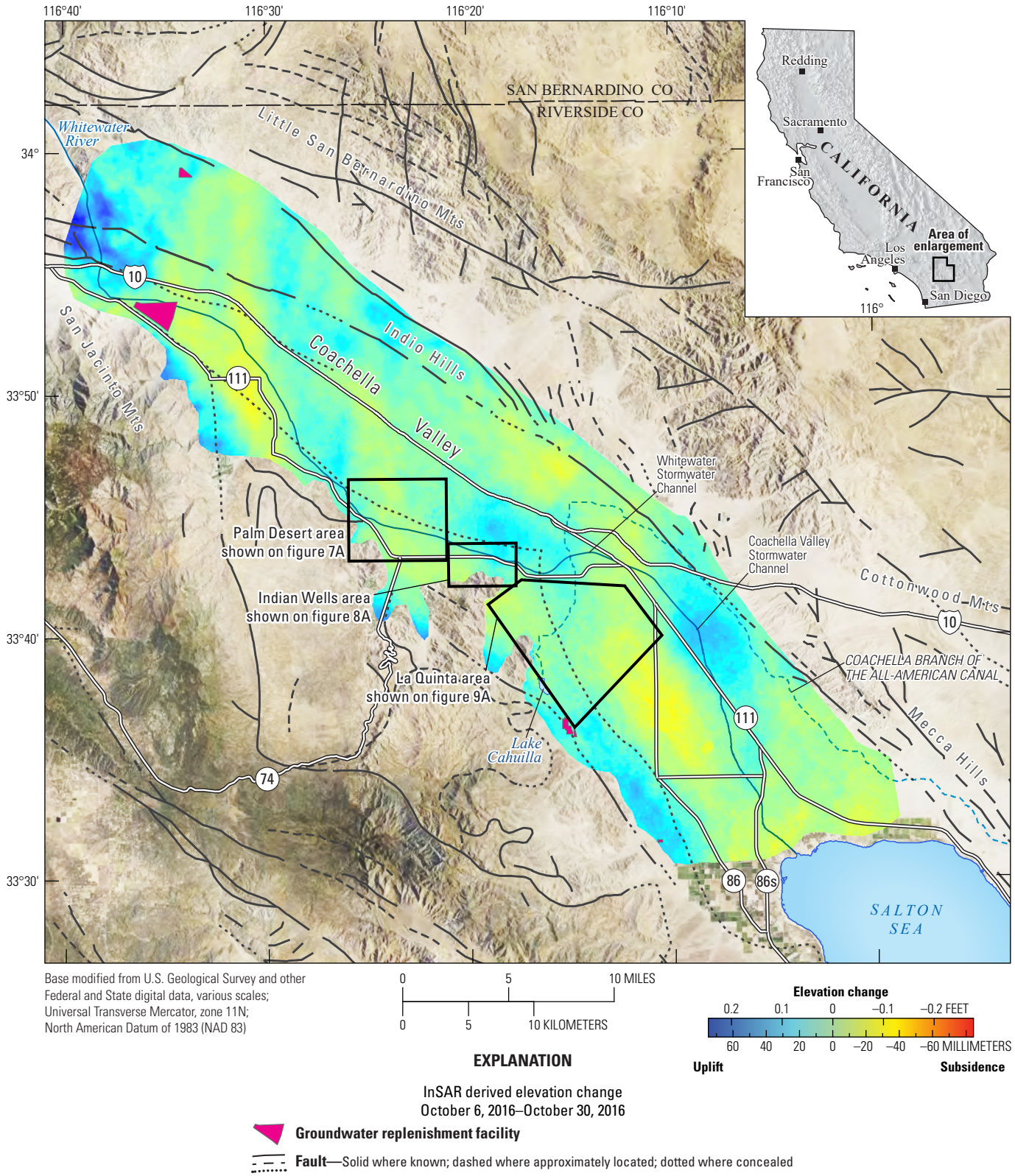
116°40'
116°30'
116°20'
116°10'
116°
34°
33°50'
33°40'
33°30'
SAN BERNARDINO CO
RIVERSIDE CO
Whitewater River
Little San Bernardino Mts
San Jacinto Mts
Indio Hills
Coachella Valley
Palm Desert area shown on figure 7A
Indian Wells area shown on figure 8A
La Quinta area shown on figure 9A
Lake Cahuilla
Whitewater Stormwater Channel
Coachella Valley Stormwater Channel
Cottonwood Mts
COACHELLA BRANCH OF THE ALL-AMERICAN CANAL
Mecca Hills
SALTON SEA
10
111
74
86
86s
Redding
Sacramento
San Francisco
CALIFORNIA
Los Angeles
Area of enlargement
San Diego
Base modified from U.S. Geological Survey and other Federal and State digital data, various scales; Universal Transverse Mercator, zone 11N; North American Datum of 1983 (NAD 83)
0 5 10 MILES
0 5 10 KILOMETERS
Elevation change
0.2 0.1 0 –0.1 –0.2 FEET
60 40 20 0 –20 –40 –60 MILLIMETERS
Uplift
Subsidence
EXPLANATION
InSAR derived elevation change
October 6, 2016–October 30, 2016
Groundwater replenishment facility
Fault—Solid where known; dashed where approximately located; dotted where concealed

Figure 1.20.

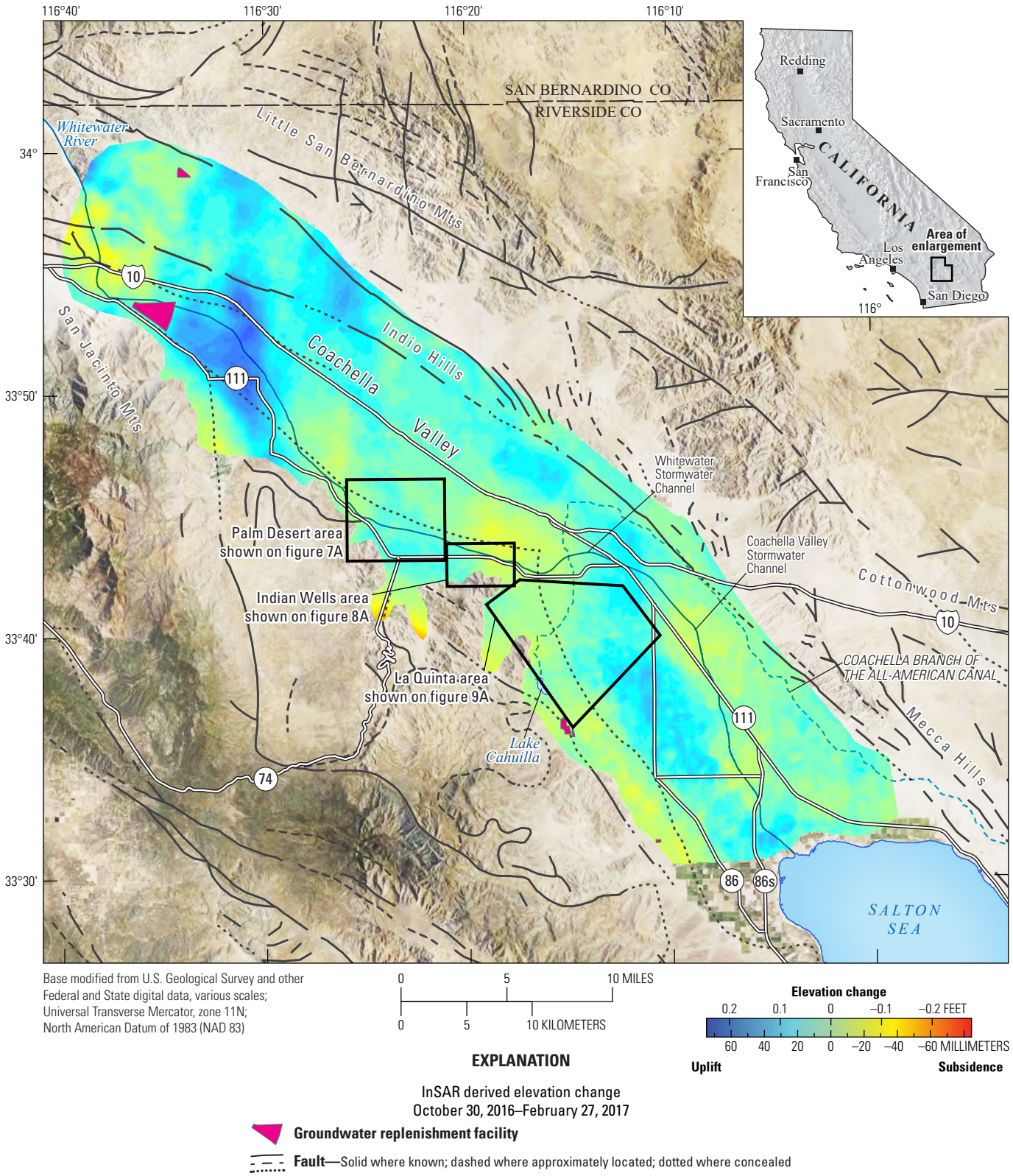
116°40'
116°30'
116°20'
116°10'
34°
33°50'
33°40'
33°30'
SAN BERNARDINO CO
RIVERSIDE CO
Whitewater River
Little San Bernardino Mts
San Jacinto Mts
Indio Hills
Coachella Valley
Whitewater Stormwater Channel
Coachella Valley Stormwater Channel
Palm Desert area shown on figure 7A
Indian Wells area shown on figure 8A
La Quinta area shown on figure 9A
Lake Cahuilla
Cottonwood Mts
COACHELLA BRANCH OF THE ALL-AMERICAN CANAL
Mecca Hills
SALTON SEA
10
111
74
86
86s
Redding
Sacramento
San Francisco
CALIFORNIA
Los Angeles
San Diego
Area of enlargement
116°
Base modified from U.S. Geological Survey and other Federal and State digital data, various scales; Universal Transverse Mercator, zone 11N; North American Datum of 1983 (NAD 83)
0 5 10 MILES
0 5 10 KILOMETERS
Elevation change
0.2 0.1 0 –0.1 –0.2 FEET
60 40 20 0 –20 –40 –60 MILLIMETERS
Uplift
Subsidence
EXPLANATION
InSAR derived elevation change
October 30, 2016–February 27, 2017
Groundwater replenishment facility
Fault—Solid where known; dashed where approximately located; dotted where concealed

Figure 1.21.

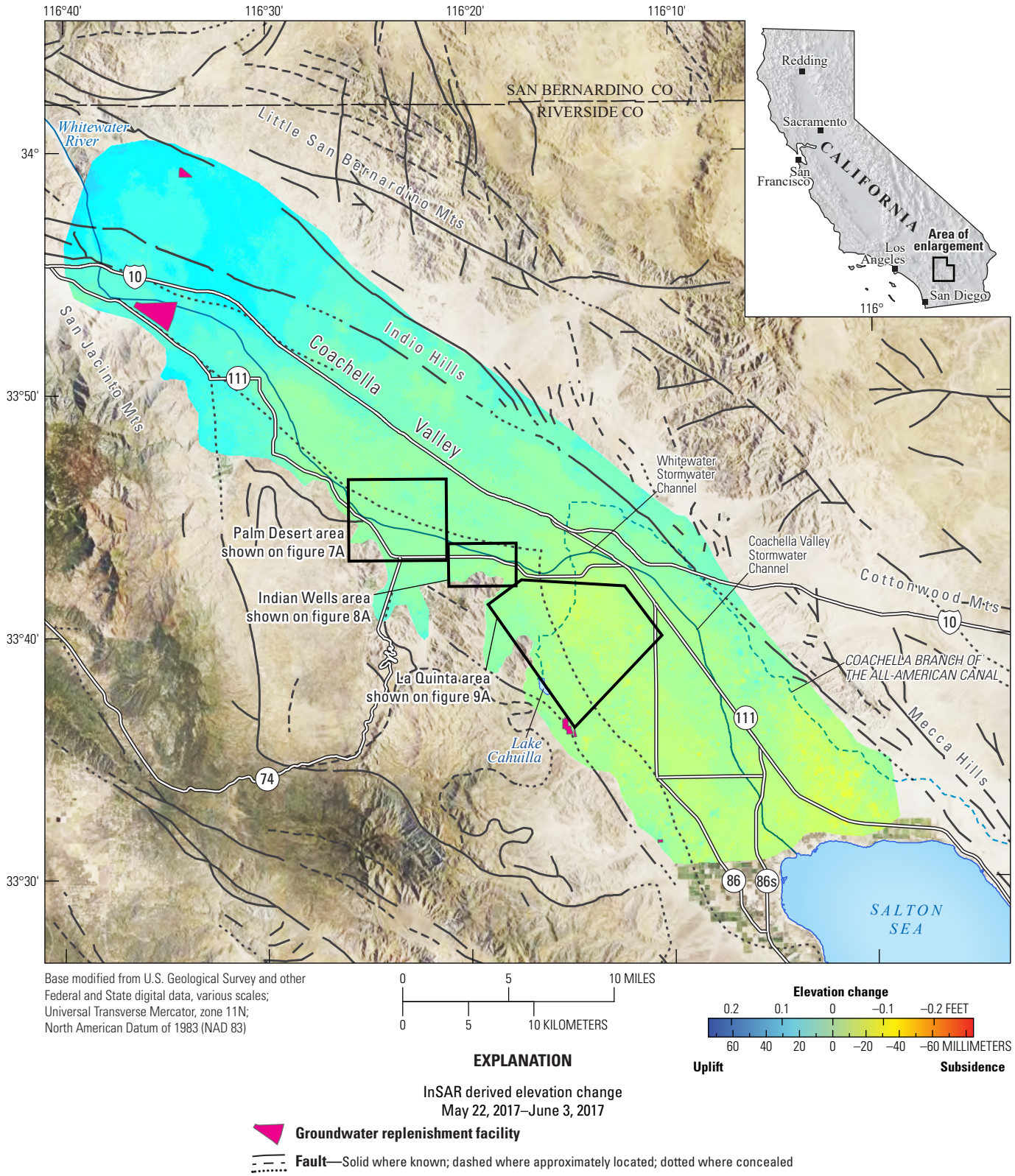
116°40'
116°30'
116°20'
116°10'
34°
33°50'
33°40'
33°30'
SAN BERNARDINO CO
RIVERSIDE CO
Whitewater River
Little San Bernardino Mts
San Jacinto Mts
Indio Hills
Coachella Valley
Palm Desert area shown on figure 7A
Indian Wells area shown on figure 8A
La Quinta area shown on figure 9A
Lake Cahuilla
Whitewater Stormwater Channel
Coachella Valley Stormwater Channel
Cottonwood Mts
COACHELLA BRANCH OF THE ALL-AMERICAN CANAL
Mecca Hills
SALTON SEA
10
111
74
86
86s
Redding
Sacramento
San Francisco
CALIFORNIA
Los Angeles
Area of enlargement
San Diego
116°
Base modified from U.S. Geological Survey and other Federal and State digital data, various scales; Universal Transverse Mercator, zone 11N; North American Datum of 1983 (NAD 83)
0 5 10 MILES
0 5 10 KILOMETERS
Elevation change
0.2 0.1 0 –0.1 –0.2 FEET
60 40 20 0 –20 –40 –60 MILLIMETERS
Uplift
Subsidence
EXPLANATION
InSAR derived elevation change
May 22, 2017–June 3, 2017
Groundwater replenishment facility
Fault—Solid where known; dashed where approximately located; dotted where concealed

Figure 1.22.

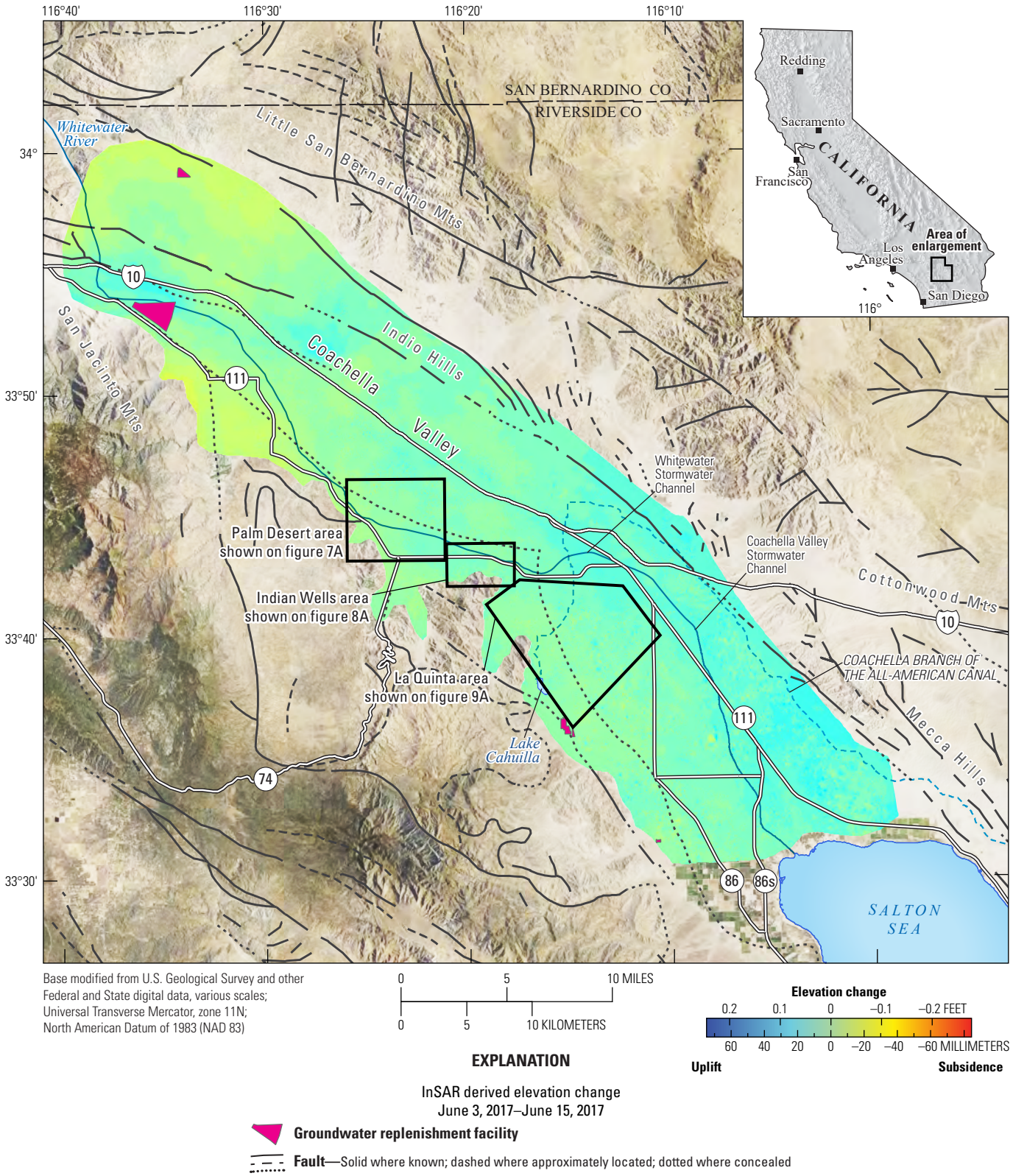
116°40'
116°30'
116°20'
116°10'
34°
33°50'
33°40'
33°30'
SAN BERNARDINO CO
RIVERSIDE CO
Whitewater River
Little San Bernardino Mts
San Jacinto Mts
Indio Hills
Coachella Valley
Whitewater Stormwater Channel
Coachella Valley Stormwater Channel
Palm Desert area shown on figure 7A
Indian Wells area shown on figure 8A
La Quinta area shown on figure 9A
Lake Cahuilla
Cottonwood Mts
COACHELLA BRANCH OF THE ALL-AMERICAN CANAL
Mecca Hills
SALTON SEA
10
111
74
86
86s
Redding
Sacramento
San Francisco
CALIFORNIA
Los Angeles
Area of enlargement
San Diego
116°
Base modified from U.S. Geological Survey and other Federal and State digital data, various scales; Universal Transverse Mercator, zone 11N; North American Datum of 1983 (NAD 83)
0 5 10 MILES
0 5 10 KILOMETERS
Elevation change
0.2 0.1 0 –0.1 –0.2 FEET
60 40 20 0 –20 –40 –60 MILLIMETERS
Uplift
Subsidence
EXPLANATION
InSAR derived elevation change
June 3, 2017–June 15, 2017
Groundwater replenishment facility
Fault—Solid where known; dashed where approximately located; dotted where concealed

Figure 1.23.

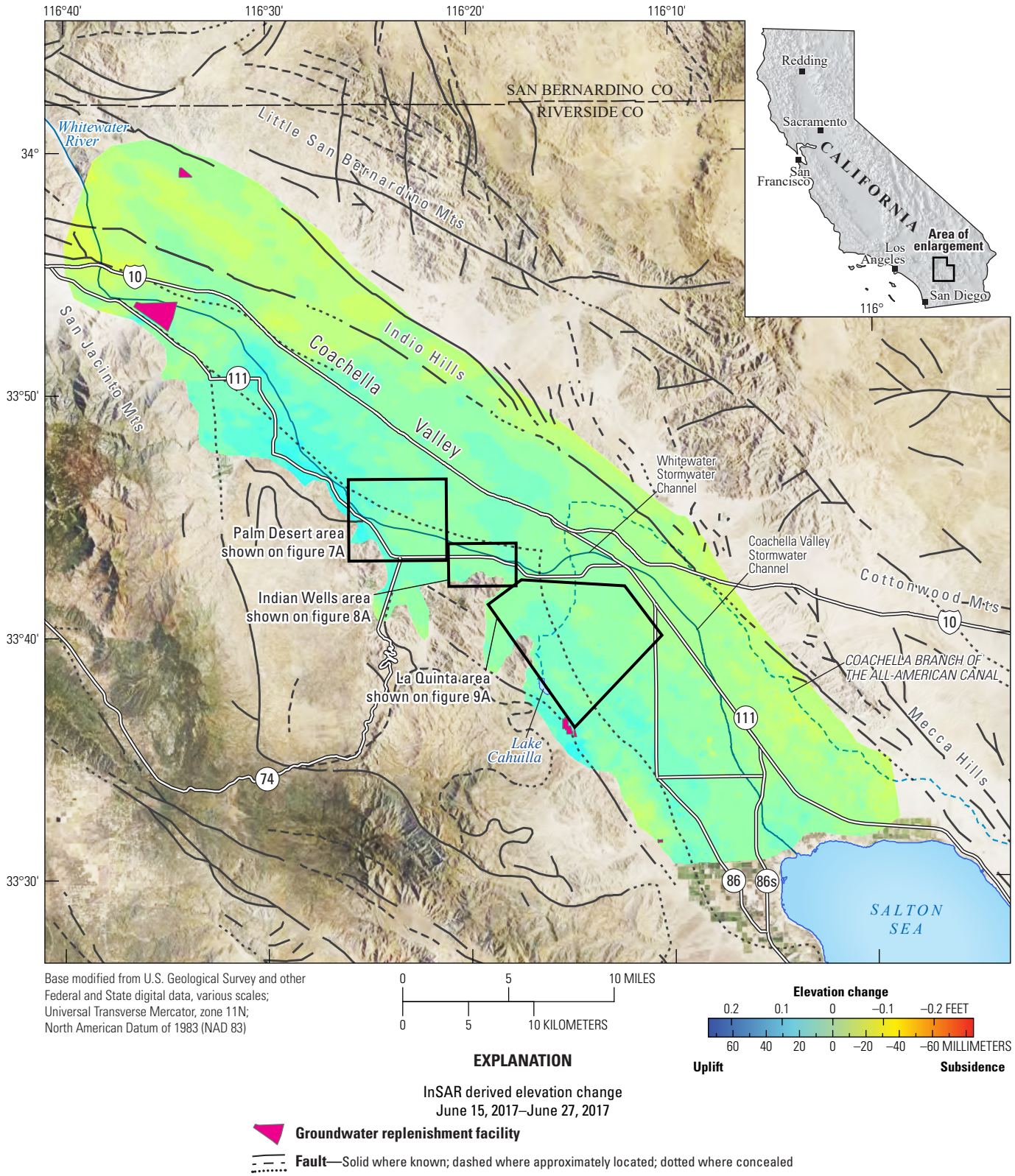
116°40'
116°30'
116°20'
116°10'
34°
33°50'
33°40'
33°30'
SAN BERNARDINO CO
RIVERSIDE CO
Whitewater River
Little San Bernardino Mts
San Jacinto Mts
Indio Hills
Coachella Valley
Palm Desert area shown on figure 7A
Indian Wells area shown on figure 8A
La Quinta area shown on figure 9A
Lake Cahuilla
Whitewater Stormwater Channel
Coachella Valley Stormwater Channel
Cottonwood Mts
COACHELLA BRANCH OF THE ALL-AMERICAN CANAL
Mecca Hills
SALTON SEA
10
111
74
86
86s
Redding
Sacramento
San Francisco
CALIFORNIA
Los Angeles
Area of enlargement
San Diego
116°
Base modified from U.S. Geological Survey and other Federal and State digital data, various scales; Universal Transverse Mercator, zone 11N; North American Datum of 1983 (NAD 83)
0 5 10 MILES
0 5 10 KILOMETERS
Elevation change
0.2 0.1 0 –0.1 –0.2 FEET
60 40 20 0 –20 –40 –60 MILLIMETERS
Uplift
Subsidence
EXPLANATION
InSAR derived elevation change
June 15, 2017–June 27, 2017
Groundwater replenishment facility
Fault—Solid where known; dashed where approximately located; dotted where concealed

Figure 1.24.

For more information concerning the research in this report, contact the
Director, California Water Science Center
U.S. Geological Survey
6000 J Street, Placer Hall
Sacramento, California 95819
https://ca.water.usgs.gov
Publishing support provided by the
U.S. Geological Survey Science Publishing Network,
Sacramento Publishing Service Center